A Fc Domain-Conjugated Adenosine 2A Receptor Ligand for Immune Checkpoint Blockade

by

Po-Yuan Hsiao

A dissertation submitted to Johns Hopkins University in conformity with the requirements for the degree of Doctor of Philosophy

Baltimore, Maryland

July, 2016

Abstract

In light of the recent success of immune checkpoint blockade in cancer treatments, new inhibitory molecules and pathways have been increasingly considered as targets for cancer immunotherapy. The adenosine A_{2A} receptor has long been regarded as an important checkpoint target given its role in anti-inflammation and immune suppression. At the same time, the tumor environment has also been found to contain high levels of adenosine as a consequence of hypoxia, inflammation, and cell death. The result of this phenomenon is often a suppression of activated lymphocytes, natural kills cells, and antigen-presenting cells, along with the up-regulation of inhibitory T cells.

To combat the evasion by the tumor cells and avoid further exploitation of the adenosine pathway, numerous strategies have been proposed including the use of monoclonal antibodies to block CD73, an adenosine-generating ecto-5'-nucleotidase expressed on the surface of tumor cells. Alternatively, potent and selective small-molecule antagonists to the A_{2A} receptor can also prevent activation of the receptor, hence the downstream signaling pathways that lead to immune suppression. However, most antagonists developed previously have drawbacks such as short pharmacokinetic half-lives and potential systemic toxicity due to the expression of $A_{2A}R$ in the brain and the heart.

In my thesis research, we conjugated a potent, selective A_{2A} receptor antagonist, ZM-241,385, to the fragment crystallizable (Fc) region of immunoglobulins to overcome these pharmacologic barriers to A_{2A} receptor inhibition. Our synthetic approach utilizes the

advantage of expressed protein ligation to site-specifically and reproducibly link the two moieties, ZM-241,385 and Fc, together. The resulting product, Fc-ZM, retained functional interactions with the A_{2A} receptor and Fc receptors as confirmed by *in vitro* binding and functional assays. More importantly, Fc-ZM was shown to have superior pharmacologic properties in blocking the adenosine checkpoint pathway in mice, thereby enhancing the immune response *in vivo*. Overall, my thesis research provides a reproducible method of synthesizing Fc-conjugated small molecules, and demonstrate the ability of Fc conjugation to enhance the pharmacologic properties of small molecule drugs.

Acknowledgements

Thesis Advisor: Philip A. Cole, M.D. Ph.D.

Thesis Reader: Jonathan D. Powell, M.D. Ph.D.

Thesis Committee Members: Jonathan D. Powell, M.D. Ph.D., Maureen Horton, M.D., Jun Liu, Ph.D.

Collaborators: Lai-Xi Wang, Ph.D., Kathleen Gabrielson, D.V.M., Ph.D., Polina Sysa-Shah, M.D., Jay Kalin, Ph.D., Meng-Jung Chiang, Ph.D., Ying-Chun Lo, M.D. Ph.D., Im-Hong Sun, Mohammed N. Amin, Ph.D., John Giddens.

Colleagues: Young-Hoon Ahn, Ph.D., David Bolduc, Ph.D., Jay Kalin, Ph.D., You Sang Hwang, Ph.D., Mary-Katherine Tarrant Connacher, Ph.D., Rong Huang, Ph.D., Beverly Dancy, Ph.D., Blair Dancy, Ph.D., Isabel Ferrando, Ph.D., Shonoi Ming, Ph.D., Zhihong Wang, Ph.D., Yun Wang, Ph.D., Beth Zucconi, Ph.D., Shridhar Bhat, Ph.D., Polina Prusevich, Ph.D., Mingxuan Wu, Ph.D., Daniel Dempsey, Ph.D., Brian Weiser, Ph.D., Nam Chu, Ph.D., Zan Chen, Sam Henager, Dawn Hayward

Pharmacology Staff: Robin Hart, Amy Paronto, Amy Forcier, Mimi Guercio, Brenda Figueroa, Paula Mattingly, Frank Williams

To Dr. Jim Stivers and Dr. Ronald Schnaar, who kindly supported me during my rotations and were patient mentors who allowed me to explore, experiment, and learn about completely new scientific fields.

To Dr. Philip Cole, my thesis advisor, who has graciously taught me how to become a great scientist, a great colleague, and a great collaborator. Without his unconditional support and mentorship, the hard times throughout my graduate career would have been disastrous. Words cannot describe my appreciation for his guidance and understanding at every step of my graduate career. I am grateful to have had him as my advisor.

To Dr. Jonathan Powell, my co-mentor, who has consistently given me generous advice, pointed me to the right direction, and reminded me that I can always improve myself further as a scientist. I am grateful to have had his support throughout the second half of my graduate career.

To Dr. Daniel Raben, Dr. Jun Liu, and Dr. Maureen Horton, my current and previous thesis committee members, who have given me great advice in solving the toughest challenges in science. I am thankful for their support and mentorship throughout the different stages in my thesis research.

To all my collaborators, colleagues, and departmental staff listed above, I want to thank them for their long-term support and friendship. Without them, I would not have been able to persist and complete my degree. My graduate life was made colorful and enjoyable because of all of you.

Lastly and most importantly, to my family, my father, Dr. Ting-Nung Shiau, my mother, Dr. Su-Chen Wang, and my brother, Pei-Yuan (Daniel) Hsiao, who has given me

unconditional love and spiritual support throughout my whole life. They are the reason why I have the strength and motivation to reach where I am today. Thank you guys and I love you.

Table of Content

List of Figures

Chapter 1:

Introduction

Cancer Immunotherapy

Technological advances in the understanding, production, and use of biologics have greatly accelerated the growth of cancer immunotherapy in the past two decades. Today, cancer immunotherapy comes in various forms including antibody-based, cell-based, virus-based, and non-targeted methods (Fig. 1). These methods help boost our immune system by doing one of two things: stimulate the immune cells to work harder and smarter, or provide the system with critical components to speed up and strengthen the immune response. This is because our immune system sometimes does not recognize cancer cells as foreign or, in cases where recognition happens, the response might not be robust enough to destroy the cancer cells. At the same time, cancer cells themselves can also release substances to dampen or even shut down the immune response. As the cancer cells evolve their immunogenicity in order to survive the attacks from the immune system, the result is often the emergence of immune-resistant tumors.

This dynamic process involving immunosurveillance and tumor progression is known as immunoediting (Fig. 2), and occurs in three steps: *elimination*, *equilibrium*, and *escape*[1]. The first phase, *elimination*, refers to the innate and adaptive immune responses to the tumor. Natural killer (NK) cells, lymphocytes, macrophages and other immune cells work together to destroy cancer cells by cytotoxic mechanisms such as perforin, TNF-

related apoptosis-inducing ligands, and reactive oxygen species[2]. Next, in the *equilibrium* phase, cancer cells that have survived the elimination enter into an equilibrium with the host immune system, wherein lymphocytes and cytokines such as IFN-γ continue to exert pressure that is sufficient to contain, but not fully extinguish, the tumor. During this relatively long period of Darwinian selection, new variants of the original tumor with reduced or non-immunogenic phenotypes arise and are selected for proliferation[2]. Lastly, during the *escape* phase, the host's immune defense system is effectively breached, with the cancer cells selected in the *equilibrium* phase expanding without any detection and elimination. Although most cancers observed clinically have progressed through the *escape* phase, it remains critically important to understand the underlying mechanisms that give rise to immune tolerance for the design and the development of better, more effective, immunotherapies.

One of the first examples of immunotherapy for cancer is the use of Bacillus Calmette-Guérin (BCG) for treating superficial forms of bladder cancer. In fact, the BCG vaccine has been used as standard of care for patients with non-muscle-invasive bladder cancer (NMIBC) since 1977, nearly 40 years ago[3]. The antitumor effect of BCG is thought to be mediated through a combination of direct effects on cancer cells and the host's immune system, resulting in improve recognition and subsequent destruction of cancer cells through non-specific and specific cell-mediated mechanisms[4]. More recent examples of cancer vaccines include Gardisil, a preventative vaccine approved by the FDA for cervical cancer in 2006, and Sipuleucel-T (Provenge®), approved by the FDA in 2010 for the treatment of prostate cancer. Sipuleucel-T is a cell-based therapeutic vaccine that

utilizes patient's own white blood cells, particularly dendritic cells, to fight off cancer. After a brief stimulation *ex vivo* with a fusion protein consisting of the antigen prostatic acid phosphatase (PAP) and the granulocyte-macrophage colony stimulating factor (GM-CSF), the resulting active blood product is reinfused into the patient (Fig. 3). In a double-blind randomized phase III clinical trial, Sipuleucel-T showed a four-month overall survival benefit to patients with castration-resistant prostate cancer[5]. For this reason, Sipuleucel-T was the first human cancer treatment vaccine to be approved in the United States.

In addition to cancer vaccines, a new type of immunotherapy known as oncolytic virus therapy gained FDA approval in October 2015. The genetically engineered virus, called talimogene laherparepvec, or T-VEC, was altered to reduce its ability to cause herpes and instead, infect and preferentially kill cancer cells (Fig. 4). In a randomized phase III clinical trial, T-VEC shrank tumours in people with advanced melanoma and extended patient survival by a median of 4.4 months[6]. While newer cancer vaccines, oncolytic viruses, and other novel approaches such as the chimeric antigen receptor (CAR) T-cell therapy display promising potential, most of the success stories up-to-date have been demonstrated by monoclonal antibodies (mAbs). Since the approval of Rituximab in 1997, more than a dozen mAbs have been approved for cancer treatment (Fig. 5). Notable examples include the recently renowned immune checkpoint blockers, anti-CTLA-4[7, 8] and anti-PD-1[9-11], which significantly extend the survival and cause rapid tumor regression in patients with melanoma[12, 13] and other cancers. The recent approval of

daratumumab[14] and elotuzumab[15], the first antibody treatments for myeloma, further highlights the importance of continual innovation in this space.

Figure 1. Key Milestones of Cancer Immunotherapy.

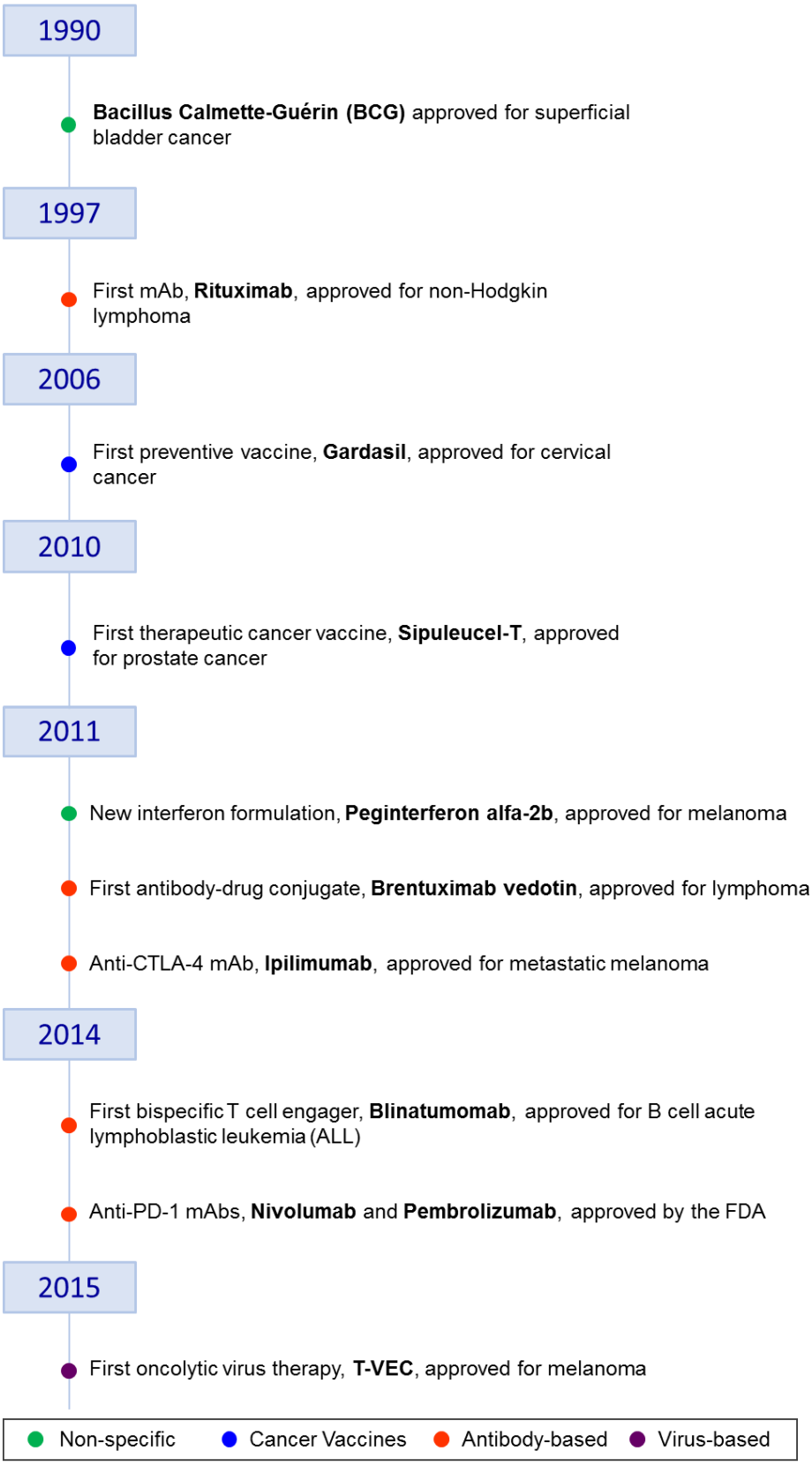

Figure 2. Three phases of Immunoediting.

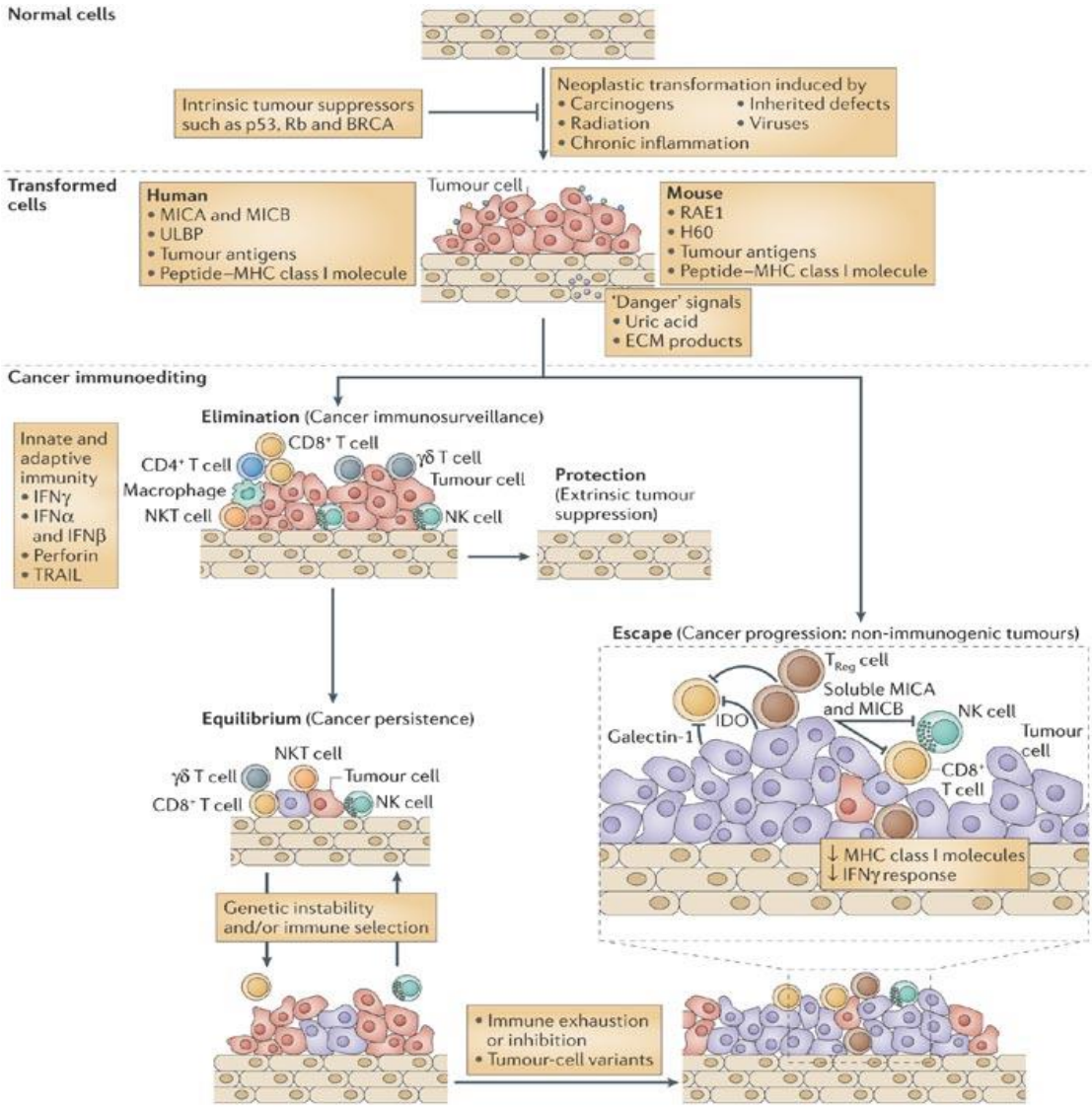

Dunn GP, Koebel CM, Schreiber RD. Interferons, immunity and cancer immunoediting. Nat Rev Immunol. 2006;6(11):836-48.

Figure 3. Mechanism of action of Sipuleucel-T.

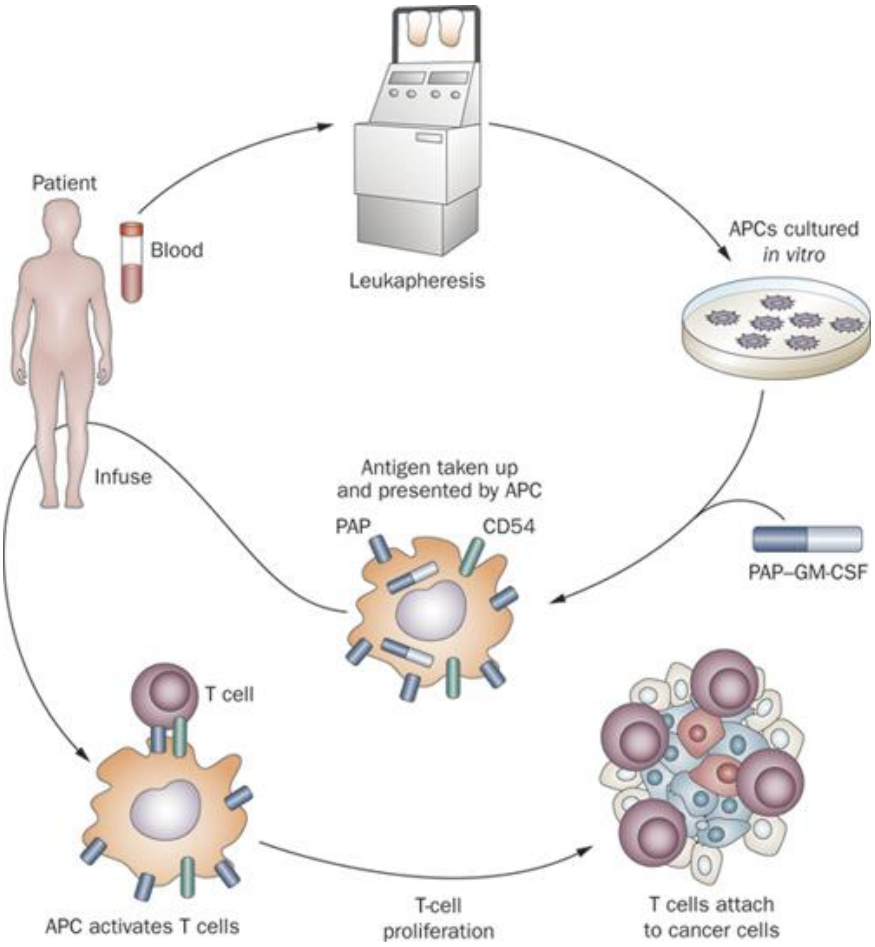

Di Iorenzo G, Buonerba C, Kantoff PW. Immunotherapy for the treatment of prostate cancer. Nat Rev Clin Oncol. 2011;8(9):551-61.

Figure 4. Mechanism of action of T-VEC.

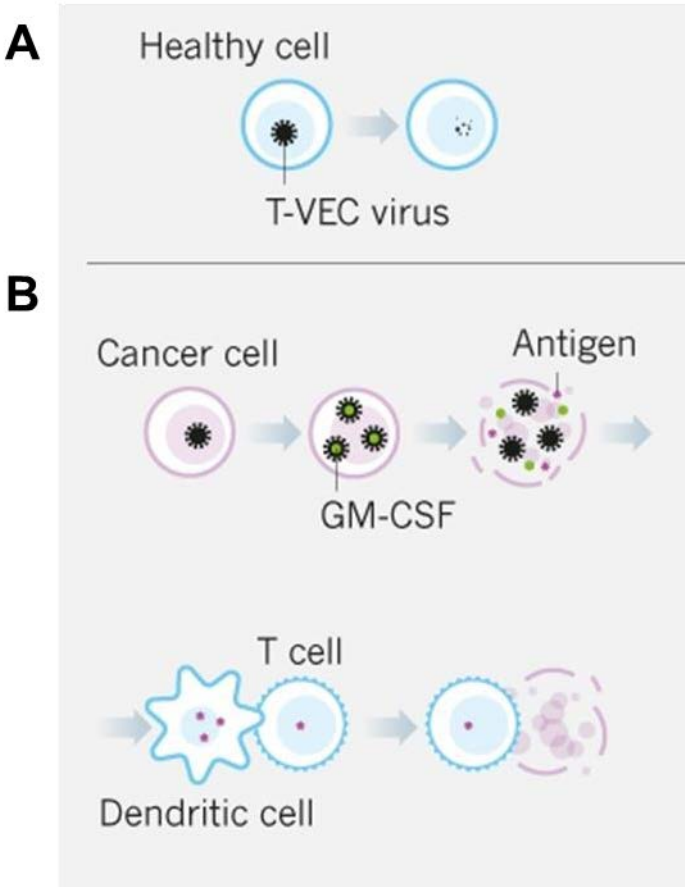

(A*) T-VEC enters but does not replicate within healthy cells. (B) T-VEC destroys malignant cells directly, releasing GM-CSF and antigens that attract and enables the immune system to further destroy cancer cells throughout the body.*

Ledford H. Cancer-fighting viruses win approval. Nature. 2015;526(7575):622-3.

Figure 5. Example FDA approved therapeutic monoclonal antibodies

Antibody	Approval date	Target	Indication (Target Cancer)
alemtuzumab	2001	CD52	Chronic lymphocytic leukemia
bevacizumab	2004	Vascular endothelial growth factor (VEGF)	Colorectal cancer
brentuximab vedotin	2011	CD30	Anaplastic large cell lymphoma (ALCL) and Hodgkin lymphoma
cetuximab	2004	Epidermal growth factor receptor	Colorectal cancer, Head and neck cancer
daratumumab	2015	CD38	Multiple Myeloma
denosumab	2010	RANK Ligand inhibitor	Solid tumor's bony metasteses
ibritumomab tiuxetan	2002	CD20	Non-Hodgkin lymphoma
ipilimumab (MDX-101)	2011	Blocks CTLA-4	Melanoma
nivolumab	2014	Blocks PD-1	Melanoma and SCC
ofatumumab	2009	CD20	Chronic lymphocytic leukemia
panitumumab	2006	Epidermal growth factor receptor	Colorectal cancer
pembrolizumab	2014	Blocks PD-1	Melanoma and NSCLC
rituximab	1997	CD20	Non-Hodgkin lymphoma
tositumomab	2003	CD20	Non-Hodgkin lymphoma
trastuzumab	1998	ErbB2	Breast cancer

Monoclonal Antibodies

Existing monoclonal antibody therapeutics on the market can be largely divided into five categories based on their mechanisms of action[16, 17]. The first category includes those that make cancer cells more susceptible to immune attacks. These mAbs achieve this by either improving the recognition of cancerous cells or preventing the immune system from shutting down via endogenous inhibitory pathways. Rituximab, for instance, binds to CD20 on B cells, rendering certain types of lymphomas more visible to the immune system. The second category of mAbs refers to those that block growth signals for the tumor. Cetuximab, a monoclonal antibody approved to treat colon cancer and head and neck cancers, attaches to the epidermal growth factor receptor on cancer cells thereby slowing or stopping their growth. The third category consists of antiangiogenic mAbs. As cancer cells rely heavily on oxygen and nutrients in the blood, angiogenesis has been found to be an important therapeutic target in controlling tumor growth and expansion. The monoclonal antibody bevacizumab targets the vascular endothelial growth factor (VEGF) and restrict the growth of new blood vessels around tumors. Monoclonal antibodies that deliver radiation and chemotherapy to cancer cells make up the fourth and fifth categories, respectively. Examples include ibritumomab, approved for non-Hodgkin's lymphoma, and trastuzumab emtansine, which is approved to treat HER2-positive breast cancer.

In terms of design, mAbs can be naked, conjugated, or bispecific. Naked mAbs are antibodies that work by themselves and are the most common form of mAbs. Conjugated antibodies are mAbs that are linked to either a chemotherapeutic or a radioactive ligand. Bispecific antibodies, on the other hand, are made up parts of two different antibodies,

allowing them to recognize and bind two antigens even if the antigens are on different cells. For example, blinatumomab, which is used to treat certain subtypes of acute lymphocytic leukemia, can bind to both CD19 and CD3 on cancer and immune cells simultaneously and by doing so, enhance immune recognition and destruction of the cancer cells.

Lastly, upon binding by tumor-specific mAbs, cancer cells can die via direct signaling-induced death or immune-mediated mechanisms such as antibody-dependent cellular cytotoxicity (ADCC) and complement-mediated cytotoxicity (CMC). Figures 6 and 7 summarizes these mAb therapeutic strategies as described above[18].

Figure 6. Monoclonal antibody-based cancer therapeutic strategies.

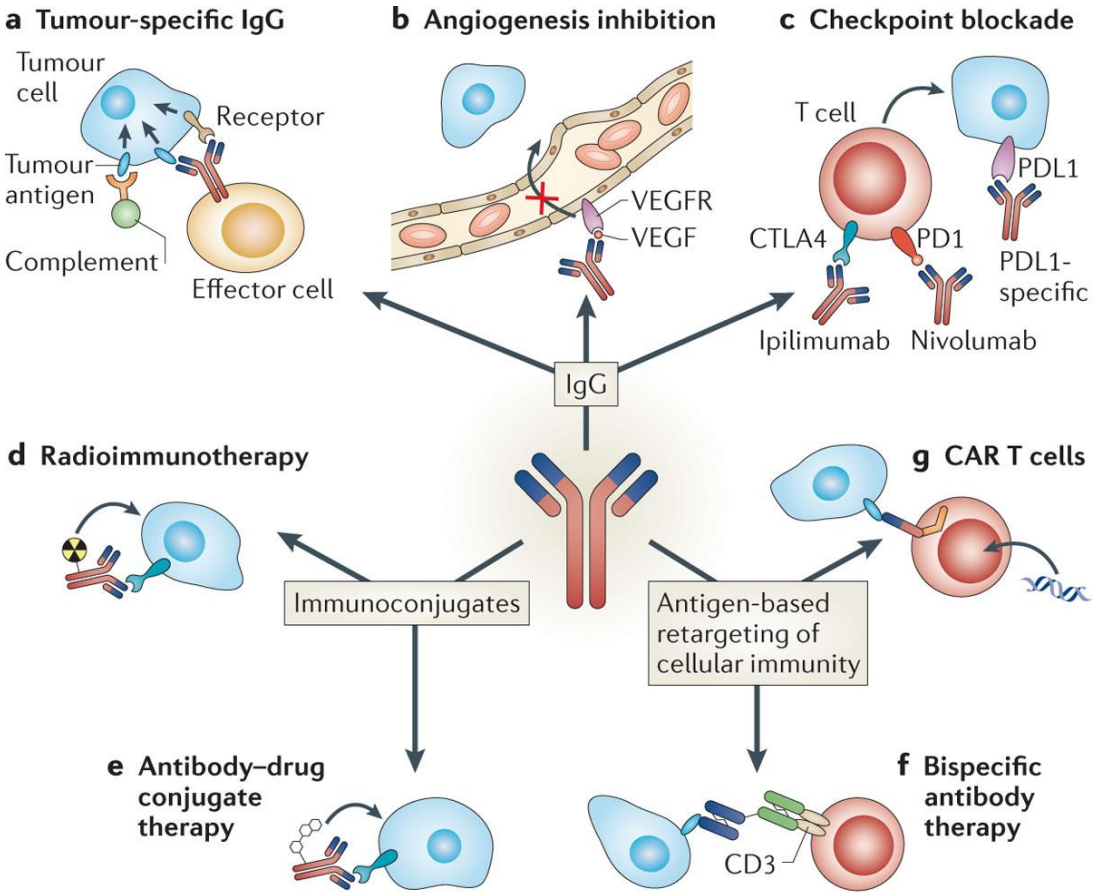

(A) Immunoglobulin G (IgG) molecules that bind to target cancer cells mediating antibody-dependent cellular cytotoxicity (ADCC), inducing complement-mediated cytotoxicity (CMC) or result in the direct signaling-induced death of cancer cells (for example, herceptin and rituximab). (B) IgG mAbs inhibiting angiogenesis (for example, bevacizumab). (C), IgG mAbs blocking inhibitory signals, thereby resulting in a stronger antitumour T cell response (for example, ipilimumab and nivolumab). (D) Radioimmunoconjugates. (E) Antibody–drug conjugates (for example, brentuximab vedotin and trastuzumab emtansine) delivering highly potent toxic drugs to the cancer cells. (F) Bispecific antibodies (for example, blinatumomab). (G) Tumor-specific T-cells with chimeric antigen receptors (CAR) are generated by a gene therapy approach in which DNA for a mAb variable region fused to signaling peptides is transferred to T cells. CD3, T cell surface glycoprotein CD3 ε-chain; CTLA4, cytotoxic T lymphocyte-associated antigen 4; PD1, programmed cell death protein 1; PDL1, PD1 ligand; VEGF, vascular endothelial growth factor; VEGFR, VEGF receptor.

Weiner GJ. Building better monoclonal antibody-based therapeutics. Nat Rev Cancer. 2015;15(6):361-70.

Figure 7. Mechanisms of action of monoclonal antibodies that target cancer cells.

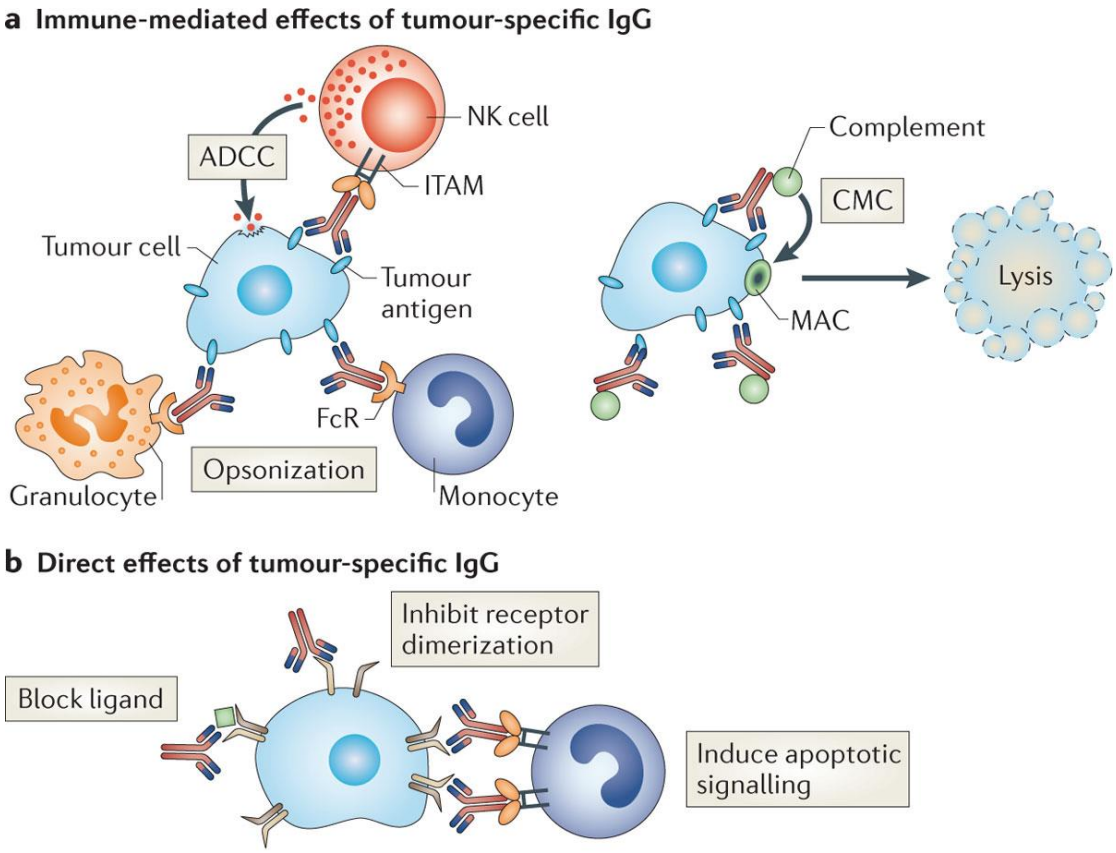

Weiner GJ. Building better monoclonal antibody-based therapeutics. Nat Rev Cancer. 2015;15(6):361-70.

Antibodies and Antibody-Drug Conjugates (ADCs)

As mentioned above, one way of enhancing the therapeutic potential of mAbs is by conjugating them to small-molecule drugs, such as the case of Brentuximab vedotin and T-DM1 (trastuzumab emtansine). These antibody-drug conjugates (ADCs) combine the efficacy of potent chemotherapeutics and the specificity from mAbs to target and destroy cancer cells without harming patient's healthy cells. However, the need to site-specifically incorporate a small-molecule drug through a linker to an antibody and produce a homogeneous mixture at a large-scale remains a major challenge in this field[19-21].

Moreover, the choice of linker is also an important consideration when designing ADCs. In general, linkers can be categorized into two groups: those that are cleavable and those that are not (Fig. 8 and 9). The decision to use a cleavable linker or a non-cleavable one is made largely based on the desired pharmacokinetic profile including the distribution and delivery of the small-molecule drug. Cleavable linkers usually contain chemical motifs such as disulfides[22, 23], hydrazones[24, 25], or peptides[26-28]. These linkages are either enzyme-sensitive or pH-sensitive within the target tissue or target cell to ensure a controlled release of potent, often cytotoxic, chemotherapeutics. After the cytotoxic payload is released, however, it can escape from the target cell and attack the neighboring cells or tissues in a process called 'bystander killing'[29]. Non-cleavable linkages such as -S-C- bonds can protect the host from such bystander killing since the small-molecule moiety stays with the antibody. In the context of clinical safety, this means non-cleavable linkers can lead to even lower side effects and wider therapeutic window. In my thesis research, we employed expressed protein ligation (EPL)[30] to connect the small molecule

ZM-241,385 (ZM), a selective antagonist of the $A_{2A}R$, via a non-cleavable linker to the immunoglobulin Fc region (Fc) as a therapeutic strategy for enhancing the immune response against cancers via immune checkpoint blockade.

Figure 8. An example of an enzyme-sensitive cleavable linker.

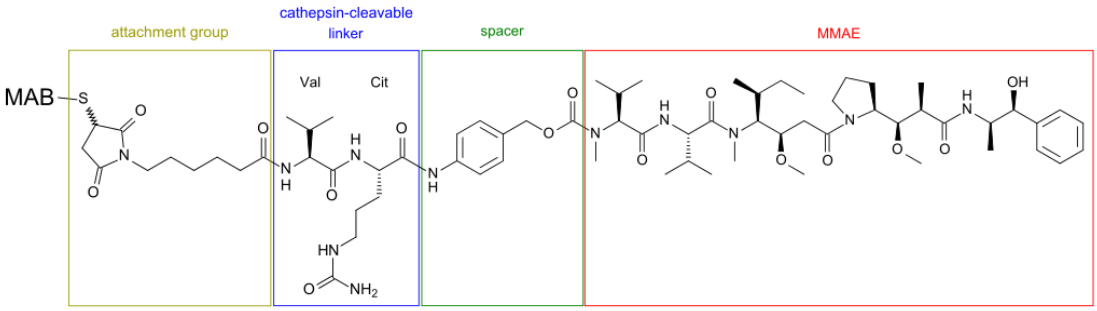

Skeletal formula of brentuximab vedotin showing an example of an enzyme-sensitive cleavable linker. 3 to 5 units of MMAE are attached to the monoclonal antibody (MAB) brentuximab via the spacer paraaminobenzoic acid (marked green), a cathepsin-cleavable linker (Cit = citrulline, Val = valine, marked blue), and an attachment group consisting of caproic acid and maleimide (marked brown).

Francisco JA, Cerveny CG, Meyer DL, et al. cAC10-vcMMAE, an anti-CD30-monomethyl auristatin E conjugate with potent and selective antitumor activity. Blood. 2003;102(4):1458-65.

Figure 9. An example of a stable, non-cleavable linker.

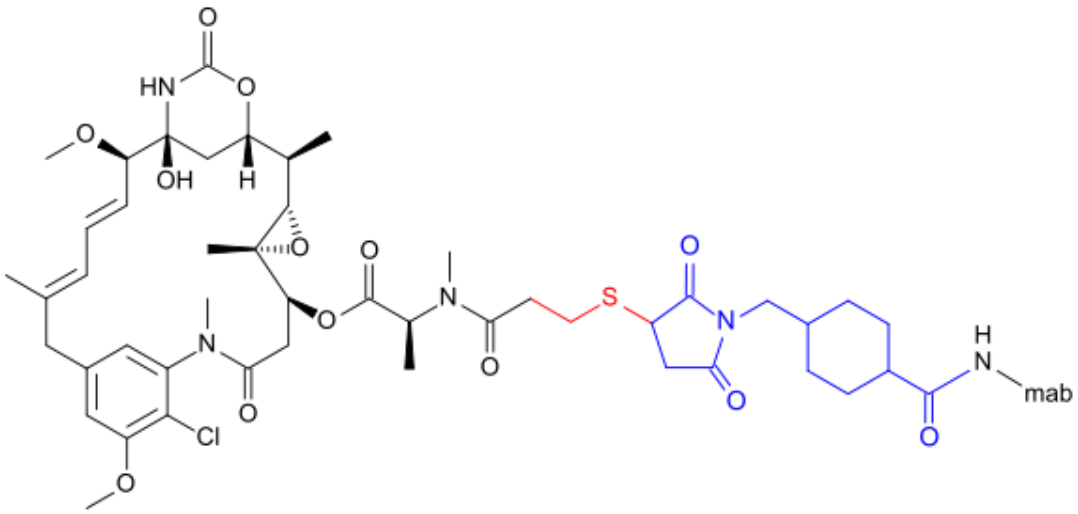

Schematic representation of trastuzumab emtansine showing an example of a stable, non-cleavable linker. The maytansine skeleton is shown in black at left. The thioether group that makes mertansine is shown in red. The linker group that makes emtansine is shown in blue at right, bound to the amino group (HN–) of a lysine residue in the trastuzumab molecule (–mab).

Lorusso PM, Weiss D, Guardino E, Girish S, Sliwkowski MX. Trastuzumab emtansine: a unique antibody-drug conjugate in development for human epidermal growth factor receptor 2-positive cancer. Clin Cancer Res. 2011;17(20):6437-47.

Immune Checkpoint Blockers

Tumor antigens are readily recognized by the immune system as foreign based on their unique and mutational profiles. However, not all interactions between the immune cells and cancer lead to destruction of the cancer cell. This phenomenon is known as immune tolerance, where the cancer cell is recognized and determined as 'self'. Immune tolerance is influenced by multiple factors, including the regulatory immune cells, anti-inflammatory cytokines, and the 'immune checkpoint' pathways. One dominant immune checkpoint pathway present in the tumor microenvironment is the programmed cell death protein 1 (PD1) and PD1 ligand 1 (PDL1) receptor–ligand pair (Fig. 10). The natural function of the PD1 pathway in maintaining immune homeostasis is exploited in many cancers. In fact, mAbs that block this pathway have demonstrated powerful clinical efficacy against unresectable metastatic melanoma and treatment-refractory metastatic non-small-cell lung cancer and renal cell carcinoma. Durable objective (partial or complete) responses range from 31 – 44% in patients with advanced melanoma[11, 13, 31-33], to 19 – 20% in patients with non-small-cell lung cancer[34-36], and 22 – 25% in patients with renal cell carcinoma[37, 38].

In addition to the PD1 pathway, there are many other receptor – ligand interactions that could be targeted as immune checkpoint pathways. For example, ipilimumab, a mAb that binds to the prototypical immune checkpoint cytotoxic T lymphocyte associated antigen 4 (CTLA4), was approved in 2011 by the FDA for advanced melanoma[7, 39]. Unlike the PD1 pathway, however, the CTLA4 immune checkpoint predominantly functions early in the immune response, during T cell priming and activation (Fig. 11).

Interestingly, a recent study in patients with advanced melanoma, a combination of anti-CTLA4 (ipilimumab) with anti-PD1 (nivolumab) mAbs showed a robust objective response rate in 53% of patients, all with tumor reduction of 80% or more[12]. Such study raises the potential for other combinational treatment regimens using immune checkpoint blockers and further highlights the need for continual identification and understanding of immune checkpoint pathways.

Figure 10. Biological importance of PD-1 signaling.

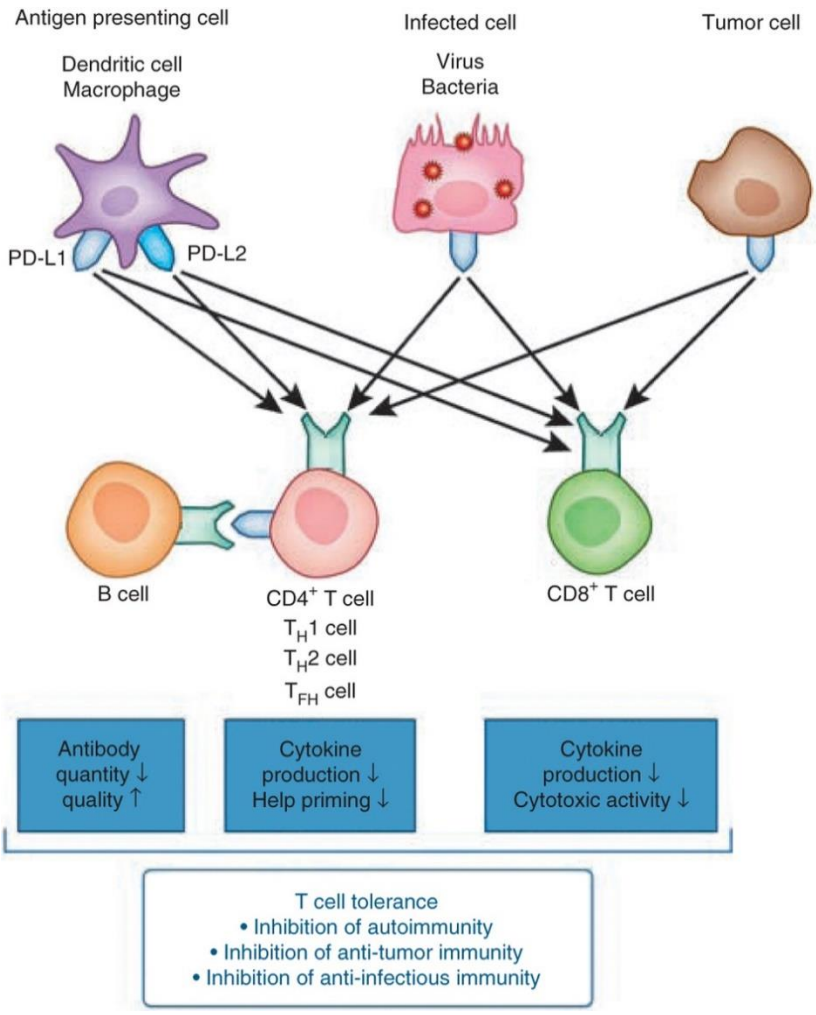

Okazaki T, Chikuma S, Iwai Y, Fagarasan S, Honjo T. A rheostat for immune responses: the unique properties of PD-1 and their advantages for clinical application. Nat Immunol. 2013;14(12):1212-8.

Figure 11. Distinct mechanisms of PD-1 and CTLA4 in immunosuppression.

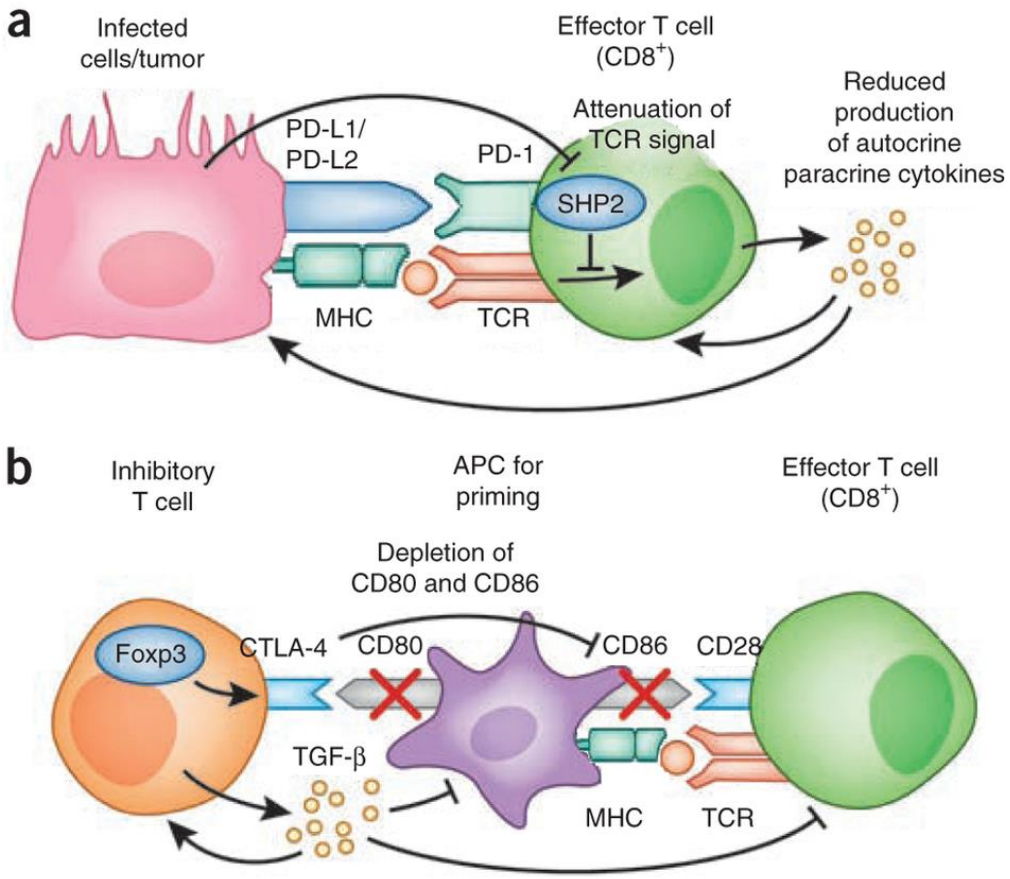

(A) PD-1 controls the effector phase of the immunity by inducing unresponsiveness through attenuating antigen-specific signals. Only CD8+ T cells are included here. MHC, major histocompatibility complex. (B) CTLA-4 controls, in particular, the function of activated CD4+ T cells that express Foxp3. CTLA-4 dominantly captures CD80 and CD86 on antigen-presenting cell (APC) and down-modulates the costimulatory activity of CD28 on effector T cells. TGF-β1, an important cytokine produced by Foxp3+ T cells, supports the growth and differentiation of Foxp3+ T cells and suppresses diverse immune responses.

Okazaki T, Chikuma S, Iwai Y, Fagarasan S, Honjo T. A rheostat for immune responses: the unique properties of PD-1 and their advantages for clinical application. Nat Immunol. 2013;14(12):1212-8.

Immunology of Adenosine and the Adenosine Receptors

Adenosine is a purine nucleoside known to affect the immune system[40]. The accumulation of adenosine is anti-inflammatory and leads to the inhibition of T cell activation and expansion[41, 42]. This normally acts as a feedback system to protect the host tissue from damage by auto-immune responses or over-inflammation[43]. However, high levels of adenosine are also found within the tumor microenvironment due to hypoxia[44] and inflammation which promote the generation and inhibit the degradation of adenosine[45]. This provides tumors a way to dampen the response and evade destruction by the immune system (Fig. 12). Fortunately, at the same time, it also provides a potential route for pharmacologic intervention and a platform for new cancer immunotherapeutic development.

The adenosine receptors (ARs) are G protein-coupled receptors (GPCRs) that can be found in four different subtypes, designated A_1, A_{2A}, A_{2B}, and A_3. They are expressed throughout the heart, the brain, and the immune system including lymphocytes, macrophages, and NK cells. Of the four subtypes of adenosine receptors, $A_{2A}R$ is the predominantly expressed subtype in most immune cells (Fig. 13)[46]. In particular, $A_{2A}R$ have been found to down-regulate activated immune cells upon activation by an agonist[47, 48]. In the context of cancer, this down-regulation translates to the inhibition of NK cell cytotoxicity and tumor-specific CD4 and CD8 cell activity[49, 50]. Surprisingly, even after the removal of $A_{2A}R$ agonists, the effector function of T cells remains impaired [48, 51], suggesting that the adenosine-rich environment in tumors may induce T cells that are

anergic to the tumor cells. Consistent with this change, $A_{2A}R$ stimulation induces immunoregulatory molecules such as CTLA-4 and PD-1 on T cells [52-54].

Besides the T cells, antigen-presenting cells (APCs) are also affected by adenosine. Studies have found $A_{2A}R$ agonists to suppress IL-12 and induce IL-10 production from APCs, discouraging cellular immune response[55, 56]. Furthermore, T cell activation in the presence of $A_{2A}R$ stimulation markedly increases $CD4^+$ $FoxP3^+$ cells[53, 57-59]. FoxP3, a key transcriptional factor for the immunosuppressive activity of Treg cells, was also found to be inducible upon $A_{2A}R$ stimulation[48]. Overall, $A_{2A}R$ antagonists, like the checkpoint blocker anti-PD-1, presents promising potential in preventing tolerance and anergy during the immune response against cancer (Fig. 14). Furthermore, $A_{2A}R$ antagonists could also be combined with other current and developing immunotherapies to achieve enhanced efficacy[60, 61].

Figure 12. Adenosine pathway in the tumor microenvironment.

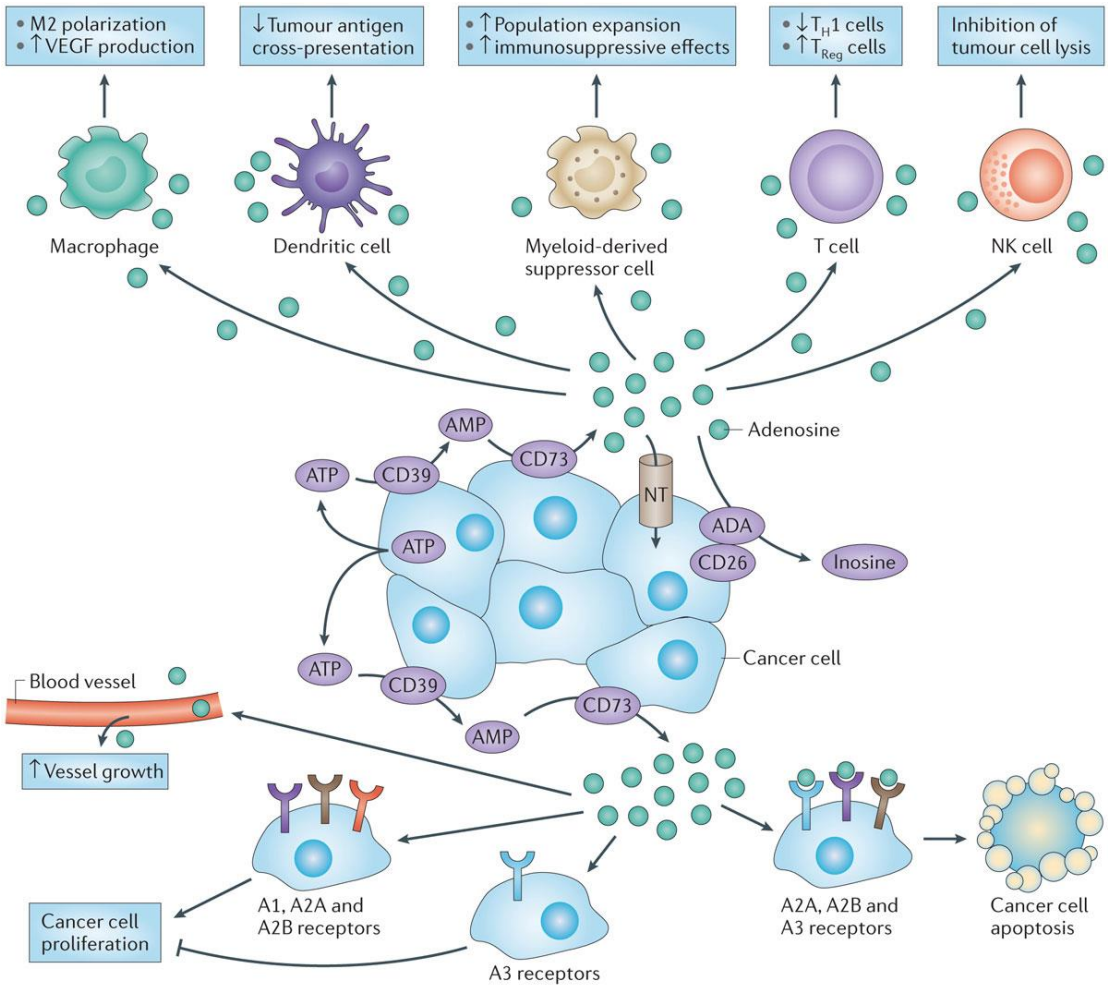

Antonioli L, Blandizzi C, Pacher P, Haskó G. Immunity, inflammation and cancer: a leading role for adenosine. Nat Rev Cancer. 2013;13(12):842-57.

Figure 13. Summary of the Distribution of Adenosine Receptors.

Data where there is correspondence between mRNA distribution and receptor distribution are given in bold. Data based mainly or exclusively on distribution of mRNA are given in ordinary letters. Ambiguous data (including major species differences) are given in italics.

A_1 Receptor	A_{2A} Receptor	A_{2B} Receptor	A_3 Receptor
High expression **Brain (cortex, cerebellum, hippocampus). Dorsal horn of spinal cord. Eye, adrenal gland, atria**	**High expression** **Spleen, thymus, leukocytes (both lymphocytes and granulocytes), blood platelets. Striatopallidal GABAergic neurons (in caudate-putamen, nucleus accumbens, tuberculum olfactorium), olfactory bulb**	**High expression** Cecum, colon, bladder	**High expression** *Testis (rat), mast cells (rat)*
Intermediate levels **Other brain regions. Skeletal muscle, liver, kidney, adipose tissue, salivary glands, esophagus, colon, antrum, testis**	**Intermediate levels** Heart, lung, blood vessels	**Intermediate levels** Lung, blood vessels, eye, median eminence, *mast cells*	**Intermediate levels** *Cerebellum (human?), hippocampus (human?), lung, spleen (sheep),* pineal
Low levels **Lung (but probably higher in bronchi), pancreas**	**Low levels** **Other brain regions**	**Low levels** Adipose tissue, adrenal gland, brain, kidney, liver, ovary, pituitary gland	**Low levels** Thyroid, most of brain, adrenal gland, *spleen (human)*, liver, kidney, heart, intestine, *testis (human)*

Fredholm BB, Ijzerman AP, Jacobson KA, Klotz KN, Linden J. International Union of Pharmacology. XXV. Nomenclature and classification of adenosine receptors. Pharmacol Rev. 2001;53(4):527-52.

Figure 14. Pro-Cancer Activities of Extracellular Adenosine and Therapeutic Targets for Cancer Immunotherapy.

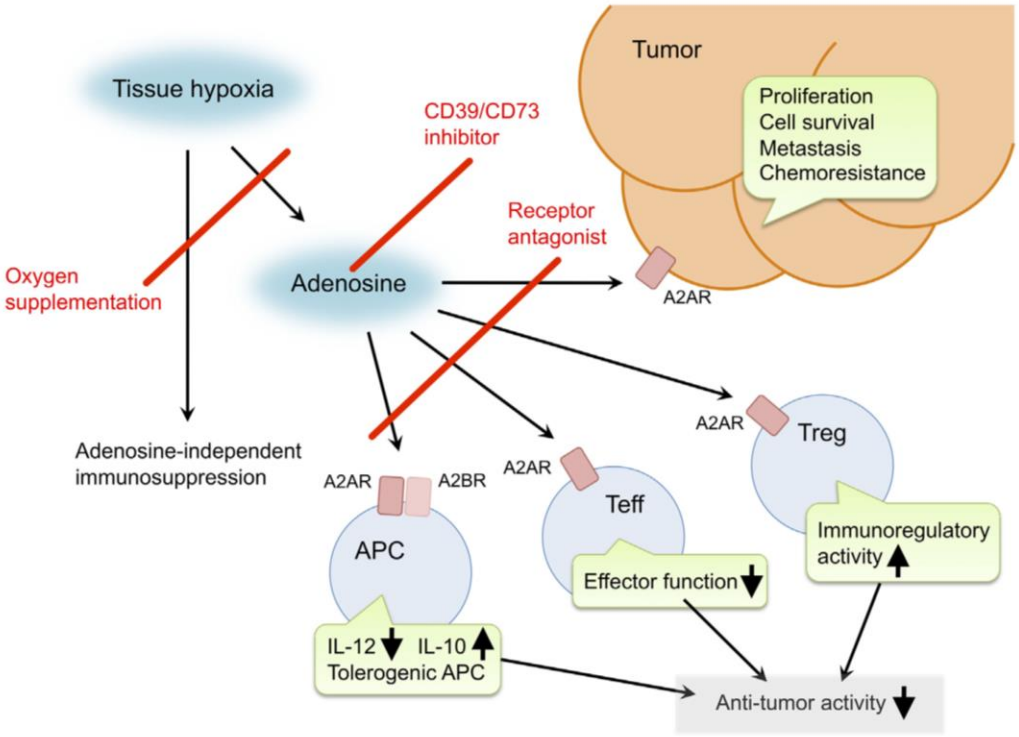

Tissue hypoxia in tumors increases extracellular adenosine production through induction of CD39 and CD73. Produced adenosine transmits immunosuppressive signals through adenosine receptors on various immune cells. Potential target molecules in include the adenosine receptors (A2AR and A2BR) and adenosine producing enzymes (CD39 and CD73). Oxygen supplementation can also decrease pro-cancer effects of the adenosine pathway.

Ohta A. A Metabolic Immune Checkpoint: Adenosine in Tumor Microenvironment. Front Immunol. 2016;7:109.

Chapter 2:

Generation of the Protein-Small Molecule Conjugate Fc-ZM

Introduction

Agonist and Antagonist of the Adenosine 2A Receptor

As discussed in Chapter 1, adenosine receptors have distinct distributions in the human body, and therefore control different functions. The A_{2A} receptor, in particular, is important in mediating vasodilation[62], supporting the synthesis of new blood vessels[63] and protecting tissues from excessive inflammatory damage. Numerous pharmacologic candidates that target the $A_{2A}R$ have been developed for this reason. Notably, a selective A_{2A} adenosine receptor agonist, Regadenoson, was approved by the FDA in 2008 for coronary vasodilation during cardiac nuclear stress tests. Many other agonists and antagonists are also currently undergoing clinical trials, validating the therapeutic potential of $A_{2A}R$ modulation.

Early attempts in the development of $A_{2A}R$ agonists found that the adenosine scaffold and its stereochemistry was critically important and must be conserved as a structural basis for agonist design. Therefore, most of the modifications were centered around the N6 of the 2-position of the purine and at the 5'-position of the ribose, with the goal to achieve better metabolic stability compared to the natural ligand, adenosine[64]. One of the molecules that culminated from these studies was CGS21680, a moderately $A_{2A}R$ selective agonist that displays binding affinities of 27 and 19 nM at the human and

rat $A_{2A}R$, respectively (Fig. 15)[65, 66]. The $A_{2A}R$ binding of CGS21680 is 10-fold selective against A_1R and has a similar potency on A_3R (hA_3 K_i = 67 nM), whereas it is highly selective against $A_{2B}R$ (hA_{2B} K_i > 10 000 nM). However, like most adenosine-based ligands, CGS21680 exhibited poor oral bioavailability and short *in vivo* half-lives due to the presence of three hydrogen bond donors in the ribose which are critical for $A_{2A}R$ activation but are subject to extensive metabolism. Later research focused on improving the pharmacokinetic and $A_{2A}R$ selectivity profiles, which led to the successful invention of Regadenoson (Fig. 16). Interesting, Regadenoson has a 2 to 3 min biological half-life, as compared with adenosine's 10-second half-life.

Unlike the agonists, antagonists of the $A_{2A}R$ lack the ribose moiety and are usually made up of mono-, bi-, or tricyclic structures that mimic the adenine part of adenosine. They are classified as xanthines and non-xanthines. Examples of xanthines include caffeine and theophylline, which are natural non-selective AR antagonists. However, due to the poor water solubility and instability associated with xanthine derivatives, scientists began to search for new classes of $A_{2A}R$ antagonists in the late 1980s. As part of this search. the Zeneca group developed ZM-241,385 (Fig. 17)[67], a potent bicyclic non-xanthine antagonist (hA_{2A} K_i = 0.8 nM) that is selective over the A_1 and A_3 receptors (hA_1 K_i = 255 nM, hA_3 K_i > 10 000 nM) although also potent at the A_{2B} AR (hA_{2B} K_i = 50 nM) (Fig. 18)[64]. In animal models, ZM has been shown to protect against beta amyloid neurotoxicity[68] and enhance L-DOPA derived dopamine release[69], and therefore was thought to be useful in the treatment of Alzheimer's disease and Parkinson's disease.

Due to its potency and selectivity against the $A_{2A}R$, we selected ZM as our candidate for the development of a novel immune checkpoint blocker. However, since ZM was originally developed for the treatment of Parkinson's disease, there are a number of design considerations when repurposing it for immune enhancement. First and foremost, ZM was found to have a short pharmacokinetic half-life (less than 20 min in cats), whether administered orally or intravenously[70, 71], with no detectable levels present in the plasma 4 h after oral administration. In a study in anaesthetized dogs, an apparent loss of cardiovascular activity was observed after 2 h following an intravenous administration[72]. Secondly, in addition to expression in T lymphocytes, $A_{2A}R$ is also abundant in the brain and heart and thus high doses of ZM could result in neuro- or cardio-toxicity. We hypothesized that by attaching ZM to Fc, the resulting conjugate Fc-ZM could overcome these obstacles as an enhanced immune checkpoint blocker.

Figure 15. Examples of adenosine A2A receptor agonists.

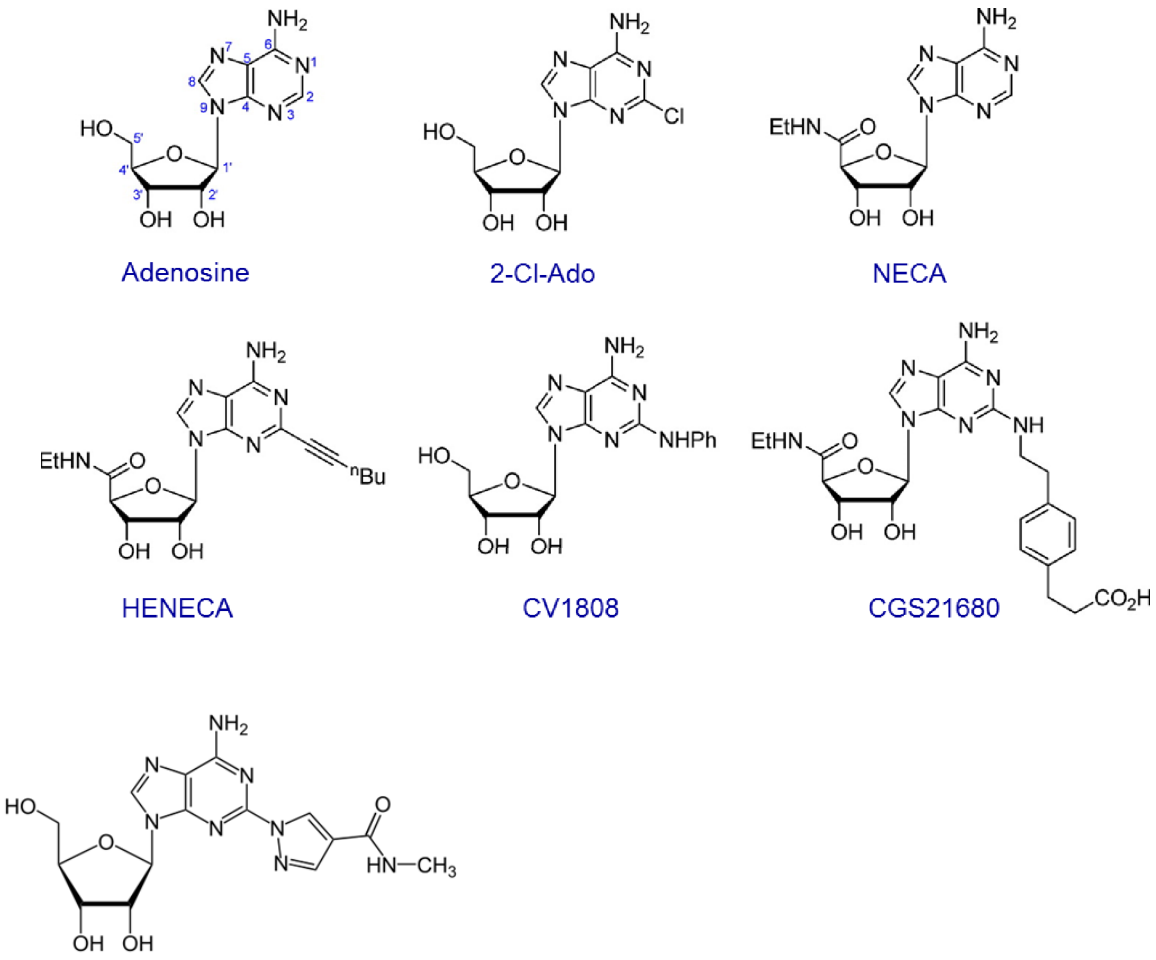

De lera ruiz M, Lim YH, Zheng J. Adenosine A2A receptor as a drug discovery target. J Med Chem. 2014;57(9):3623-50.

Figure 16. Affinities of A2AR Agonists in Binding and Functional Assays at A1, A2A, A2B, and A3 Adenosine Receptors.

Agonist	A_{2A} K_i (nM)	A_{2B} EC_{50} (nM)	A_1 K_i (nM)[a]	A_3 K_i (nM)
adenosine	700	24000	310	290
2-Cl-Ado	180	ND	1.39	19
NECA	20	330	14	6.2
HENECA	6.4	6100	60	2.4
CV1808	100 (r)	ND	400 (r)	ND
CGS21680	27	361000	290	67
binodenoson (WRC0470)	270	>100000	48000	903
apadenoson (ATL146e)	0.5	ND	77	45
regadenoson (CVT3146)	290	10000	3770	10000
GW328267	46	1300	369	92
UK432097	4	ND	ND	ND
sonedenoson (MRE0094)	490	10000	10000	ND
25	167	ND	107 (r)	92

De lera ruiz M, Lim YH, Zheng J. Adenosine A2A receptor as a drug discovery target. J Med Chem. 2014;57(9):3623-50.

Figure 17. Examples of adenosine A2A receptor antagonists.

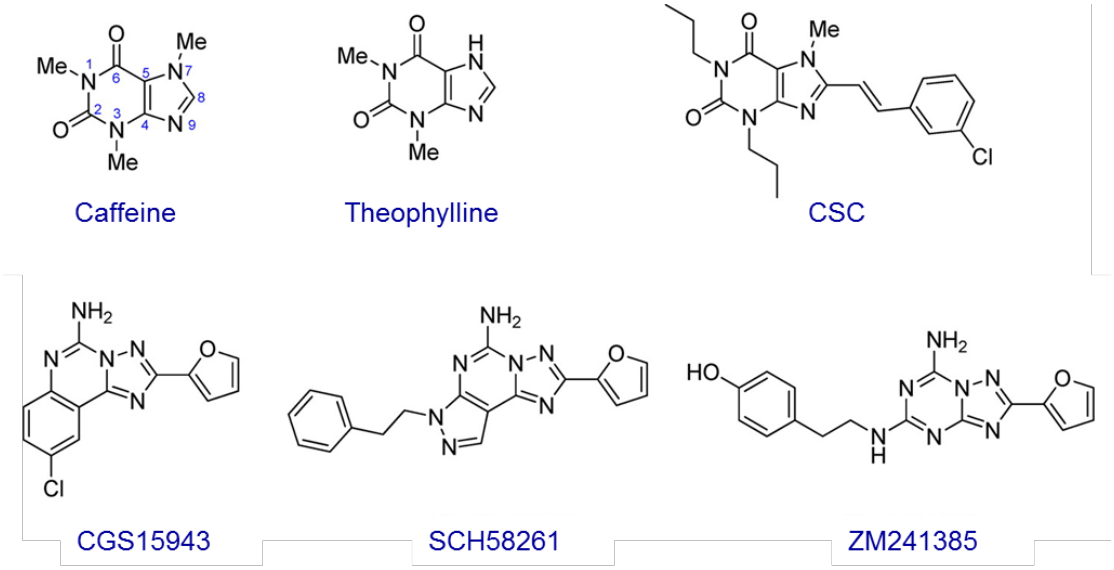

De lera ruiz M, Lim YH, Zheng J. Adenosine A2A receptor as a drug discovery target. J Med Chem. 2014;57(9):3623-50.

Figure 18. Affinities of A2AR Antagonists in Binding and Functional Assays at A1, A2A, A2B, and A3 Adenosine Receptors.

Antagonists	A_{2A} K_i (nM)	A_{2B} K_i (nM)	A_1 K_i (nM)	A_3 K_i (nM)
caffeine	23400	20500	44900	>100000 (r)
theofylline	25000 (r)	ND	8500 (r)	ND
CSC	54 (r)	ND	28000 (r)	>10000 (r)
MSX-2	5, 8 (r)	2900	2500, 900 (r)	>10000 (r)
istradefylline	36, 12	1800	2830, 9600	>3000
CGS15943	0.4, 1.2 (r)	44	3.5, 6 (r)	95
SCH58261	1.1	1110	549	1200
ZM241385	0.8	50	255	>10000

De lera ruiz M, Lim YH, Zheng J. Adenosine A2A receptor as a drug discovery target. J Med Chem. 2014;57(9):3623-50.

Structure of Adenosine 2A Receptor and Binding of ZM-241,385

The adenosine receptors display the topology typical of GPCRs, with a central core consisting of seven transmembrane helices. At the amino acid level, the human A_{2A} AR shares 49% sequence identity with human A_1 AR, 58% with human A_{2B} AR, and only 41% with the human A_3 AR. Considering residues responsible for the ligand binding, however, the average sequence identity is 71%, indicating high degrees of conservation. In 2008, Jaakola et al. published the crystal structure of A_{2A}R bound to ZM[73], and three years after, crystal structures of the A_{2A}R bound to the agonists adenosine and 5'-*N*-ethylcarboxamidoadenosine (NECA) were resolved[74]. Binding interactions of the A_{2A}R with adenosine and ZM are illustrated in Figure 19.

As shown in Figure 20, the bicyclic triazolotriazine core of ZM is anchored by an aromatic stacking interaction with Phe168 and an aliphatic hydrophobic interaction with Ile274. Analysis of the shape of the binding pocket shows that it consists of a deep, planar, and narrow cavity[75]. Importantly, the phenolic hydroxyl group extending from the ethylamine chain forms a hydrogen bond with an ordered water molecule towards the solvent-exposed extracellular regions, while the phenyl ring forms hydrophobic interactions with Leu267 and Met270. Additionally, affinity to the A_{2A}R was found to be unaffected when the phenylmethylene group is replaced by a cycloalkyl substituent[76], demonstrating a high degree of substituent flexibility in this area of the pharmacophore. For this reason, we chose the phenolic hydroxyl group as our point of attachment for the linker and the Fc protein.

Figure 19. Crystal Structure: Binding Pocket of Adenosine 2A Receptor.

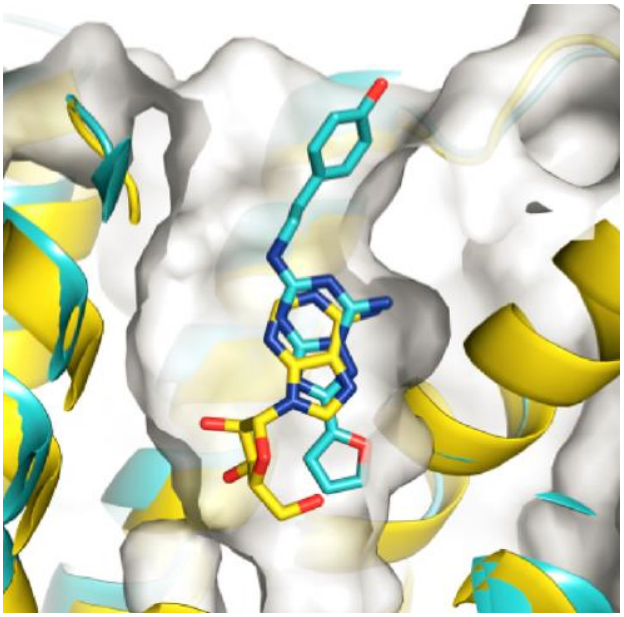

Overlap between the crystal structures solved with the agonist adenosine (yellow) and the antagonist ZM241385 (cyan).

De lera ruiz M, Lim YH, Zheng J. Adenosine A2A receptor as a drug discovery target. J Med Chem. 2014;57(9):3623-50.

Figure 20. Binding interactions at the adenosine A2A receptor by antagonist ZM241385.

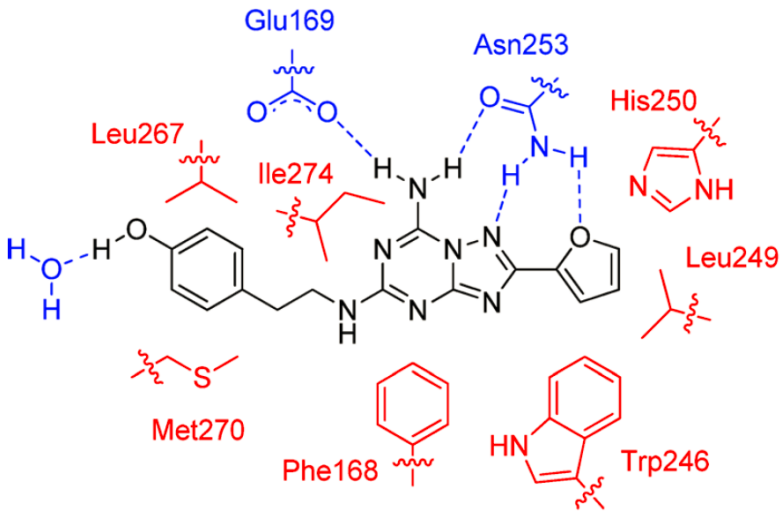

De lera ruiz M, Lim YH, Zheng J. Adenosine A2A receptor as a drug discovery target. J Med Chem. 2014;57(9):3623-50.

Fc-Fusion Protein Therapeutics

Many of the biological and pharmacological properties of mAbs can be found in the immunoglobulin (Ig) constant region Fc domain. In fact, fusing Fc to other molecules have shown to dramatically increase the *in vivo* half-life, as seen in the case of the anti-TNFα drug etanercept. This increase in half-life could be attributed to the slower renal clearance for macromolecules as well as recycling through the neonatal Fc receptor (FcRn)[77]. Indeed, in a review published by Levin et al., the authors reported a correlation between the *in vivo* half-lives of Fc-fusion drugs and therapeutic mAbs and their FcRn-binding affinities (Fig. 21)[78]. In addition to the improved serum half-life, Fc fusion has also shown to enhance other properties such as stability and solubility. In the case of ZM, the attachment of Fc could further prevent it from liver metabolism, additionally contributing to prolonged therapeutic activity. Moreover, Fc-ZM may show enhanced localization to tumors and other inflamed tissue sites given the presence of Fc receptors on antigen presenting cells and the enhanced permeability and retention effect[79] in the surrounding vasculature. From an industrial perspective, the use of Fc can be advantageous for the manufacturing process, as the production and purification processes offer the opportunity to be simpler than mAbs and ADCs.

One common but important concern in the development of biologics is immunogenicity. For Fc-fusion therapeutics, additional consideration is needed due to the immunological consequences resulting from interactions between the Fc domain and its canonical receptors. In addition to binding the FcRn, the Fc of IgG molecules also interacts

with various FcγRs and has critical biological effector functions like activating complement, mediating phagocytosis, and antibody-dependent cell-mediated cytotoxicity. Whether an interaction leads to an activating or inhibitory immune response depends on the specific motif associated with the receptor[80]. The activating receptors contain or associate with the immunoreceptor tyrosine-based activation motif (ITAM) as part of their intracytoplasmic structure, whereas the only inhibitory receptor in both humans and mice, namely FcγRIIB, has an immunoreceptor tyrosine-based inhibition motif (ITIM). Furthermore, the IgG receptors also vary in their binding affinities to each IgG subclass (1, 2, 3, and 4 in humans and 1, 2a, 2b, and 3 in mice) as shown in Figures 22 and 23. In our studies, we chose the Fc domain of mouse IgG3 for its low affinity to essentially all IgG receptors except FcRn.

Lastly, it is worth noting that furthering the understanding of the biology in Fc–FcR interactions would be helpful in assessing the risks associated with this class of therapies as more engineered protein therapeutics that incorporate the Fc moiety enters the drug development pipeline. More importantly, this knowledge can be used to improve the pharmacologic profiles of the drugs based on the clinical needs of individual diseases. For example, Fc from the IgA molecule can be used to target conditions involving the mucosa and Fc from the IgE molecule targeting the IgE FcR (FcεR) can inhibit allergic responses[81-83].

Figure 21. Properties of the Fc fragment of fusion-protein drugs compared with therapeutic mAbs and human IgG1.

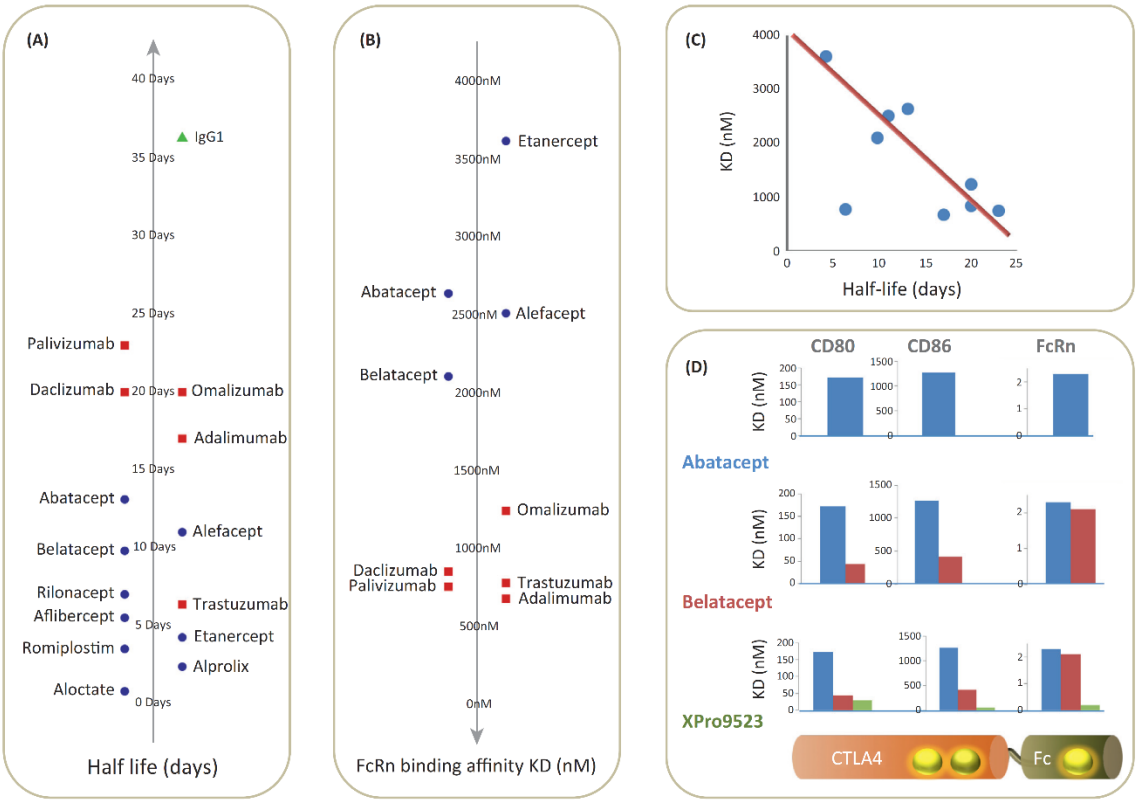

(A) Comparison of the half-life of Fc-fusion drugs (blue circles), therapeutic mAbs (red squares), and IgG1 (green triangle). (B) FcRn-binding affinities (nM) of Fc-fusion drugs (blue circles) and therapeutic mAbs (red squares). (C) Correlation between half-life and FcRn-binding affinities of Fc-fusion drugs and therapeutic mAbs. (D) Binding affinities for therapeutic targets (CD80, CD86) and FcRn are depicted for three generations of CTLA-4–Fc-fusion drugs. The active moiety CTLA-4 (orange cylinder) and Fc (green cylinder) were both engineered. Abatacept is the parent molecule and affinities are depicted as blue bars. The CTLA-4 domain was engineered in the second-generation belatacept, resulting in increased binding affinity for CD80 and CD86 but with no effect on affinity for FcRn (red bars). In the third-generation XPro9523, both the CTLA-4 and Fc domains were engineered, resulting in increased affinity for CD80, CD86, and FcRn (green bars).

Levin D, Golding B, Strome SE, Sauna ZE. Fc fusion as a platform technology: potential for modulating immunogenicity. Trends Biotechnol. 2015;33(1):27-34.

Figure 22. Human IgG receptors.

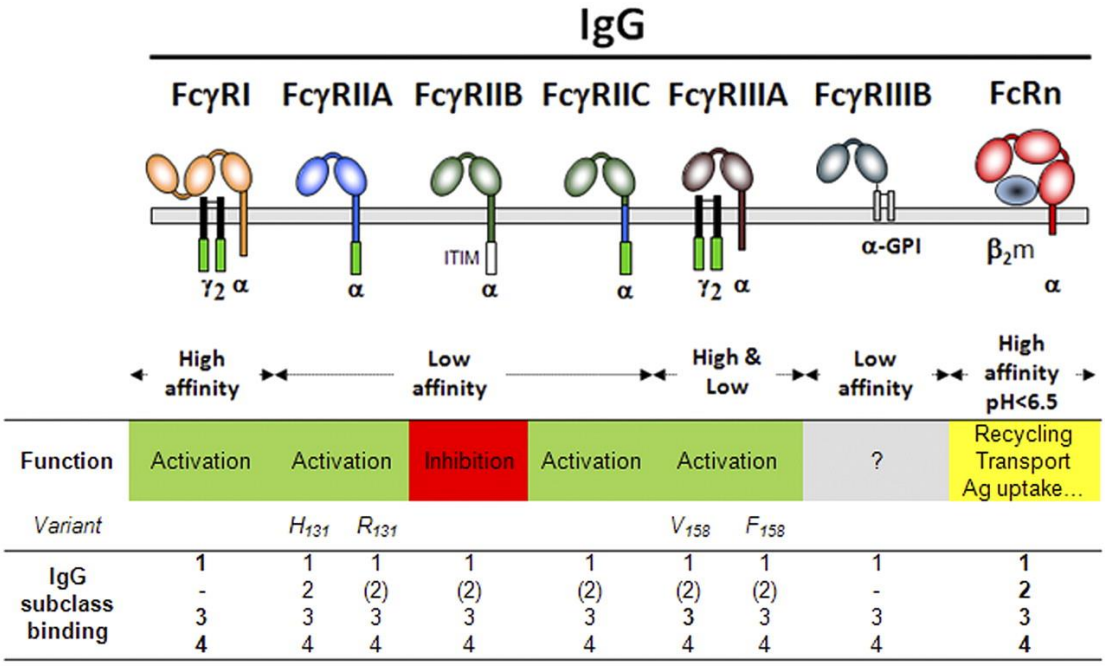

Function	Activation	Activation		Inhibition	Activation	Activation		?	Recycling Transport Ag uptake…
Variant		H_{131}	R_{131}			V_{158}	F_{158}		
IgG subclass binding	**1**	1	1	1	1	1	1	1	**1**
	-	2	(2)	(2)	(2)	(2)	(2)	-	**2**
	3	3	3	3	3	3	3	3	3
	4	4	4	4	4	4	4	4	**4**

Schematic representation of human IgG receptors at the cell membrane (gray bar) and their association or not to the FcRγ-chain dimer (black). Green boxes represent ITAMs; and the white box, the ITIM. Binding of a human IgG subclass is indicated in bold (high affinity), plain (low affinity), or between parentheses (very low affinity). - indicates no binding.

Bruhns P. Properties of mouse and human IgG receptors and their contribution to disease models. Blood. 2012;119(24):5640-9.

Figure 23. Mouse IgG receptors.

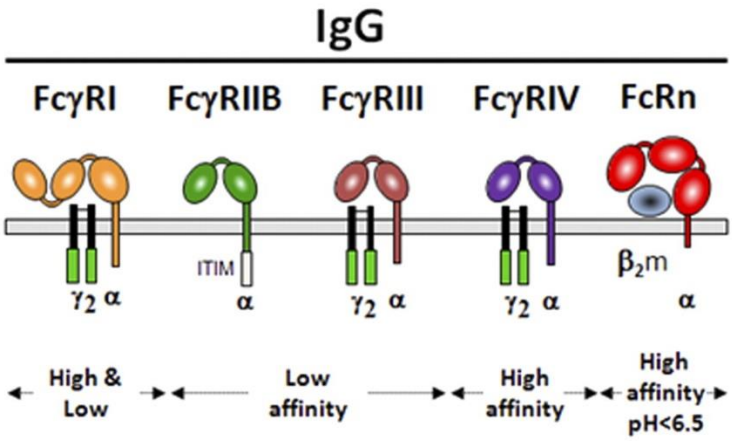

Function	Activation	Inhibition	Activation	Activation	Recycling Transport Ag uptake
IgG subclass binding	- **2a** 2b (3)	1 2a 2b -	1 2a 2b -	- **2a** **2b** -	**1** **2a** **2b** 3

Schematic representation of mouse IgG receptors at the cell membrane (gray bar) and their association or not to the FcRγ-chain dimer (black). Green boxes represent ITAMs; and the white box, the ITIM. Binding of a mouse IgG subclass is indicated in bold (high affinity), plain (low affinity), or between parentheses (very low affinity). - indicates no binding.

Bruhns P. Properties of mouse and human IgG receptors and their contribution to disease models. Blood. 2012;119(24):5640-9.

Expressed Protein Ligation (EPL)

Expressed protein ligation (EPL) is a technique that allows for the incorporation of an N-terminal cysteine-containing peptide to the C-terminus of a recombinant protein with a C-terminal thioester group in a precise and efficient manner[30]. For this reason, EPL is commonly used for flourophore labeling[84], isotope incorporation for NMR spectrometry[85], and generation of semi-synthetic proteins containing specific post-translational modifications of interest[86]. Here, we have employed EPL to install ZM onto the C-terminus of the truncated mouse IgG3 Fc domain.

EPL involves the action of inteins (internal protein sequences), which are protein domains that act analogously to the introns of RNA molecules[87]. Specifically, the inteins are engineered in EPL so that the self-splicing reaction is interrupted in the first step during the intramolecular *N,S*-acyl shift (Fig. 24). In this project, we designed the expression construct so that the mouse IgG3 Fc is secreted with a intein fused with a chitin binding domain (CBD) at the C-terminus. The CBD domain is used as an affinity tag for chitin bead binding. The junction between Fc and the intein is induced by the intein to form a C-terminal thioester, which is in equilibrium state with the native amide bond. This transient thioester can then react with sodium mercaptoethanesulfonate (MESNA), and then C-ZM (modified ZM with a linker containing six ethylene glycol units and a terminal Cysteine) to make Fc-ZM as the final product (Fig. 25).

Figure 24. Expressed protein ligation.

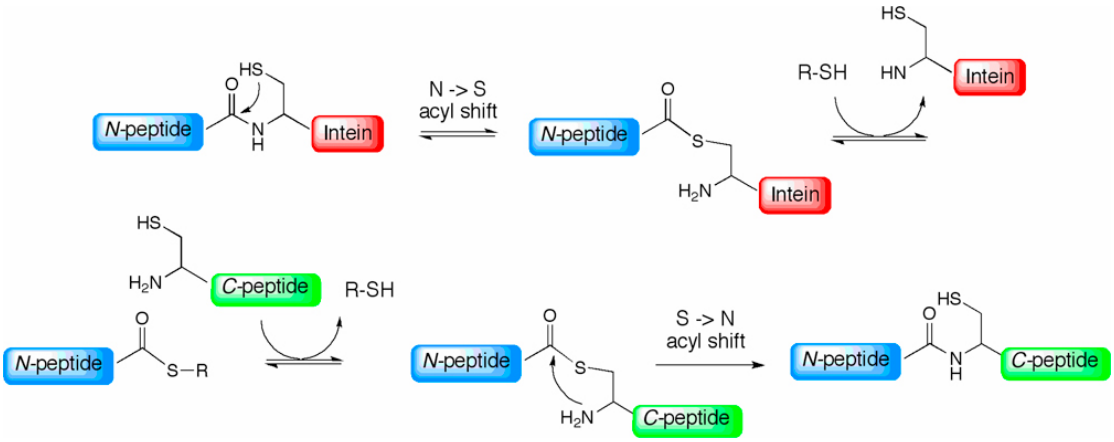

The amino-terminal peptide of the target protein is expressed in cells as a fusion protein with an intein that has been modified to eliminate the branched ligation. Thiols (R = benzyl, phenyl, alkyl, CH2CH2SO3Na) are used to cleave the intein and generate a reactive carboxy-terminal thioester. This construct is then reacted with a peptide generated by solid phase peptide synthesis that contains an amino-terminal cysteine and an unnatural amino acid(s) in the position of interest. Reaction between the two constructs results in thiotransesterification, followed by S to N acyl shift to regenerate a peptide.

Minnihan EC, Yokoyama K, Stubbe J. Unnatural amino acids: better than the real things?. F1000 Biol Rep. 2009;1:88.

Figure 25. Synthetic scheme for Fc-ZM.

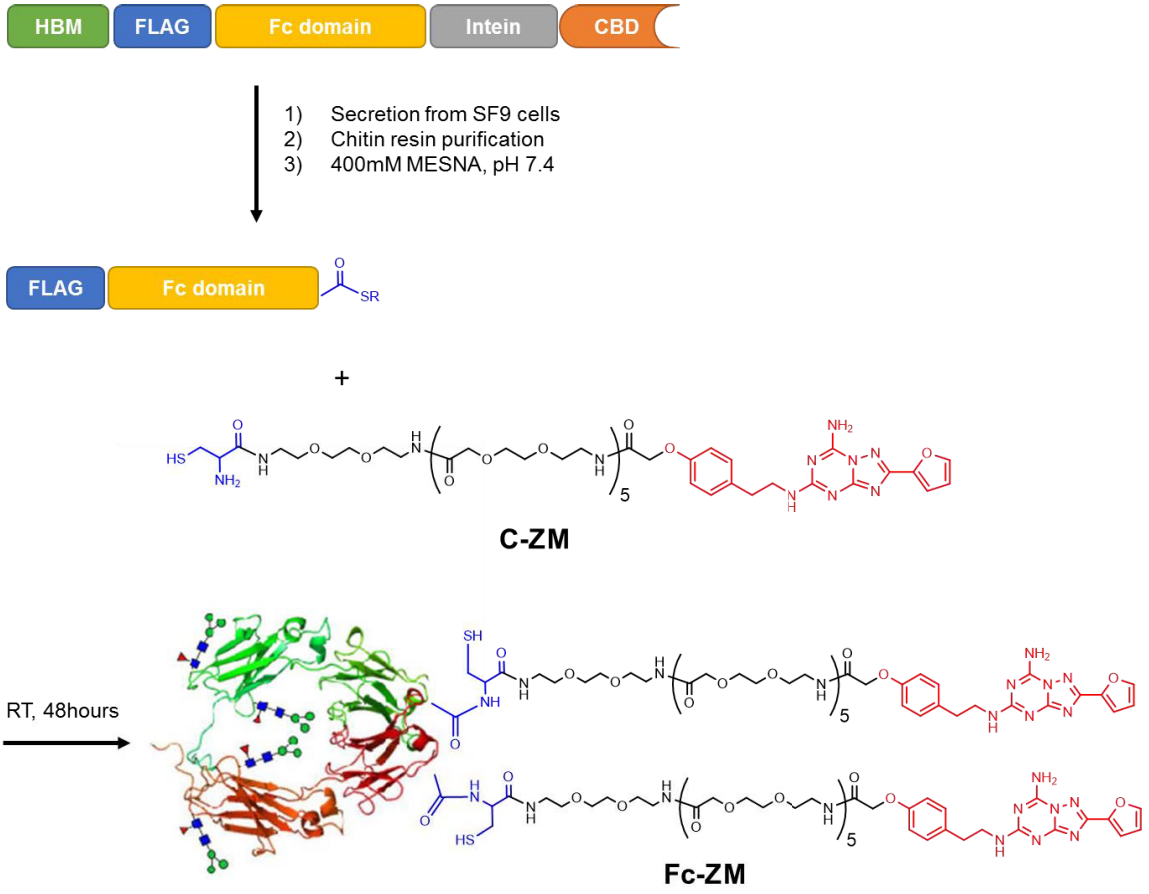

Materials and Methods

Synthesis of A-ZM.

***tert*-Butyl (*E*)-3-(4-(cyanomethyl)phenyl)acrylate (*Intermediate A*)**.

A mixture of 4-hydroxybenzyl cyanide (**1**, 5.00 g, 37.6 mmol) and powdered K_2CO_3 (12.7 g, 76.6 mmol) were dissolved in *N*,*N*-dimethylformamide (40 mL). Then, *tert*-butyl bromoacetate (7.4 mL, 50 mmol) was dissolved in *N*,*N*-dimethylformamide (10 mL) and added dropwise to the reaction at room temperature. The mixture was vigorously stirred at 40 °C for 16 h resulting in the formation of a white precipitate. The reaction was allowed to cool and then poured into water (150 mL). The organic products were extracted with dichloromethane (3 x 25 mL) and the combined organic extracts were washed with water (3 x 100 mL), brine (50 mL), dried with anhydrous sodium sulfate, filtered, and concentrated in vacuo. The crude yellow oil was purified by column chromatography (SiO_2, 10-25% EtOAc/hexanes) to yield the desired product as a slightly yellow, viscous oil (7.6 g, 81%). ^{1}H NMR (500 MHz, $CDCl_3$): δ 1.41 (s, 9H), 3.58 (s, 2H), 4.44 (s, 2H), 6.80 (d, J = 8.8 Hz, 2H), 7.15 (d, J = 8.8 Hz, 2H). ^{13}C NMR (125 MHz, $CDCl_3$): δ 22.22, 27.59, 65.19, 81.94, 114.71, 117.85, 122.53, 128.75 157.19, 167.34. ESI-LRMS: $[M+H]^+$ = *m/z* 248.2.

3-(Furan-2-yl)-1*H*-1,2,4-triazol-5-amine (3).

2-Furonitrile (**2**, 5.0 g, 0.05 mmol) was first dissolved in 3 mL of absolute ethanol and cooled to 0 °C in an ice bath. Dry hydrogen chloride gas was then bubbled into the mixture for 3 min after which diethyl ether was added to precipitate a solid intermediate.

The isolated solid was then dissolved in pyridine (30 mL) and to it was added aminoguanidine nitrate (7.4 g, 0.05 mmol). The mixture was heated to reflux for 4 h after which it was cooled to RT, filtered, and the filtrate concentrated in vacuo. The resulting crude oil was placed on ice and treated with an aqueous solution 8M HNO_3 (40 mL). The newly formed precipitate was isolated by filtration and washed with cold H_2O (10 mL) and ethanol (5 mL). The nitrate salt was suspended in near boiling H_2O (30 mL) with stirring and to it was added sodium carbonate in small portions (~1.30 g). Heating was continued until solids were completely dissolved, then the solution was allowed to cool to RT and subsequently placed on ice. The resulting precipitate was isolated by filtration, washed with H_2O (3 x 5 mL), and dried to provide the title compound as a colorless prism (**3**, 2.37 g, 29%). ^{1}H NMR (500 MHz, DMSO-d_6): δ 6.06 (s, 2H), 6.54 (s, 1H), 6.68 (s, 1H), 7.68 (s, 1H), 12.08 (s, 1H). ^{13}C NMR (125 MHz, DMSO-d_6): δ 107.53, 111.30, 142.68, 147.68, 152.15, 157.05. ESI-LRMS: $[M+H]^+$ = *m/z* 151.2.

2-(Furan-2-yl)-5-(methylthio)-[1,2,4]triazolo[1,5-*a*][1,3,5]triazin-7-amine (4).

Compound **3** (2.18 g, 14.5 mmol) and dimethyl *N*-cyanodithioiminocarbonate (2.33 g, 16.0 mmol) were placed in a round-bottomed flask fitted with a condenser under argon. The neat mixture was heated to 170 °C for 1 h with stirring being initiated after compounds began to melt. . The reaction was then cooled to RT and the resulting solid was dry loaded and chromatographed on silica (0-50% EtOAc/DCM) to yield the desired compound as a colorless solid (**4**, 1.71 g, 48%). ^{1}H NMR (500 MHz, DMSO-d_6): δ 2.51 (s, 3H), 6.71 (dd, *J* = 3.4 Hz, 1.8 Hz, 1H), 7.16 (dd, *J* = 3.4 Hz, 0.7 Hz, 1H), 7.92 (dd, *J* = 1.7 Hz, 0.8 Hz,

1H), 8.86 (br, 2H). ^{13}C NMR (125 MHz, DMSO-d_6): δ 13.60, 112.12, 112.57, 145.25, 145.52, 149.59, 156.19, 157.20, 173.35. ESI-LRMS: $[M+H]^+$ = *m/z* 249.2.

2-(Furan-2-yl)-5-(methylsulfonyl)-[1,2,4]triazolo[1,5-*a*][1,3,5]triazin-7-amine (Intermediate B).

A solution of 3-chloroperoxybenzoic acid (6.88 g, 39.7 mmol) in dichloromethane (60 mL) was added to a stirred, ice-cooled suspension of compound **4** (1.5 g, 6.1 mmol) in dichloromethane (60 mL). The resulting suspension was allowed to warm to ambient temperature and stirring was continued for 16 h. The solvent was evaporated and the resulting solid triturated in ethanol (30 mL). The suspension was then cooled on ice and the precipitate isolated by filtration to provide the desired material as a white, crystalline solid (1.4 g, 83%). ^{1}H NMR (500 MHz, DMSO-d_6): δ 3.37 (s, 3H), 6.76 (dd, *J* = 3.3 Hz, 1.7 Hz, 1H), 7.27 (d, *J* = 3.5 Hz, 1H), 7.99 (m, 1H), 9.65 (br, 2H). ^{13}C NMR (125 MHz, DMSO-d_6): δ 38.89, 112.34, 113.42, 144.97, 145.79, 152.19, 156.84, 157.32, 165.30. ESI-LRMS: $[M+H]^+$ = *m/z* 281.0.

2-(4-(2-((7-Amino-2-(furan-2-yl)-[1,2,4]triazolo[1,5-*a*][1,3,5]triazin-5-yl)amino)ethyl)phenyl)acetic acid (*A-ZM*).

Intermediate A (3.80 g, 15.4 mmol) was dissolved in 100 mL of 2-propanol in a Parr shaker together with 25 mL of 1N HCl and 1 g of the 10% Pd/C catalyst. The reaction mixture was hydrogenated at 50 psi and shaken for 6 h at room temperature. The reaction

was then filtered through a bed of Celite and the filter cake was washed with isopropanol (100 mL). The combined filtrate and wash were concentrated in vacuo and then partitioned between saturated aqueous sodium bicarbonate (50 mL) and diethyl ether (50 mL). The organic layer was isolated and the aqueous layer was further extracted with diethyl ether (30 mL). The combined organic extracts were dried with anhydrous sodium sulfate, filtered, and concentrated in vacuo to yield compound **5** as a colorless oil that was used in the next step without further purification. Compound **5** was then diluted in acetonitrile (5 mL) and slowly added to a solution of Intermediate B, also dissolved in acetonitrile (5 mL). The reaction mixture was stirred for 16 h at room temperature after which the solvent was removed in vacuo and the reaction chromatographed on silica (5% MeOH/DCM) to provide a viscous yellow oil. The oil was taken up in ethyl acetate and recrystallized to yield the penultimate ester, *tert*-butyl 2-(4-(2-((7amino-2-(furan-2-yl)-[1,2,4]triazolo[1,5-*a*][1,3,5]triazin-5-yl)amino)ethyl)phenyl)acetate, as a white solid (yield: 0.6 g, 76%). ^{1}H NMR (500 MHz, DMSO-d_6): δ 1.41 (s, 9H), 2.78 (m, 2H), 3.45 (m, 2H), 4.59 (s, 2H), 6.67 (s, 1H), 6.82 (d, J = 8.3 Hz, 2H), 7.05 (d, J = 3.1 Hz, 1H), 7.16 (d, J = 8.2 Hz, 2H), 7.46 (m, 1H), 7.86 (s, 1H), 8.28 (m, 2H). ^{13}C NMR (125 MHz, DMSO-d_6): δ 27.69, 33.87, 42.36, 65.00, 81.29, 111.61, 111.90, 114.32, 129.58, 132.11, 144.61, 146.19, 150.01, 155.80, 156.06, 159.19, 161.08, 167.96. ESI-LRMS: $[M+H]^+$ = *m/z* 452.2.

The *tert*-butyl ester (0.40 g, 0.89 mmol) was dissolved in a 3:1:1 mixture of tetrahydrofuran/methanol/water (20 mL) and to it was added lithium hydroxide (0.17 g, 7.1 mmol). The reaction was stirred at room temperature for 1 h after which it was complete as evidenced by TLC. Then, the mixture was acidified to pH 2 with 1N HCl and the

resulting precipitate was isolated by filtration and washed with water to provide the title compound as a white solid (0.28 g, 79%). ^{1}H NMR (500 MHz, DMSO-d_6): δ 2.78 (t, J = 7.5 Hz, 2H), 3.44 (m, 2H), 4.62 (s, 2H), 6.67 (dd, J = 3.3 Hz, 1.7 Hz, 1H), 6.84 (d, J = 8.6, 2H), 7.05 (dd, J = 3.5 Hz, 0.8 Hz, 1H), 7.17 (m, 2H), 7.50 (m, 1H), 7.86 (s, 1H), 8.30 (m, 2H) (Fig. 26). ^{13}C NMR (125 MHz, DMSO-d_6): δ 33.82, 42.44, 64.48, 112.01, 112.38, 114.30, 129.59, 131.94, 144.91, 145.14, 145.53, 149.94, 156.16, 158.53, 160.99, 170.26 (Fig. 27). ESI-HRMS: calcd. for $C_{18}H_{18}N_7O_4$: $[M+H]^+$ = *m/z* 396.1420, found: $[M+H]^+$ = *m/z* 396.1415 (Fig. 28).

Figure 26. 1H-NMR of A-ZM.

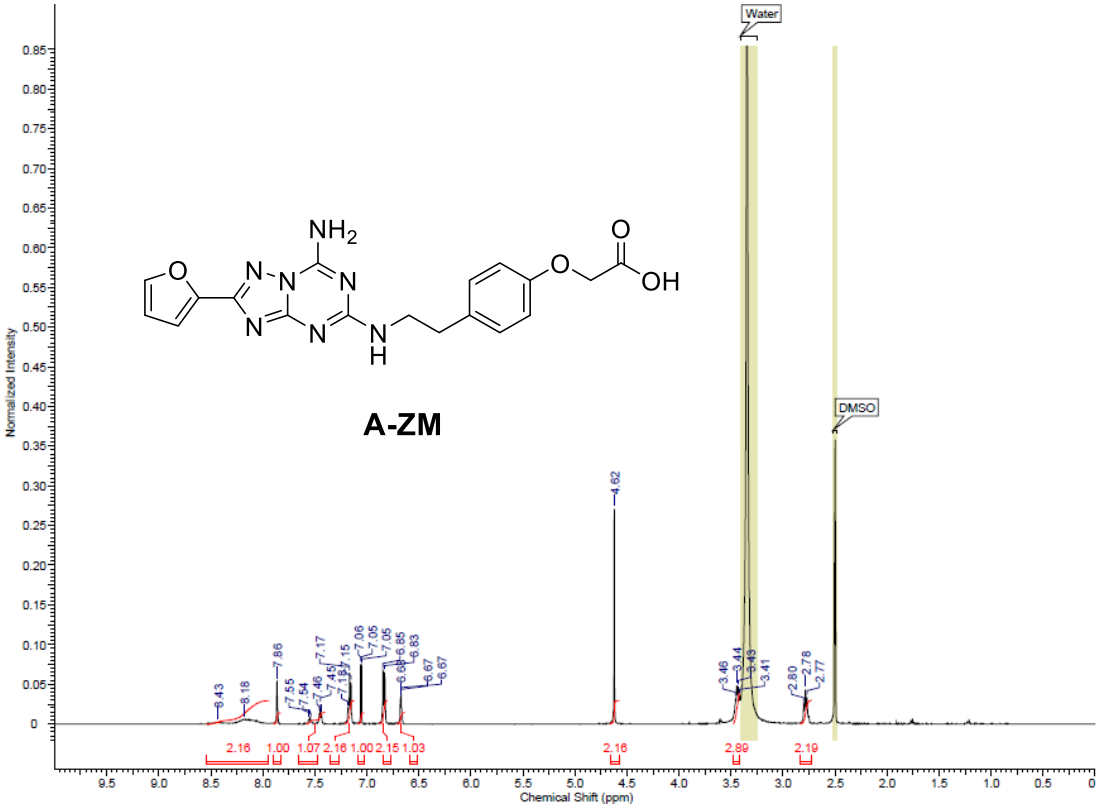

Figure 27. 13C-NMR of A-ZM.

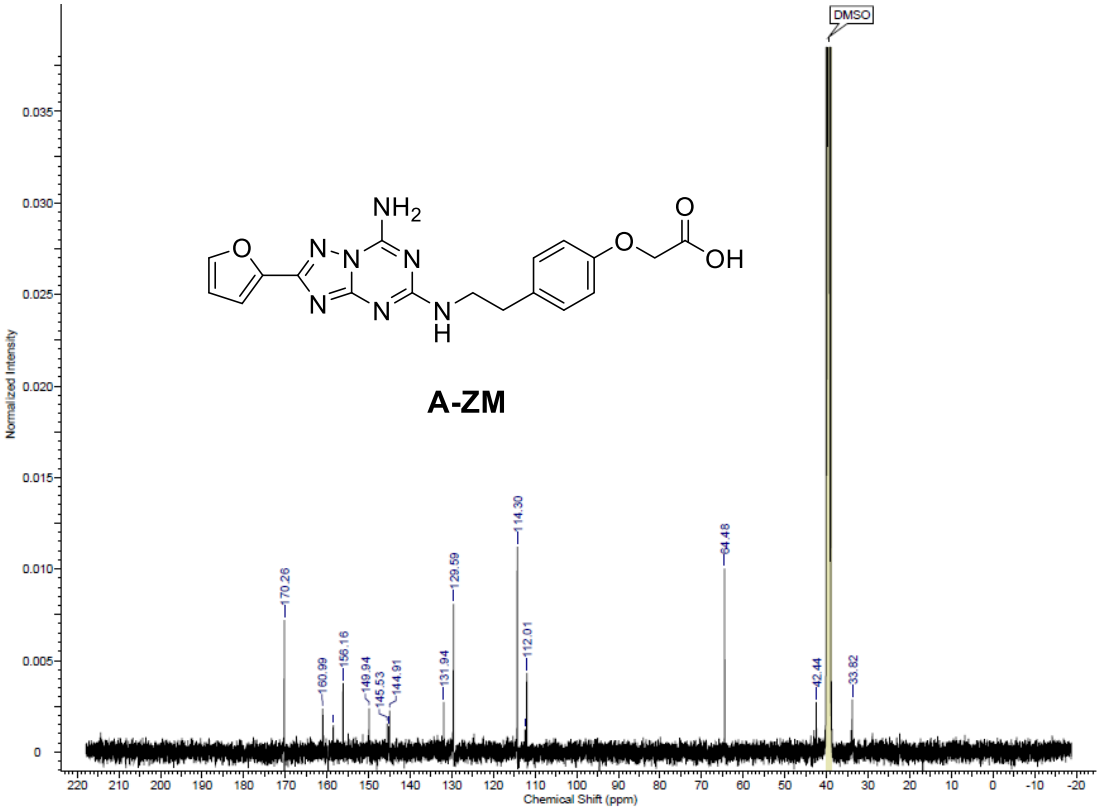

Figure 28. A-ZM High-Resolution Mass Spectrum

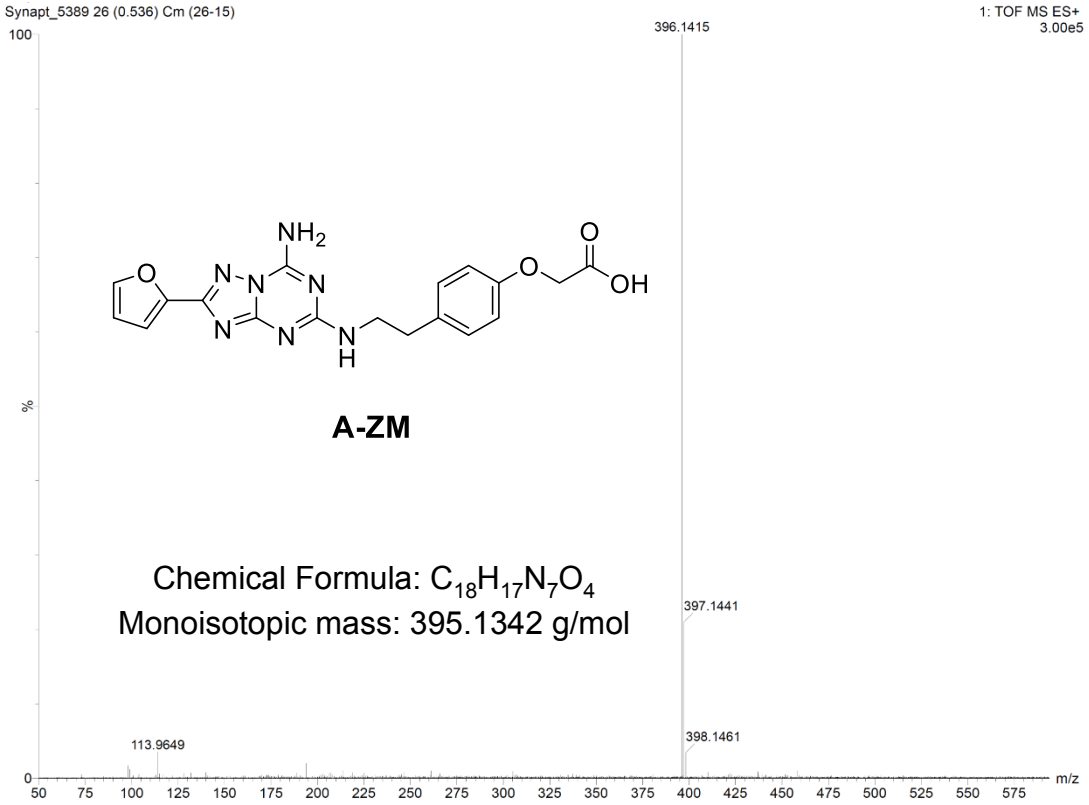

Synthesis of C-ZM.

tert-Butyl (14-amino-5-oxo-1,1,1-triphenyl-9,12-dioxa-2-thia-6-azatetra decan-4-yl) carbamate (0.20 g, 0.33 mmol), synthesized as previously described[88], was dissolved in anhydrous tetrahydrofuran (3 mL) and added to PAL resin (MidWest Bio-Tech) (0.10 g, 0.09 mmol) suspended in anhydrous THF (2 mL). Glacial acetic acid (0.10 mL) was added to this mixture and the reaction was allowed to stir at room temperature for 1 h. Then, $NaBH(OAc)_3$ (0.16 g, 0.77 mmol) was added and stirring was continued overnight. The resin was then washed with methanol (5 x 5 mL), *N*,*N*-dimethylformamide (5 x 5 mL) and dichloromethane (5 x 5 mL) in a Bio-Rad Poly-Prep Chromatography Column. The subsequent coupling reactions with Fmoc-8-amino-3,6-dioxaoctanoic acid (139 mg, 0.35 mmol each reaction) and A-ZM (17.8 mg, 0.045 mmol prepared as previously described) were based on standard solid phase peptide synthesis methodology. Coupling was carried out at room temperature for 3 h with 5% diisopropylethylamine (1.8 mL) and *O*-(Benzotriazol-1-yl)-*N,N,N',N'*-tetramethyluronium hexafluorophosphate (HBTU, 133 mg, 0.35 mmol). Fluorenylmethoxycarbonyl deprotection was carried out at room temperature for 1 h with 20% piperidine (3 mL). The solvent used for both reactions was *N*-methyl-2-pyrrolidone (NMP). The crude product was cleaved from the PAL resin with 4 mL of a 95% TFA (trifluoroacetic acid), 2.5% ddH2O and 2.5% triisopropylsilane solution at room temperature for 1 hour, dried under vacuum, resuspended in 7 mL of ddH_2O containing 0.05% TFA and then filtered through a 0.2 μm filter to remove all insoluble particles. The filtrate was further purified by reverse-phase high performance liquid chromatography (HPLC), Varian Dynamax Microsorb 100-5 C18 column (250 x 21.4 mm), gradient: 5% to 60% acetonitrile/ddH_2O over 50 min; 60%-100% acetonitrile/H_2O, 5 min, 100%

acetonitrile, 10 min; 100%-5%, 10 minutes, the flow rate was 10 mL per minute. The final purified product, C-ZM, was lyophilized and isolated as a fine brownish powder (16 mg, 13%). Compound characterization was done via analytical HPLC and electrospray ionization (ESI) mass spectrometry (Figures 29 and 30).

Figure 29. HPLC Spectrum of C-ZM.

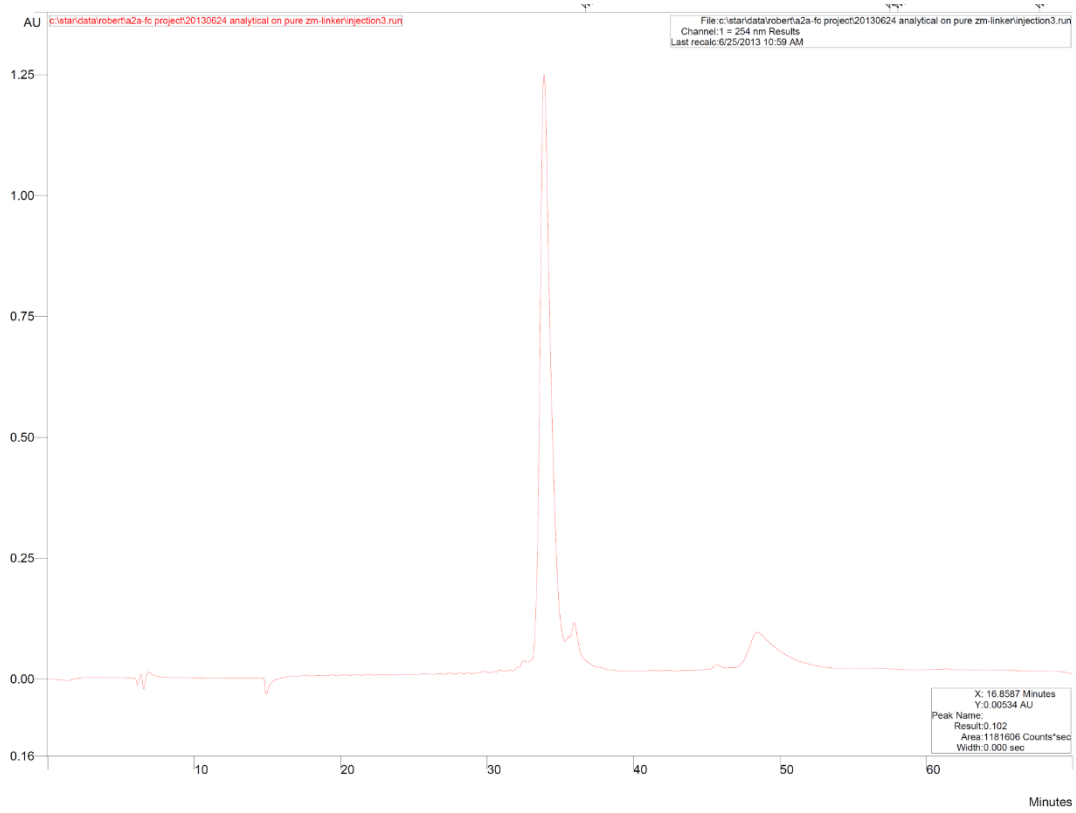

Figure 30. Electrospray mass spectrum of C-ZM.

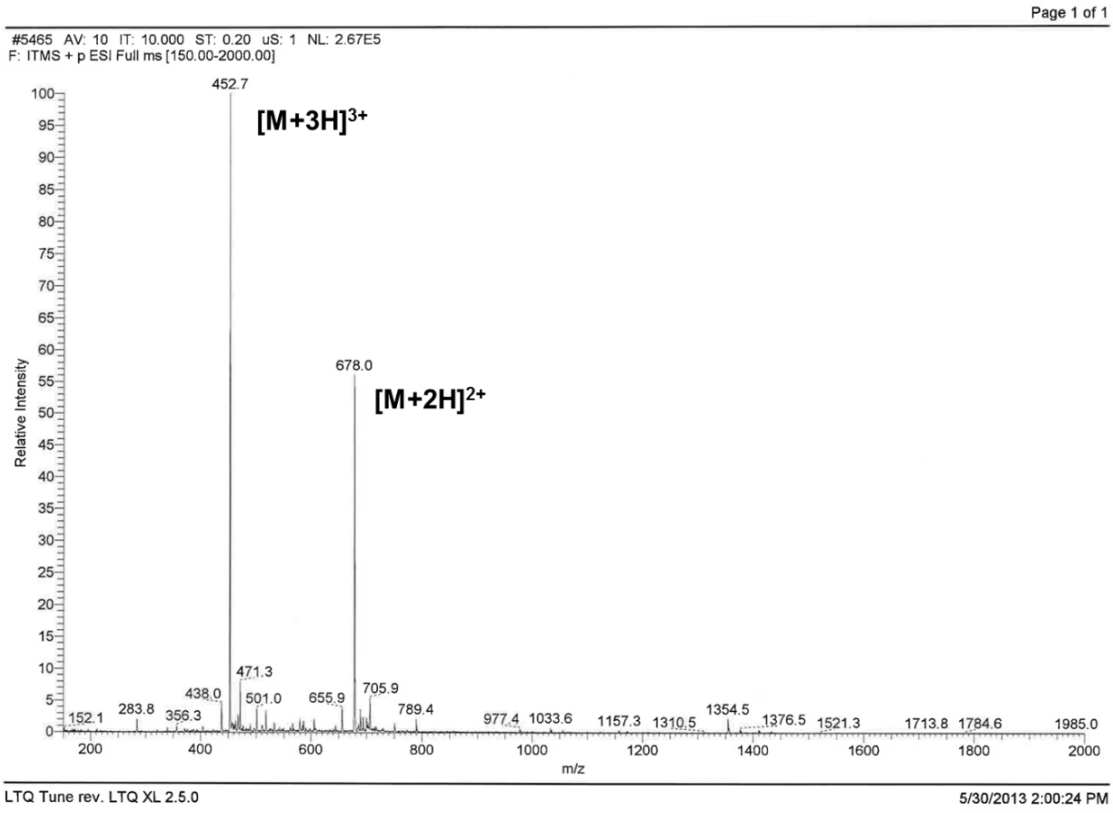

Exact mass of C-ZM is 1353.62 amu. Major peaks at 452.7 and 678.0 corresponds to the 3+ and 2+ charged states, respectively.

Synthesis of Fc-ZM.

The Fc domain of mouse IgG3 gene (aa 104-330) was expressed and isolated as previously described[88]. Briefly, Sf9 insect cells were grown in serum-free media (Sf-900 III, Invitrogen) in suspension culture at 27°C. Fc-intein-CBD recombinant protein was expressed and secreted by Sf9 insect cells to the supernatant, which was collected by centrifugation at 1,500 rpm for 10 minutes and filtering through a 0.2μm filter to remove the cell pellet and debris. The Fc-intein-CBD fusion protien was then purified by passing the supernatant over a bed of chitin beads (NEB, 2 mL bed volume per liter culture) by gravity flow. The beads were washed with 50 mL of phosphate buffered saline (PBS) 5 times before subjected to ligation with C-ZM. To initiate the ligation with C-ZM, 1-2 column volumes of 400 mM sodium 2-mercaptoethanesulfonate in PBS (pH = 7.4) containing more than 100 molar equivalents of C-ZM was added to the column. The column was purged with argon and the reaction was carried out at room temperature over 72 hours. The ligated product was eluted from the column with 1 column volume of PBS 5 times, and dialyzed against 4 liters of PBS using a 10 kDa molecular weight cutoff (MWCO) dialysis cassette (Slidealyzer). Each buffer exchange lasted at least 6 hours, with a total of six buffer exchanges. The final Fc-ZM was further concentrated to 0.5-1 mg/mL and stored at -80 °C. Typical yield was about 0.5 mg Fc-ZM per liter of Sf9 cell culture.

Liquid Chromatography Mass Spectrometry (LC-MS) analysis of Fc-ZM.

LC-MS was performed on a LXQ system (Thermo Scientific) with a Poroshell 300SB-C8 column (5 um, 75 x 1.0 mm). Fc-ZM was first digested with PNGase F (New England Biolabs) according to the protocol provided by the manufacturer. The digested sample was then treated with 50 mM DTT and heated at 55 °C for 20 minutes before subjecting to LC-MS analysis. The LC was performed at 60 °C eluting with a linear gradient of 20-40% acetonitrile:water containing 0.1% formic acid within 10 minutes at a flow rate of 0.25 mL/min.

Results and Discussions

Synthesis of Fc-ZM.

In designing Fc-ZM, we considered the key role that derivatizing the ZM small molecule would play that would preserve its potent antagonist function. We thus pursued the chemical synthesis of A-ZM (Fig. 31), a form of ZM in which the phenol would be derivatized with a carbolic acid that could be convenient for connecting a synthetic linker. Prior X-ray crystallographic studies of ZM in complex with the $A_{2A}R$ revealed that the phenol was relatively solvent exposed[73]. We thus predicted that A-ZM would retain the pharmacodynamic properties of the parent compound ZM. The synthesis of A-ZM began with commercially available 4-hydroxybenzonitrile **1** which was alkylated with *t*butyl bromoacetate to generate intermediate **A**. At the same time, the sulfone building block, intermediate **B**, was prepared according to previously published procedures[89-91]. Briefly, the commercially available 2-furonitrile starting material **2** was cyclized with aminoguanidine to generate amniotriazole **3**. Condensation of **3** with *N*-cyanodithioiminocarbonate provided heterocyclic thioether **4** which was subsequently oxidized with mCPBA to yield sulfone intermediate **B**. With the two building blocks **A** and **B** in hand, A-ZM was generated by first hydrogenating intermediate **A** to afford phenethylamine **5**. Nucleophilic displacement of the sulfone with the resulting primary amine and subsequent base-catalyzed removal of the *t*-butyl group provided the desired compound in seven overall steps. Separately, we prepared an ethylene-oxy linker terminating in a Cys resiude by solid phase synthesis for use in expressed protein ligation. The size of this linker was projected to be of sufficient length, about 100 angstroms in extended conformation, to allow for dual engagement of the ZM with $A_{2A}R$ and the Fc

domain with Fc receptors, present on different cell types. Given previous success with Fc-CGS, this consisted of the structure shown for C-ZM (Fig. 32).

With C-ZM in hand, it was ligated to the Fc protein via expressed protein ligation. In order to produce Fc in its glycosylated, disulfide-linked form, we expressed an Fc-intein-chitin binding domain (CBD) construct containing the mouse IgG3 Fc domain (Scheme 1) in Sf9 insect cells via the baculovirus expression system as previously described. The secreted Fc-intein-CBD was isolated, purified with chitin resin, and treated with 2-mercaptoethanesulfonate sodium (MESNA) to form the free Fc thioester. The Fc thioester was then reacted with C-ZM or cysteine to make Fc-ZM and Fc, respectively. We chose EPL to ensure chemoselective ligation at the C-terminus of the Fc protein and for its technical simplicity to perform with high yields in comparison to other methods. SDS-PAGE revealed Fc and Fc-ZM with more than 90% purity based on Coomassie staining (Fig. 33). LC-MS confirmed the expected mass after deglycosylation by PNGase F (Fig. 34).

Figure 31. Synthetic scheme of A-ZM.

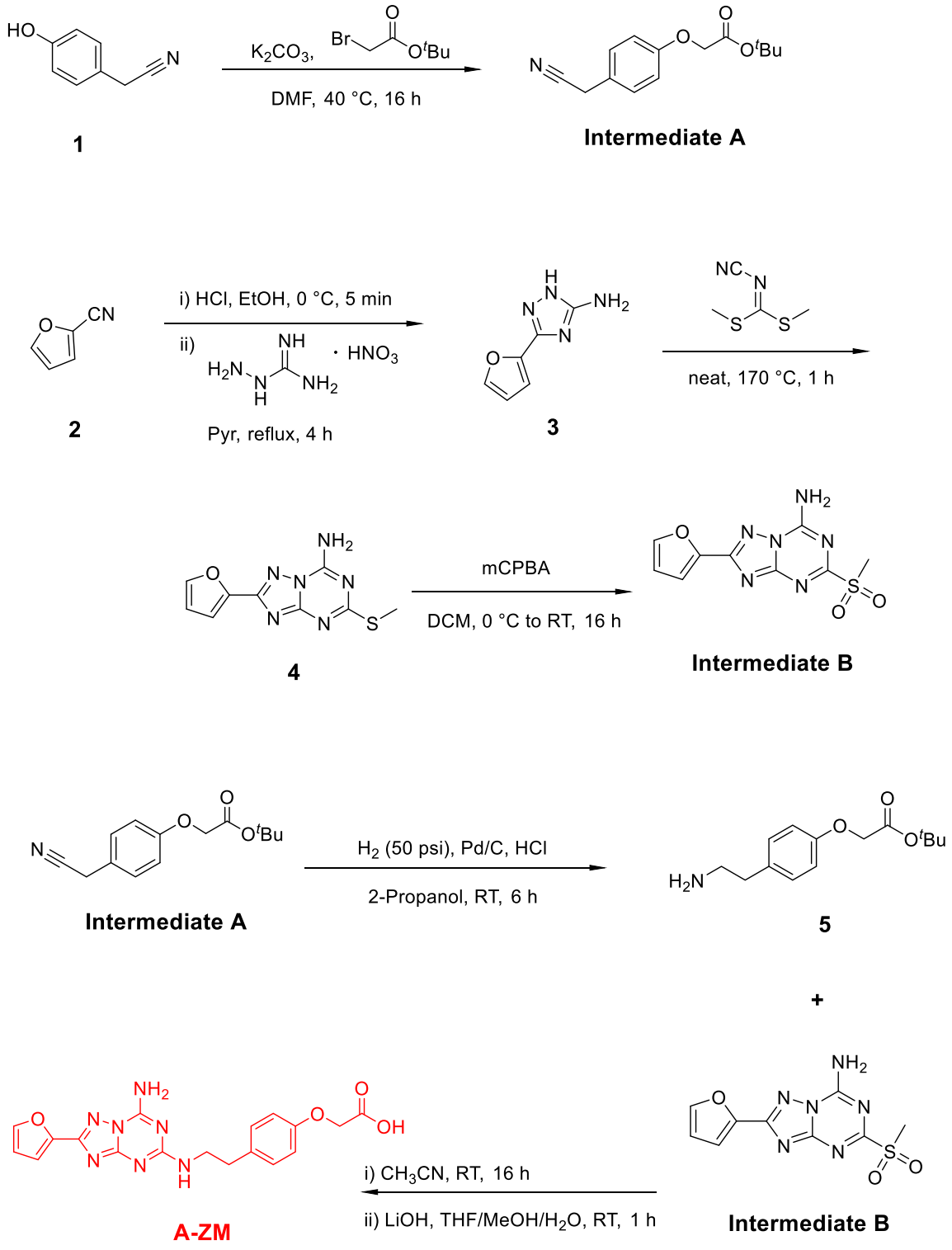

Figure 32. Synthetic scheme of C-ZM.

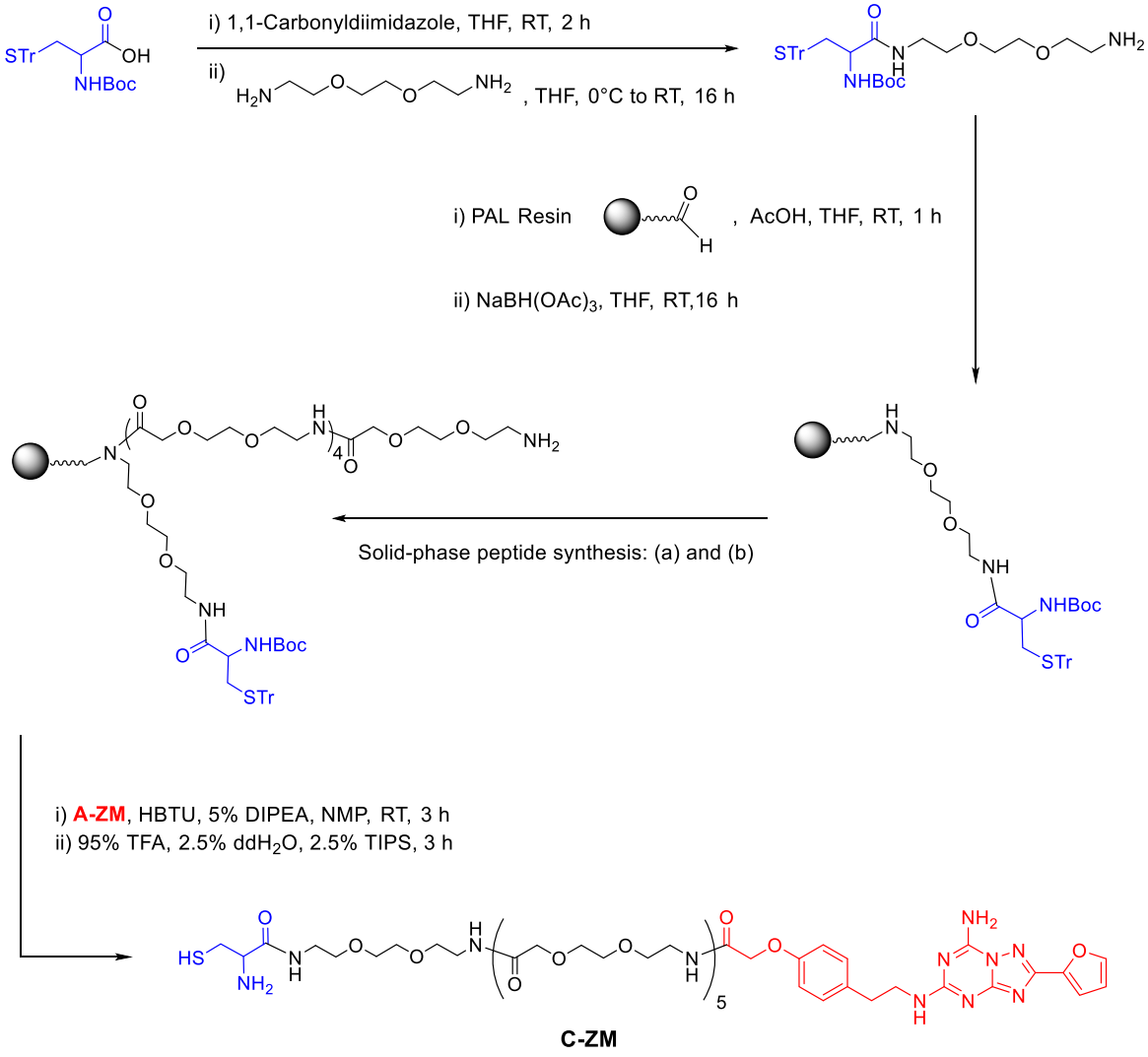

Synthesis of C-ZM. A-ZM was attached to an ethylene-oxy linker terminating in a Cys residue, which was generated via solid-phase peptide synthesis (SPPS) techniques. SPPS conditions include: (a) coupling: Fmoc-NH-(PEG)-COOH, HBTU, 5% DIPEA, NMP, RT, 3 h, and (b) deprotection: 20% piperidine, NMP, RT, 1 h.

Figure 33. Characterization of Purified Fc and Fc-ZM by SDS-PAGE.

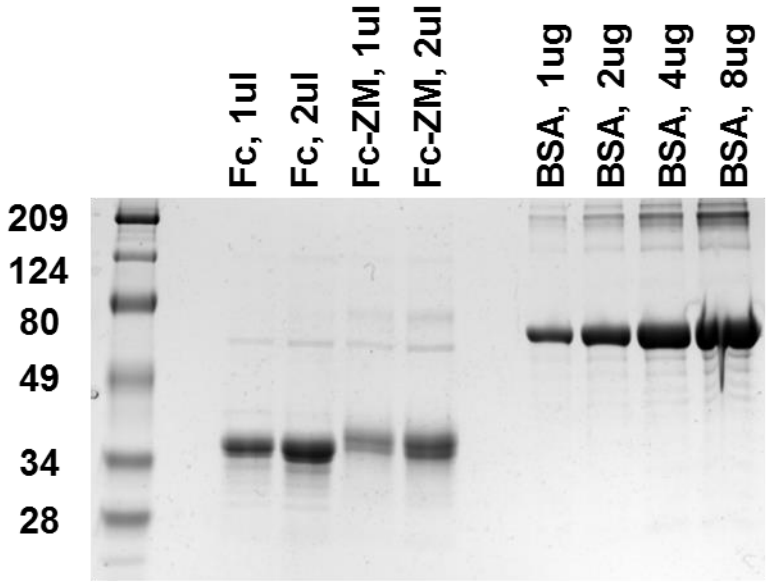

	Exact Mass* (amu)
Fc	29912.83
Fc-ZM	31163.44

**Calculated without glycans*

Fc and Fc-ZM stained with Coomassie blue in a 10% SDS-PAGE gel.

Figure 34. Liquid chromatography mass spectrometry (LC-MS) spectrum of Fc-ZM

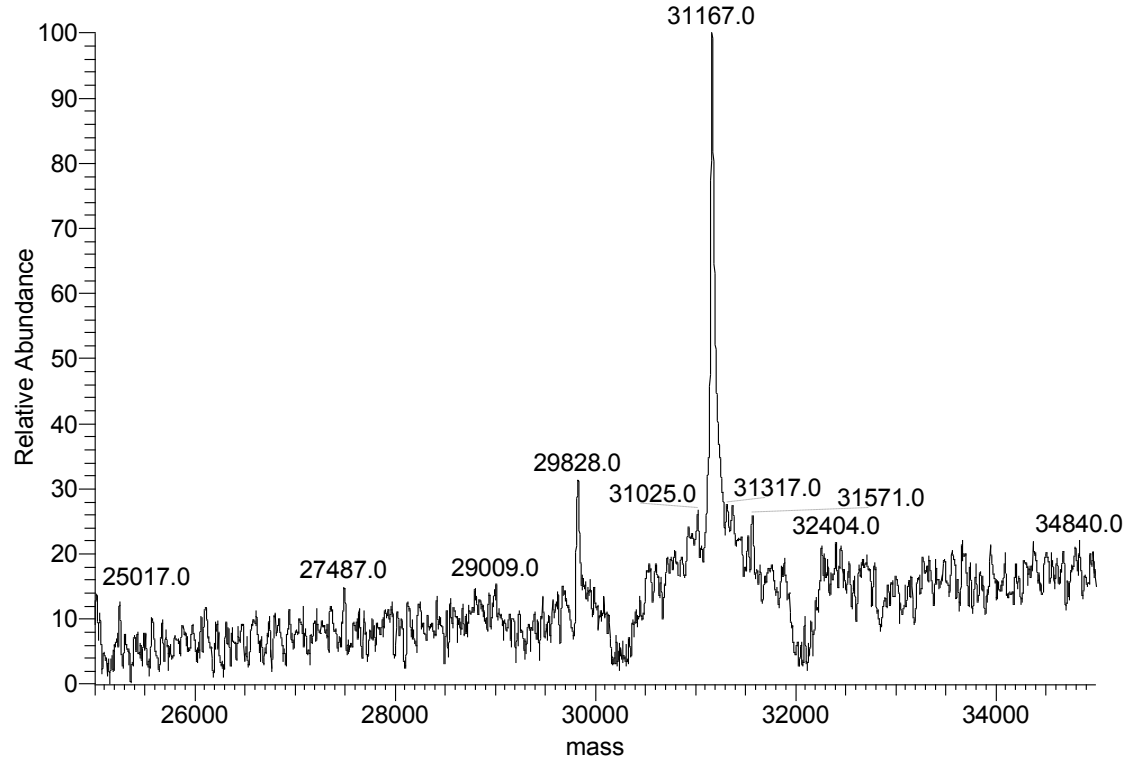

Liquid chromatography mass spectrometry (LC-MS) spectrum confirming the expected mass of Fc-ZM deglycosylated using PNGase F.

Chapter 3:

Ex vivo and *in vivo* characterization of Fc-ZM

Introduction

In Chapter 2, we demonstrated the successful synthesis and purification of Fc-ZM. Here, we characterize the functionality, efficacy, and safety of Fc-ZM in various *ex vivo* and *in vivo* immune models.

Suppression of the Adenosine Pathway in Murine Models

One of the sources of extracellular adenosine is from ATP metabolism by the surface nucleotidases, CD39 and CD73. CD39 catalyzes hydrolysis of ATP/ADP to AMP, and CD73 converts AMP to adenosine. As mentioned in Chapter 1, inflammation within the tumor environment induces focal hypoxia in the surrounding tissue. Hypoxia, in turn, increases the mRNA levels and enzymatic activities of CD39 and CD73[92, 93], and reduces the rate of adenosine removal by adenosine kinases[94, 95]. Interestingly, CD73 expression has been reported in mouse tumor cell lines[96-98] and tumor cells from patients with various cancers[99-106]. The expression of CD73 was also found to correlate with poor prognosis of breast, ovarian, prostate, brain cancers, and leukemia. Knockdown of CD73 in tumor cells led to reduced growth *in vivo* and increased susceptibility to antitumor immune cells[107, 108]. Similarly, anti-CD73 antibody therapy also reduced tumor growth and metastasis from primary tumors in an $A_{2A}R$-dependent fasion[107, 109].

In addition to targeting the production of adenosine, others have focused on blocking the pathway at the receptor level. Preclinical studies using $A_{2A}R$ antagonists and knock-out mouse models have illustrated the significance of adenosine in tumor survival by demonstrating tumor regression after the inactivation of adenosine receptors (Fig. 35)[61, 110]. In 2006, Ohta et al. showed that $A_{2A}R$-deficient mice could spontaneously regress the inoculated tumor, whereas no wild-type mice exhibited similar tumor regression[110]. Likewise, $A_{2A}R$ antagonists were also beneficial in tumor-bearing wild-type animals. Importantly, depletion of T cells and NK cells impaired the retardation of tumor growth by $A_{2A}R$ antagonists, suggesting the effector functions of these immune cells are susceptible to $A_{2A}R$ modulation[111].

Interesting, a recent report published by Cekic and Linden found that although $A_{2A}R$-deficient T cells can effectively elicit antitumor activities in the adenosine-rich tumor microenvironment, they may disappear prematurely before complete tumor regression and hence result in tumor regrowth[112]. In a separate study by Koszałka et al., the authors actually found the activation of any adenosine receptor to significantly inhibit B16F10 melanoma growth but only at its early stages[113]. Therefore, further studies to understand better dosing and timing of $A_{2A}R$ antagonists is important in improving current treatment regimens to achieve persistent immune response.

Figure 35. Overview of experimental strategies to test the hypothetical mechanism of tumor protection via the adenosine pathway.

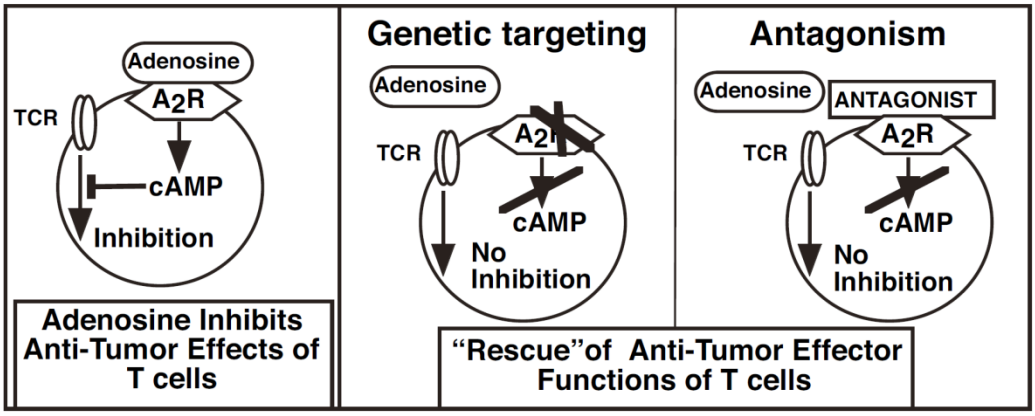

It is assumed that adenosine and A2AR, which inhibit overactive immune cells to protect normal tissues, may protect malignant tissues from antitumor T cells. Genetic targeting of A2AR may de-inhibit CD8+ T cells and thereby facilitate their antitumor effector functions. A similar outcome could be accomplished by using A2AR antagonists.

Ohta A, Gorelik E, Prasad SJ, et al. A2A adenosine receptor protects tumors from antitumor T cells. Proc Natl Acad Sci USA. 2006;103(35):13132-7.

Expected Pharmacologic Properties of Fc-ZM

As discusses earlier, Fc-conjugated therapeutics and ADCs have been found to exhibit elimination half-lives in the range of days to weeks[78]. For the clinically approved ADCs in their first-in-human Phase 1 studies: trastuzumab emtansine decayed with a half-life of 3.10 days, brentuximab vedotin decayed with a half-life of 4.43 days, and a previously approved ADC gemtuzumab ozogamicin decayed with a 3.02 days (Fig. 36)[114]. Consistent with these observations, our previous study using immunohistochemistry revealed Fc-CGS at the target tissue site even weeks after the final dose[88]. Therefore, in the *ex vivo* and *in vivo* experiments described later in this Chapter, we sought to test whether Fc-ZM has similar half-life in the range of days. In addition to pharmacokinetic improvements, we also anticipated a pharmacodynamics effect from covalently linking Fc and ZM. Specifically, Fc-ZM may display high functional affinity against the $A_{2A}R$ due to engagements at both $A_{2A}R$ and FcRs on the same cell or neighboring cells. This enhanced functional affinity, or avidity, is based on the accumulated strength of multiple individual receptor binding events, where any binding interaction increases the likelihood of another to occur (Fig. 37)[115]. The implication of such enhanced affinity could mean the use of lower dose to achieve the same efficacy, thereby reducing off-target or mechanism-based toxicity.

Figure 36. Comparative Pharmacokinetic Parameters of ADCs in Humans.

Table 2. Comparative PK parameters of ADCs at MTD or nearest dose level, at Cycle 1

ADC Name	Dosing regimen	Dose (mg/kg)	MTD (mg/kg)	Cytotoxin	Isotype	DAR	Cleavable	Cmax (µg/mL)	AUC (µg.day/mL)	CL (mL/day/kg)	t½ (days)	Vss (mL/kg)
Mylotarg®	q2w	0.220	0.220	calicheamicin	IgG4	2.5	c	2.86	5.13	90.8	3.02	300
CMC544	q4w	0.045	0.040	calicheamicin	IgG4	6	c	0.969	0.600	91.2	0.710	89.1
IMGN901	q1w	2.77	2.77	DM1	IgG1	3.5	c	55.1	62.6	52.6	0.890	56.3
HuC242-DM1	q3w	5.81	5.81	DM1	IgG1	3.5	c	241	285	24.3	2.02	42.7
Kadcyla®	q3w	3.60	3.60	DM1	IgG1	3.5	ncl	76.2	300	12.7	3.10	58.4
MLN2704	q3w	8.48	not reached	DM1	IgG1	3.5	c	209	404	26.6	2.50	nc
AVE9633	q3w	6.43	not reached	DM4	IgG1	3.5	c	119	468	12.6	3.93	68.1
BT062	q3w	3.95	3.95	DM4	IgG4	3.5	c	89.4	183	24.0	2.12	nc
SAR3419	q3w	3.95	3.95	DM4	IgG1	3.5	c	95.4	720	6.49	6.90	53.6
Adcetris®	q3w	1.80	1.80	MMAE	IgG1	4	c	32.0	79.4	25.1	4.43	117
CDX-011	q3w	1.88	1.88	MMAE	IgG2	4	c	36.3	59.7	40.8	1.18	48.7
PSMA-ADC	q3w	2.20	2.50	MMAE	IgG1	4	c	41.6	67.8	32.9	1.65	62.5
MEDI-547	q3w	0.08	0.08	MMAF	IgG1	4	ncl	2.14	nc	nc	nc	nc

MTD, Maximum Tolerated Dose; DAR, Drug-to-Antibody Ratio; Cmax, maximum (or peak) serum concentration; AUC, Area Under the Curve; CL, Clearance; t1/2, Half-life; Vss, Apparent Volume of Distribution at Steady State.

Deslandes A. Comparative clinical pharmacokinetics of antibody-drug conjugates in first-in-human Phase 1 studies. MAbs. 2014;6(4):859-70.

Figure 37. Multivalency in Ligand Design.

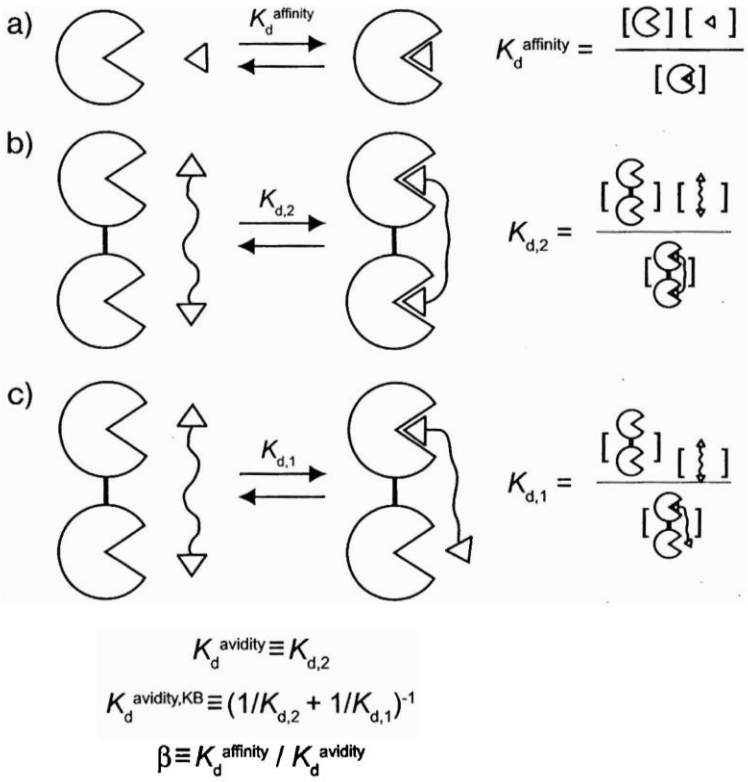

(A) A monovalent ligand binds a monovalent receptor with a dissociation constant Kd affinity. (B) A bivalent ligand binds a receptor of the same valency with a dissociation constant of Kd,2 (avidity). (C) The bivalent receptor binds its ligand with only one receptor-ligand interaction, with a dissociation constant of Kd,1. The enhancement (β) is the ratio of affinity to avidity.

Krishnamurthy, V. M., Estroff, L. A. and Whitesides, G. M. (2006) Multivalency in Ligand Design, in Fragment-based Approaches in Drug Discovery (eds W. Jahnke and D. A. Erlanson), Wiley-VCH Verlag GmbH & Co. KGaA, Weinheim, FRG. doi: 10.1002/3527608761.ch2

Materials and Methods

Intracellar cAMP (cyclic AMP) measurements via enzyme-linked immunosorbent assay.

Spleens from wild type (C57BL/6) mice were harvested and crushed on a cell strainer (BD Bioscience). The red blood cells were then removed using ACK lysis buffer. The isolated splenocytes were seeded in 96-well plates with AE7 medium (45% RPMI 1640, 45% EHAA Clicks, 10% fetal bovine serum, 1% antibiotics, 1% L-Glutamine, 0.1% Gentamycin, 0.05% 2-Mercaptoethanol) and activated by 2ug/ml of soluble anti-CD3 and anti-CD28 for 48 hours, then rested in fresh medium without anti-CD3 or anti-CD28 for 24 hours before drug treatments. To determine the effects of CGS, ZM, A-ZM, C-ZM, Fc, and Fc-ZM on $A_{2A}R$ function, the amount of total cAMP produced in wild type (C57BL/6) splenocytes was assayed with the cAMP Biotrak EIA system (GE Healthcare Life Science) according to manufacturer's instructions.

Surface Plasmon Resonance (SPR) Measurements.

SPR measurements were performed on a Biacore T200 instrument (GE Healthcare). FcRn and FcgRI were immobilized in different channels on a CM5 sensor chip (GE Healthcare) using amine coupling kit provided by the manufacturer. The sensor chip surface was activated with NHS and EDC followed by flowing of receptors until 2000 resonance units (RU) were obtained. A blank reference cell was use as a reference. Fc and drug conjugated Fc (Fc-ZM) were flown over the cell as analytes. HBS-P+ buffer (10 mM HEPES, 150 mM NaCl, 0.05% surfactant P20, pH 7.4 or 6.4) were used as sample buffer

and running buffer. Association of analytes Fc and Fc-ZM were measured for three minutes with a flow rate of 20 μL/min and allowed to dissociate for another three minutes. The surface regeneration was achieved by 3M $MgCl_2$ at a flow rate of 20 μL/min for 60 s. The analytes were injected in a series of two-fold diluted concentration of the highest concentration used (2 μM, 1 μM, 500 nM, 250 nM, 125 nM, 62.5 nM, and 31.25 nM etc and blanks). Multiple individual experiments were carried out and a typical curve is presented in the figures. All sensorgrams were reference channel and blank subtracted for analyses. Kinetics data were obtained by global fitting of the binding data to a 1:1 steady state affinity of Langmuir binding model using BIAcore T200 evaluation software (GE healthcare).

Mice.

Mice above six-weeks of age were used for all the experiments in this study. All mouse procedures were approved by the Johns Hopkins University Institutional Animal Care and Use Committee. C57BL/6 mice were obtained from the Jackson Laboratory. $A_{2A}R$ knock-out mice were bred and housed in pathogen-free conditions on the Johns Hopkins School of Medicine East Baltimore campus. Mice deficient of the γ-chain subunit of FcγR1, FcγRIII, and FcεRI were purchased from Taconic Biosciences (Model 583).

***Ex vivo* T cell response via Interferon γ ELISA.**

Splenocytes from wild type (C57BL/6) mice, $A_{2A}R$ knock-out mice, and mice deficient of the γ-chain subunit of FcγR1, FcγRIII, and FcεRI (Model 583, Taconic) were isolated and cultured in round-bottom 96-well plates with AE7 medium (45% RPMI 1640, 45% EHAA Clicks, 10% fetal bovine serum, 1% antibiotics, 1% L-Glutamine, 0.1% Gentamycin, 0.05% 2-Mercaptoethanol) over 48 hours, in the presence of 0.5 μg/ml of anti-CD3 and various drug treatments. Supernatants were harvested and the level of interferon γ was determined via ELISA (Mouse IFN gamma ELISA Ready-SET-Go!®, Affymetrix eBioscience).

***In vivo* CD8 acute response to Vaccinia virus infection.**

Wild type C57BL/6 (WTB6) mice were infected with Vaccinia virus expressing ovalbumin on day 1 via retro-orbital injections at 1 million plaque-forming unit (PFU) per mouse. Throughout days 2 to 6, various treatments were given via intraperitoneal injections, including vehicle (20% DMSO in PBS), CGS (5.0 μmol/kg, b.i.d.), CGS (5.0 μmol/kg, b.i.d.) and ZM (8.9 μmol/kg, b.i.d.), CGS (5.0 μmol/kg, b.i.d.) and Fc (100 nmol/kg, on days 2 and 4), CGS (5.0 μmol/kg, b.i.d.) and Fc-ZM (100 nmol/kg, on days 2 and 4). Importantly, Fc and Fc-ZM was given one hour before CGS injections. On day 7, splenocytes were harvested as previously described and counted using a hemocytometer.

Statistical analysis.

All graphs were created using GraphPad Prism software, and statistical analysis was performed with GraphPad Prism. Comparisons between three or more independent groups were assessed by one-way ANOVA with a Tukey's multiple-comparisons test. A P value less than 0.05 was considered statistically significant.

***In vivo* cardiovascular toxicity study with CGS and Fc-CGS.**

Wild type (C57BL/6) mice were anesthetized with 3% isoflurane and maintained under 2% isoflurane anesthesia throughout EKG acquisition. Anesthetized mice were placed in a supine position on a temperature controlled heating pad. Body temperature was monitored with rectal probe and maintained at 37–38°C. EKG probes were inserted subcutaneously and EKG signal (Standard lead II) was obtained using a PowerLab data acquisition system (ML866) and Animal Bio Amp (ML136; AD Instruments, Colorado Springs, CO, USA). Vehicle (PBS), 5 μmol/kg of CGS, or 50 nmol/kg of Fc-CGS was administered via intraperitoneal injections. 5 minutes of EKG signal were recorded prior to each injection, followed by 20 minutes of recording after the injection. LabChart Pro 7.2 software (AD Instruments, Colorado Springs, CO, USA) was used for automated EKG tracing analysis.

Results and Discussion

Binding to the $A_{2A}R$.

To explore the potential of Fc-ZM to bind and antagonize the $A_{2A}R$, we treated WT mouse splenocytes with Fc-ZM and control compounds for 1 hour and measured the subsequent production of cyclic AMP (cAMP), a known second messenger in response to A2AR activation. The treatments were either done alone (Fig. 38A) or in combination with the $A_{2A}R$ agonist, CGS-21680 (Fig. 38B), to assess receptor antagonism. Moreover, the mouse splenocytes were pre-activated with 2 μg/ml of anti-CD3 and anti-CD28 to ensure maximal $A_{2A}R$ expression on the cell surface. As expected with $A_{2A}R$ activation, CGS treatment led to a dose-dependent increase in intracellular cAMP production. Treatments with ZM, A-ZM, C-ZM, or Fc demonstrated no changes in cAMP levels. When treated in combination with CGS, Fc-ZM and its ZM-containing precursors inhibited the production of cAMP in a dose-dependent manner. Notably, Fc-alone does not affect cAMP production induced by CGS, indicating the antagonism by Fc-ZM is due to a functional ZM moiety that is able to bind and inhibit $A_{2A}R$ activation.

Figure 38. Assessment of A2AR binding via intracellular cAMP assay.

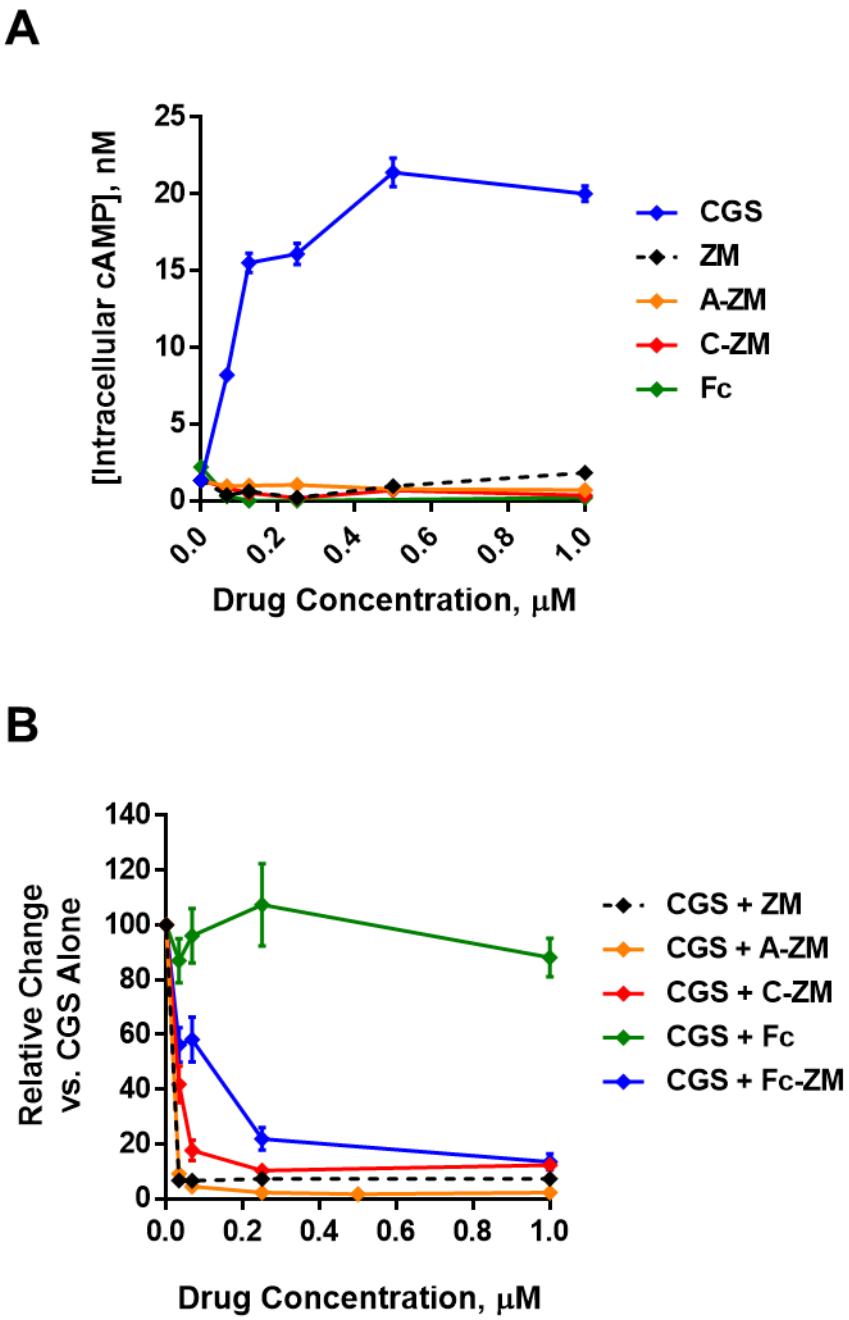

(A) Intracellular cAMP produced by wild-type mouse splenocytes after 1 h incubation in media containing various drugs with concentrations ranging from 0 to 1 μM. (B) Relative changes in the level of intracellular cAMP produced by splenocytes treated with various drugs in the presence of 1 μM CGS when compared to splenocytes treated with 1 μM CGS alone. Drug concentrations on the x-axis denotes the concentration of ZM, A-ZM, C-ZM, Fc, and Fc-ZM.

Binding to Fc Receptors.

Next we examined the ability and affinity of Fc-ZM to bind the Fc receptors. Mouse IgG3 is known to bind at low and high affinities to two Fc receptor isotypes: FcγRI and FcRn. FcγRI is typically found on dendritic cells where receptor binding leads to cell activation via the immunoreceptor tyrosine-based activation motif (ITAM). On the other hand, FcRn expression is found on most myeloid and lymphoid cell types except T cells, NK cells, and eosinophils. Functionally, FcRn is responsible for uptake, transport, and recycling of antibodies. Binding to FcRn occurs at the C_H2-C_H3 hinge region independent of Fc glycosylation[116, 117]. Unlike other Fc receptors, FcRn preferentially binds Fc at acidic pH[118], such as in endocytic vacuoles. Given the tumor microenvironment is highly acidic[119] due to glycolytic metabolism, hypoxia, and lack of blood perfusion, this characteristic of FcRn presents a potential mechanism by which Fc-conjugates can be recycled and concentrated locally within solid tumors. Therefore, we investigated the potential of Fc-ZM to bind both FcγRI the FcRn at pH 7.4 and pH 6.4 via surface plasmon resonance (SPR). In order to measure the affinities at low pH, we immobilized FcγRI and FcRn through amine coupling to the chips and injected Fc and Fc-ZM as analytes. As shown in Figure 39, both Fc and Fc-ZM were able to bind FcγRI and FcRn at pH 6.4, with the affinity to FcRn being approximately one order of magnitude higher than FcγRI. When the pH is increased from 6.4 to 7.4, affinity to FcγRI also increased by about 2-fold, whereas the affinity to FcRn decreased by 6- to 10-fold (Fig. 40).

Figure 39. Assessment of FcRn and FcγRI Binding via surface plasmon resonance at pH 6.4.

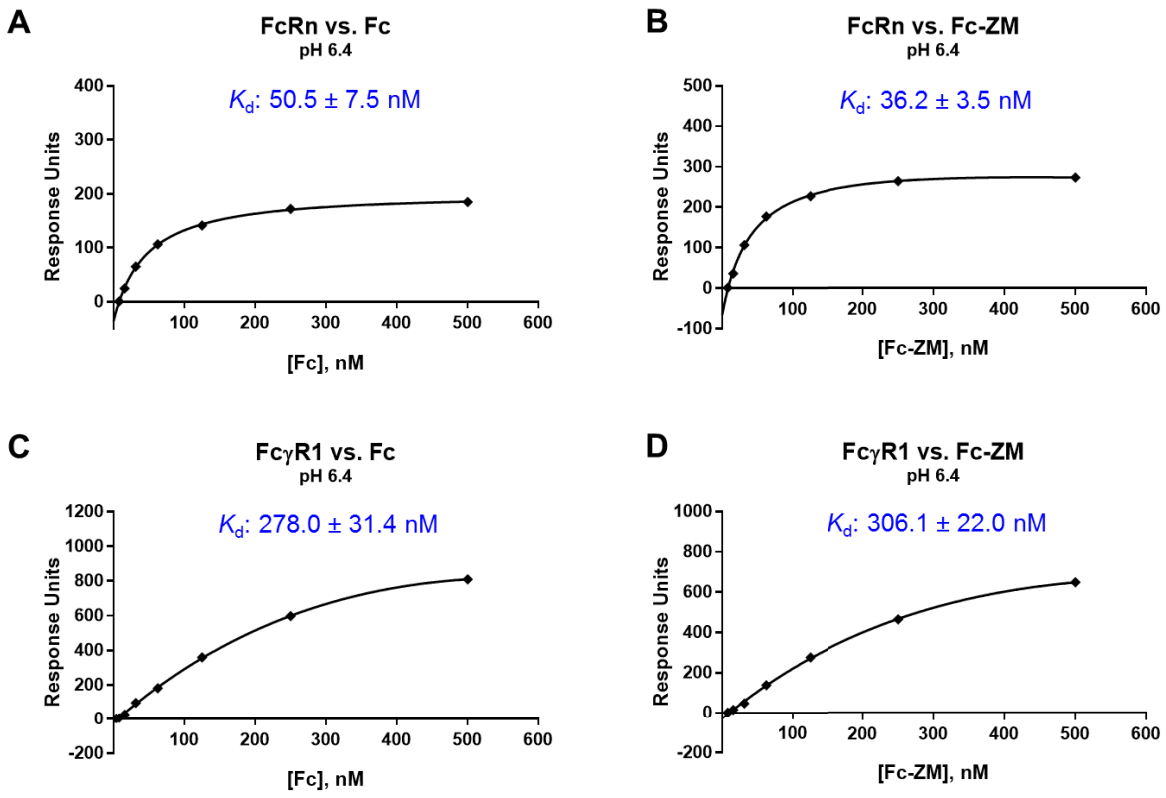

(A) and (B) shows the binding of Fc and Fc-ZM, respectively, to the immobilized mouse neonatal Fc receptor (FcRn). (C) and (D) shows the binding of Fc and Fc-ZM, respectively, to the immobilized mouse FcγR1.

Figure 40. Assessment of FcRn and FcγRI Binding via surface plasmon resonance at pH 7.4.

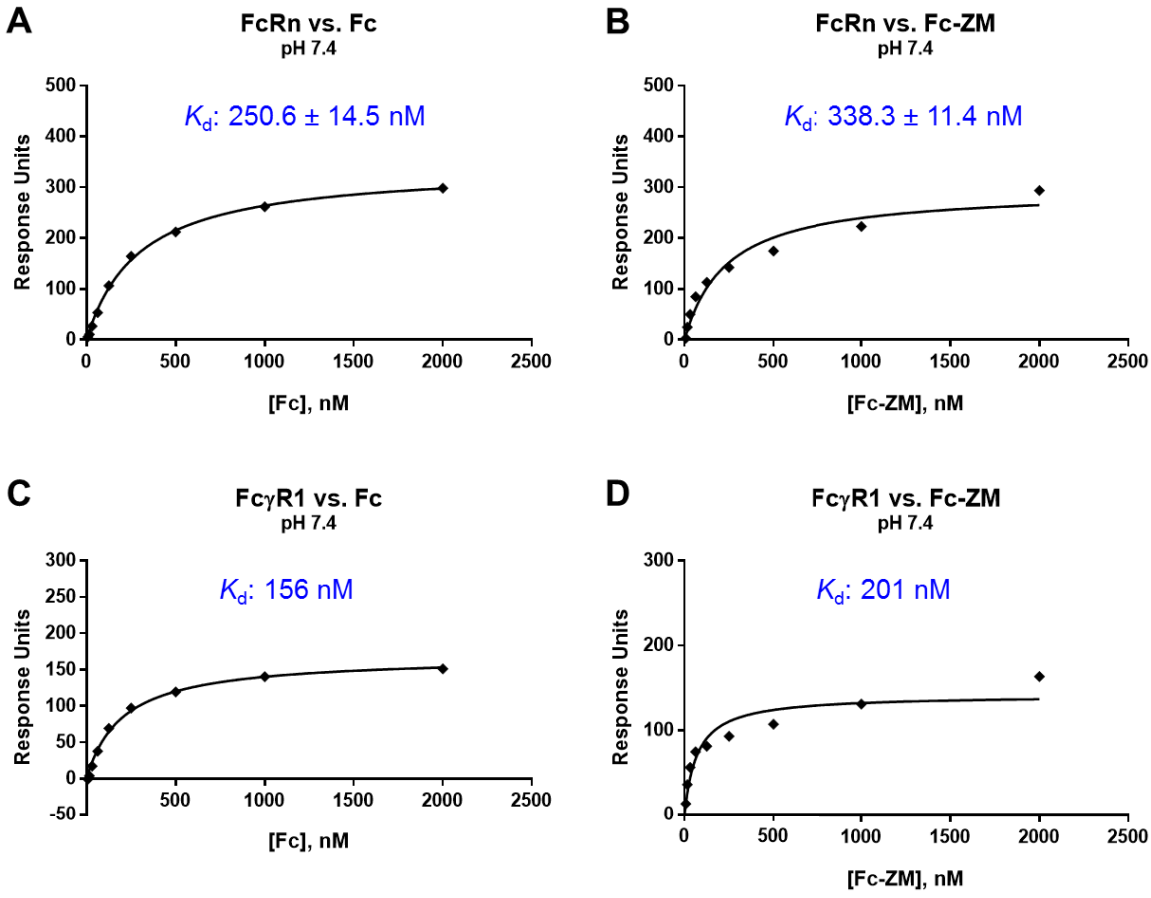

(A) and (B) shows the binding of Fc and Fc-ZM, respectively, to the immobilized mouse neonatal Fc receptor (FcRn). (C) and (D) shows the binding of Fc and Fc-ZM, respectively, to the immobilized mouse FcγR1.

***Ex vivo* T-cell Response.**

We hypothesized that the covalent linkage between Fc and ZM through a short polyethylene glycol linker would enhance the immune response further than either moiety alone. To test this, we harvested and treated wild-type C57BL/6 mice splenocytes with Fc-ZM and controls, in the presence of 0.5 μg/ml of anti-CD3 without or without CGS inhibition for 48 hours, and measured the level of interferon γ (IFNγ) accumulated in the supernatant. As expected, $A_{2A}R$ activation by CGS decreased the amount of IFNγ produced by the splenocytes whereas ZM had no effect on their IFNγ production (Fig. 41A). Interestingly, treatment with Fc alone resulted in increased level of IFNγ in the supernatant, presumably through the activation of immune cells via FcRs engagements. The addition of ZM with Fc did not further stimulate the cells except when the two molecules are covalently linked, as in the case of Fc-ZM. In fact, cells that were treated with Fc-ZM were robust producers of IFNγ, leading to extracellular levels that were 6-fold higher than that of the untreated cells. This increase caused by Fc-ZM suggests potential strengthening of cell-cell interactions between lymphocytes and antigen-presenting cells. In addition, the increase was observable even in the presence of a high concentration of CGS (9-fold molar excess, Fig. 41B), further confirming that the ZM remained active its ability to bind and inhibit the $A_{2A}R$.

Furthermore, testing the same treatments in mice splenocytes lacking the $A_{2A}R$ (Fig. 42A and 42B) or the FcγRs (Fig. 43A and 43B) did not yield similar results, suggesting that the observed phenomenon is specific to the $A_{2A}R$ and the FcγRs. Overall,

the observation that Fc-ZM can increase IFNγ production from wild-type splenocytes significantly more than either drug alone demonstrates the benefits of a covalent linkage and is consistent with our hypothesis that a short linker of approximately 100 Å could enhance the immune response by facilitating cell-cell interactions between lymphocytes and antigen-presenting cells.

Figure 41. ex vivo T-cell response via interferon γ ELISA with wild-type splenocytes.

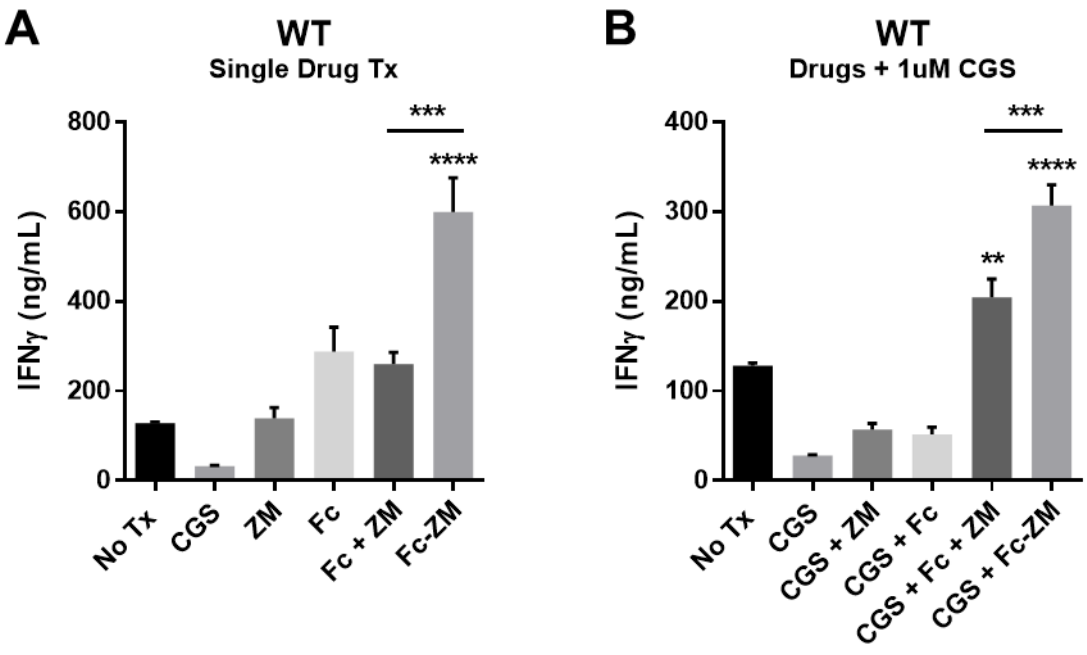

(A) shows the level of IFNγ secreted following a 48 hour incubation with various drug treatments at 111 nM. (B) shows the level of IFNγ secreted following a 48 hour incubation with various drug treatments at 111 nM, in the presence of 1 μM CGS.

Figure 42. ex vivo T-cell response via interferon γ ELISA with A2AR knock-out splenocytes.

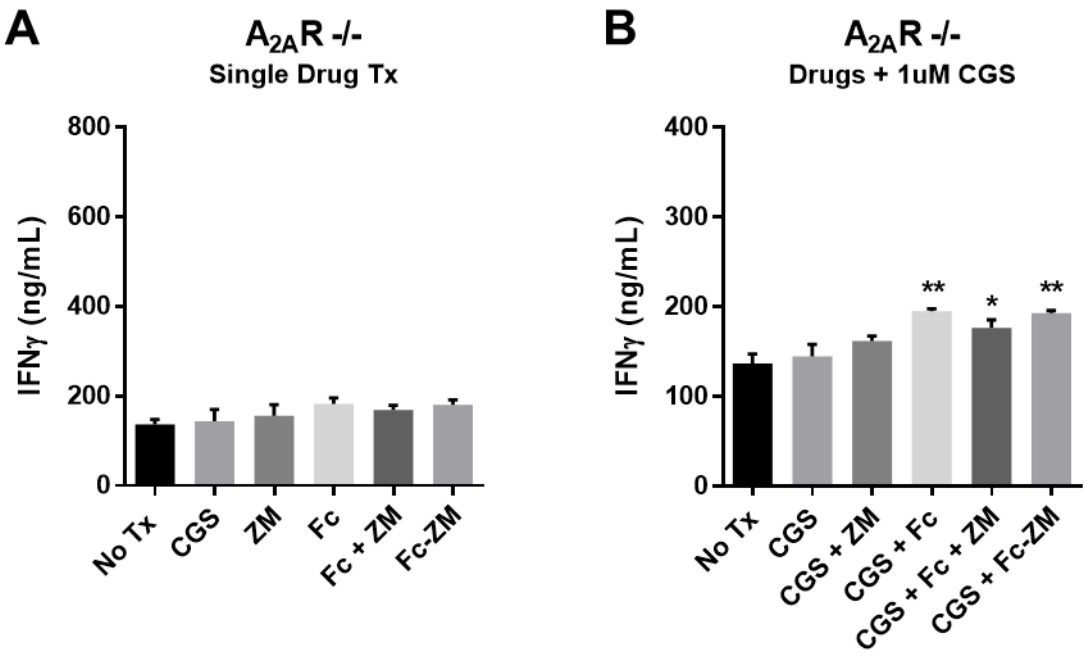

(A) shows the level of IFNγ secreted following a 48 hour incubation with various drug treatments at 111 nM. (B) shows the level of IFNγ secreted following a 48 hour incubation with various drug treatments at 111 nM, in the presence of 1 μM CGS.

Figure 43. ex vivo T-cell response via interferon γ ELISA with FcγR1 knock-out splenocytes.

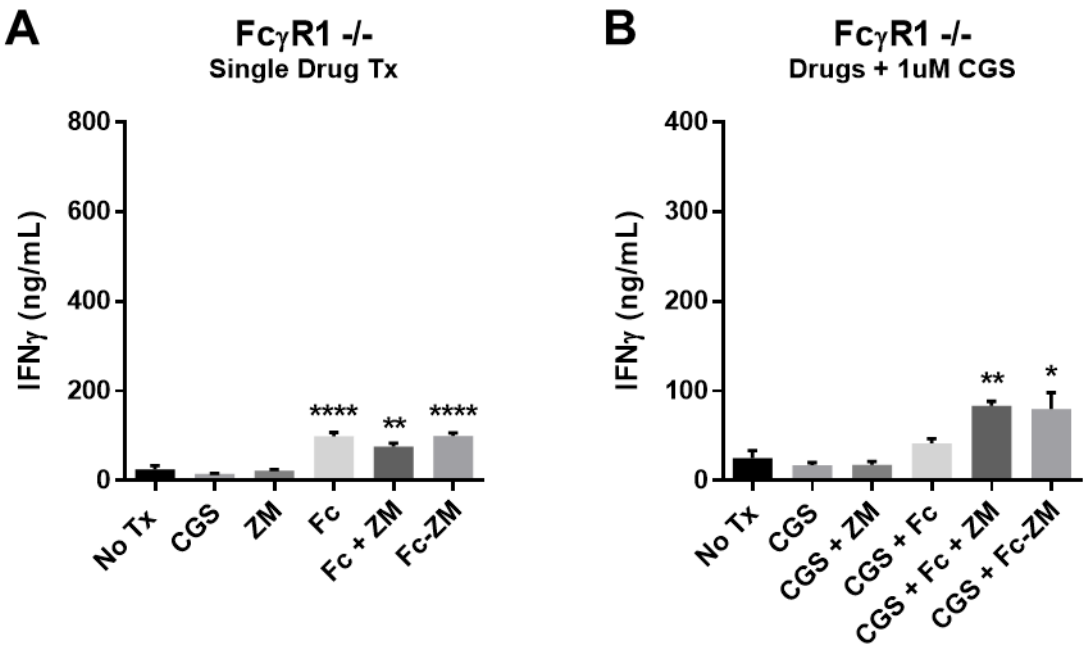

(A) shows the level of IFNγ secreted following a 48 hour incubation with various drug treatments at 111 nM. (B) shows the level of IFNγ secreted following a 48 hour incubation with various drug treatments at 111 nM, in the presence of 1 μM CGS.

***In vivo* Response to Vaccinia infection.**

To examine whether the reversal of CGS effects by Fc-ZM observed *ex vivo* can be translated *in vivo*, we looked at its effects on the acute response to Vaccinia virus infection. In this model, we infected wild type C57BL/6 mice with Vaccinia virus expressing ovalbumin and treated them with various drug combinations over the five days post-infection. Spleens were harvested on the sixth day post-infection and the number of splenocytes was quantified by counting (Fig. 44). In comparison to vehicle treatment, CGS treatment decreased the number of splenocytes by approximately three-fold. This inhibition was reversed by ZM when given twice daily to match the dosing schedule of CGS. When ZM was given once daily, the reversal was incomplete, suggesting that ZM is largely metabolized and/or cleared from the system by the time the second dose of CGS is administered (at least 4 hours after the first dose). By contrast, Fc-ZM, but not Fc, was able to reverse the inhibitory effects of CGS when given only two intraperitoneal injections total (day 1 and day 3 post-infection).

Consistent with our hypothesis, this ability of Fc-ZM to match ZM in reversing the immuno-inhibitory effects of CGS, even at a significantly reduced dosing frequency, is indicative of a prolonged half-life resulting in extended periods of antagonism at the $A_{2A}R$. It is also important to note that the dose of Fc-ZM was 50-fold less in molar amounts compared to that of CGS. Given that the small-molecule ZM only has a 33-fold higher affinity to the $A_{2A}R$ than CGS[64], this matched reversal suggests that Fc-ZM, as a bivalent molecule, has an enhanced apparent affinity to the $A_{2A}R$, potentially by engaging with

multiple A_{2A}Rs or with A_{2A}Rs and FcRs on neighboring lymphocytes and antigen-presenting cells simultaneously.

Figure 44. In vivo response to Vaccinia virus infection.

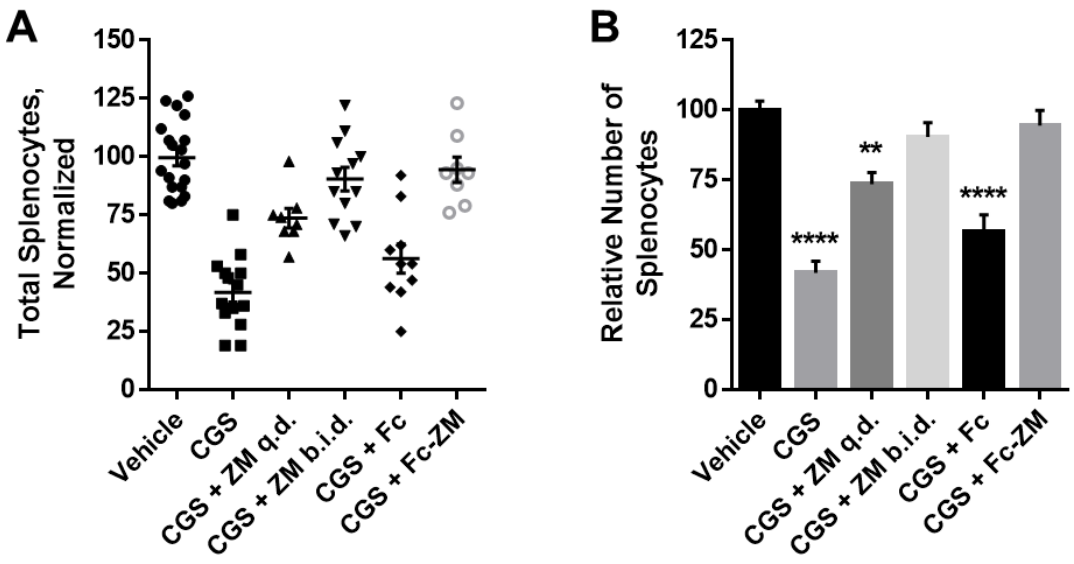

Number of splenocytes was quantified in spleens collected from mice treated with vehicle (n = 19), CGS (n = 14), CGS + ZM q.d. (n = 8), CGS + ZM b.i.d. (n = 12), CGS + Fc (n = 10), or CGS + Fc-ZM (n = 8). The results were normalized to the vehicle treatment and shown in (A) a scatter plot and (B) a bar graph. Statistical significance was determined by one-way ANOVA test ($P < 0.0001$) followed by a Tukey's multiple comparisons test (, $P < 0.05$; **, $P < 0.01$; ***, $P < 0.001$; ****, $P < 0.0001$).*

***In vivo* Cardiotoxicity of Fc-small molecule conjugates.**

Previously, we synthesized a similar Fc protein-small molecule conjugate, Fc-CGS, which demonstrated enhanced pharmacokinetics and pharmacodynamics when compared to its small molecule counterpart, CGS, in treating pneumonitis in mice. Since the heart was known to have high levels of $A_{2A}R$ expression, we hypothesized that the improved therapeutic profile of Fc-CGS would lead to reduced cardiovascular toxicity when compared to CGS. To test this, we administered PBS, CGS (5 μmol/kg), and Fc-CGS (50 nmol/kg) into anesthetized wild-type mice and monitored their heart rate changes via an electrocardiogram (EKG) for 20 minutes (Fig. 45A). Approximately 5 minutes following the intraperitoneal injection, CGS induced a significant increase in heart rate, or tachycardia (Fig. 45B). On the contrary, neither PBS nor Fc-CGS induced tachycardia in mice. This observation is consistent with our hypothesis that conjugation with Fc can enhance the pharmacologic properties of small-molecules such as CGS and ZM, resulting in more efficacious and safer dosing.

Figure 45. In vivo cardiovascular response to CGS and Fc-CGS.

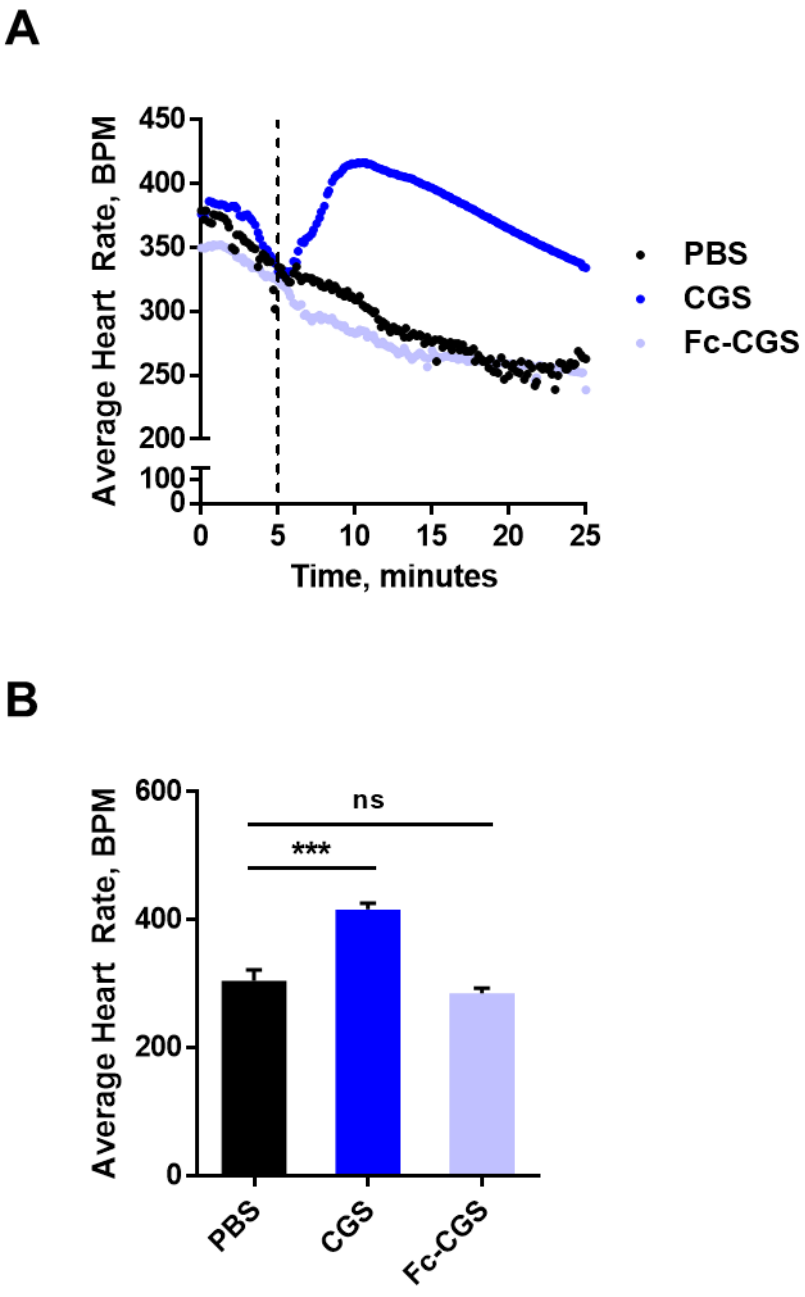

*(A) Average heart rate of mice treated with PBS (n = 3), CGS (n = 4), or Fc-CGS (n = 3), monitored over 20 minutes post-administration of the treatments. Dashed line indicates the timing of the drug injections. (B) Average heart rate at 5.5 minutes following the injection. Results were analyzed using one-way ANOVA test (***, P = 0.0002) followed by a Tukey's multiple comparisons test (***, P < 0.001).*

Summary

My thesis research has focused on the design, synthesis, and testing of a novel Fc protein-small molecule conjugate, Fc-ZM, for the purpose of immune enhancement. The design strategy allowed for a controlled, site-specific conjugation between the Fc domain protein and the modified $A_{2A}R$ antagonist, A-ZM. Binding studies *in vitro* demonstrated the ability of Fc-ZM to bind FcRn and FcγRI, and functionally inhibit the activation of $A_{2A}R$ in a manner similar to its small-molecule precursor, ZM. In both *ex vivo* and *in vivo* immune response models, Fc-ZM exhibited superior pharmacokinetics and pharmacodynamics in antagonizing the $A_{2A}R$ when compared to ZM. Overall, we have illustrated a reproducible method of synthesizing Fc-conjugated small molecules, and its ability to enhance the pharmacologic properties of small molecule drugs.

Bibliography

1. **Dunn, G.P., L.J. Old, and R.D. Schreiber, *The three Es of cancer immunoediting.* Annu Rev Immunol, 2004. 22: p. 329-60.**
2. **Kim, R., M. Emi, and K. Tanabe, *Cancer immunoediting from immune surveillance to immune escape.* Immunology, 2007. 121(1): p. 1-14.**
3. **Fuge, O., et al., *Immunotherapy for bladder cancer.* Res Rep Urol, 2015. 7: p. 65-79.**
4. **Alexandroff, A.B., et al., *BCG immunotherapy of bladder cancer: 20 years on.* Lancet, 1999. 353(9165): p. 1689-94.**
5. **Kantoff, P.W., et al., *Sipuleucel-T immunotherapy for castration-resistant prostate cancer.* N Engl J Med, 2010. 363(5): p. 411-22.**
6. **Andtbacka, R.H., et al., *Talimogene Laherparepvec Improves Durable Response Rate in Patients With Advanced Melanoma.* J Clin Oncol, 2015. 33(25): p. 2780-8.**
7. **Hodi, F.S., et al., *Improved survival with ipilimumab in patients with metastatic melanoma.* N Engl J Med, 2010. 363(8): p. 711-23.**
8. **Robert, C., et al., *Ipilimumab plus dacarbazine for previously untreated metastatic melanoma.* N Engl J Med, 2011. 364(26): p. 2517-26.**
9. **Brahmer, J.R., et al., *Safety and activity of anti-PD-L1 antibody in patients with advanced cancer.* N Engl J Med, 2012. 366(26): p. 2455-65.**
10. **Topalian, S.L., et al., *Safety, activity, and immune correlates of anti-PD-1 antibody in cancer.* N Engl J Med, 2012. 366(26): p. 2443-54.**
11. **Hamid, O., et al., *Safety and tumor responses with lambrolizumab (anti-PD-1) in melanoma.* N Engl J Med, 2013. 369(2): p. 134-44.**
12. **Wolchok, J.D., et al., *Nivolumab plus ipilimumab in advanced melanoma.* N Engl J Med, 2013. 369(2): p. 122-33.**

13. **Topalian, S.L., et al.,** ***Survival, durable tumor remission, and long-term safety in patients with advanced melanoma receiving nivolumab.*** **J Clin Oncol, 2014. 32(10): p. 1020-30.**

14. **Lokhorst, H.M., et al.,** ***Targeting CD38 with Daratumumab Monotherapy in Multiple Myeloma.*** **N Engl J Med, 2015. 373(13): p. 1207-19.**

15. **Lonial, S., et al.,** ***Elotuzumab Therapy for Relapsed or Refractory Multiple Myeloma.*** **N Engl J Med, 2015. 373(7): p. 621-31.**

16. **Breedveld, F.C.,** ***Therapeutic monoclonal antibodies.*** **The Lancet. 355(9205): p. 735-740.**

17. **Carter, P.,** ***Improving the efficacy of antibody-based cancer therapies.*** **Nat Rev Cancer, 2001. 1(2): p. 118-29.**

18. **Weiner, G.J.,** ***Building better monoclonal antibody-based therapeutics.*** **Nat Rev Cancer, 2015. 15(6): p. 361-70.**

19. **Hurwitz, E., et al.,** ***A conjugate of adriamycin and monoclonal antibodies to Thy-1 antigen inhibits human neuroblastoma cells in vitro.*** **Ann N Y Acad Sci, 1983. 417: p. 125-36.**

20. **Shen, B.Q., et al.,** ***Conjugation site modulates the in vivo stability and therapeutic activity of antibody-drug conjugates.*** **Nat Biotechnol, 2012. 30(2): p. 184-9.**

21. **Perez, H.L., et al.,** ***Antibody-drug conjugates: current status and future directions.*** **Drug Discov Today, 2014. 19(7): p. 869-81.**

22. **Carlsson, J., H. Drevin, and R. Axen,** ***Protein thiolation and reversible protein-protein conjugation. N-Succinimidyl 3-(2-pyridyldithio)propionate, a new heterobifunctional reagent.*** **Biochem J, 1978. 173(3): p. 723-37.**

23. **Chari, R.V., et al., *Immunoconjugates containing novel maytansinoids: promising anticancer drugs.* Cancer Res, 1992. 52(1): p. 127-31.**

24. **Trail, P.A., et al., *Cure of xenografted human carcinomas by BR96-doxorubicin immunoconjugates.* Science, 1993. 261(5118): p. 212-5.**

25. **Greenfield, R.S., et al., *Evaluation in vitro of adriamycin immunoconjugates synthesized using an acid-sensitive hydrazone linker.* Cancer Res, 1990. 50(20): p. 6600-7.**

26. **Koblinski, J.E., M. Ahram, and B.F. Sloane, *Unraveling the role of proteases in cancer.* Clin Chim Acta, 2000. 291(2): p. 113-35.**

27. **Sanderson, R.J., et al., *In vivo drug-linker stability of an anti-CD30 dipeptide-linked auristatin immunoconjugate.* Clin Cancer Res, 2005. 11(2 Pt 1): p. 843-52.**

28. **Toki, B.E., et al., *Protease-mediated fragmentation of p-amidobenzyl ethers: a new strategy for the activation of anticancer prodrugs.* J Org Chem, 2002. 67(6): p. 1866-72.**

29. **Kovtun, Y.V. and V.S. Goldmacher, *Cell killing by antibody-drug conjugates.* Cancer Lett, 2007. 255(2): p. 232-40.**

30. **Muir, T.W., D. Sondhi, and P.A. Cole, *Expressed protein ligation: a general method for protein engineering.* Proc Natl Acad Sci U S A, 1998. 95(12): p. 6705-10.**

31. **Robert, C., et al., *Pembrolizumab versus Ipilimumab in Advanced Melanoma.* N Engl J Med, 2015. 372(26): p. 2521-32.**

32. **Robert, C., et al., *Nivolumab in previously untreated melanoma without BRAF mutation.* N Engl J Med, 2015. 372(4): p. 320-30.**

33. **Larkin, J., et al., *Combined Nivolumab and Ipilimumab or Monotherapy in Untreated Melanoma.* N Engl J Med, 2015. 373(1): p. 23-34.**

34. **Garon, E.B., et al., *Pembrolizumab for the treatment of non-small-cell lung cancer.* N Engl J Med, 2015. 372(21): p. 2018-28.**

35. **Brahmer, J., et al., *Nivolumab versus Docetaxel in Advanced Squamous-Cell Non-Small-Cell Lung Cancer.* N Engl J Med, 2015. 373(2): p. 123-35.**

36. **Borghaei, H., et al., *Nivolumab versus Docetaxel in Advanced Nonsquamous Non-Small-Cell Lung Cancer.* N Engl J Med, 2015. 373(17): p. 1627-39.**

37. **Motzer, R.J., et al., *Nivolumab for Metastatic Renal Cell Carcinoma: Results of a Randomized Phase II Trial.* J Clin Oncol, 2015. 33(13): p. 1430-7.**

38. **Motzer, R.J., et al., *Nivolumab versus Everolimus in Advanced Renal-Cell Carcinoma.* N Engl J Med, 2015. 373(19): p. 1803-13.**

39. **Schadendorf, D., et al., *Pooled Analysis of Long-Term Survival Data From Phase II and Phase III Trials of Ipilimumab in Unresectable or Metastatic Melanoma.* J Clin Oncol, 2015. 33(17): p. 1889-94.**

40. **Linden, J., *Molecular approach to adenosine receptors: receptor-mediated mechanisms of tissue protection.* Annu Rev Pharmacol Toxicol, 2001. 41: p. 775-87.**

41. **Apasov, S., et al., *Role of extracellular ATP and P1 and P2 classes of purinergic receptors in T-cell development and cytotoxic T lymphocyte effector functions.* Immunol Rev, 1995. 146: p. 5-19.**

42. **Cronstein, B.N., D. Naime, and G. Firestein, *The antiinflammatory effects of an adenosine kinase inhibitor are mediated by adenosine.* Arthritis Rheum, 1995. 38(8): p. 1040-5.**

43. **Ohta, A. and M. Sitkovsky, *Role of G-protein-coupled adenosine receptors in downregulation of inflammation and protection from tissue damage.* Nature, 2001. 414(6866): p. 916-20.**

44. **Harris, A.L., *Hypoxia--a key regulatory factor in tumour growth.* Nat Rev Cancer, 2002. 2(1): p. 38-47.**

45. **Blay, J., T.D. White, and D.W. Hoskin, *The extracellular fluid of solid carcinomas contains immunosuppressive concentrations of adenosine.* Cancer Res, 1997. 57(13): p. 2602-5.**

46. **Fredholm, B.B., et al., *International Union of Pharmacology. XXV. Nomenclature and classification of adenosine receptors.* Pharmacol Rev, 2001. 53(4): p. 527-52.**

47. **Huang, S., et al., *Role of A2a extracellular adenosine receptor-mediated signaling in adenosine-mediated inhibition of T-cell activation and expansion.* Blood, 1997. 90(4): p. 1600-10.**

48. **Zarek, P.E., et al., *A2A receptor signaling promotes peripheral tolerance by inducing T-cell anergy and the generation of adaptive regulatory T cells.* Blood, 2008. 111(1): p. 251-9.**

49. **Raskovalova, T., et al., *Adenosine-mediated inhibition of cytotoxic activity and cytokine production by IL-2/NKp46-activated NK cells: involvement of protein kinase A isozyme I (PKA I).* Immunol Res, 2006. 36(1-3): p. 91-9.**

50. **Raskovalova, T., et al., *Inhibition of cytokine production and cytotoxic activity of human antimelanoma specific CD8+ and CD4+ T lymphocytes by adenosine-protein kinase A type I signaling.* Cancer Res, 2007. 67(12): p. 5949-56.**

51. **Ohta, A., et al., *A2A adenosine receptor may allow expansion of T cells lacking effector functions in extracellular adenosine-rich microenvironments.* J Immunol, 2009. 183(9): p. 5487-93.**

52. **Sevigny, C.P., et al., *Activation of adenosine 2A receptors attenuates allograft rejection and alloantigen recognition.* J Immunol, 2007. 178(7): p. 4240-9.**

53. **Ohta, A., et al.,** ***The development and immunosuppressive functions of CD4(+) CD25(+) FoxP3(+) regulatory T cells are under influence of the adenosine-A2A adenosine receptor pathway.*** **Front Immunol, 2012. 3: p. 190.**

54. **Allard, B., et al.,** ***Targeting CD73 enhances the antitumor activity of anti-PD-1 and anti-CTLA-4 mAbs.*** **Clin Cancer Res, 2013. 19(20): p. 5626-35.**

55. **Hasko, G., et al.,** ***Adenosine inhibits IL-12 and TNF-[alpha] production via adenosine A2a receptor-dependent and independent mechanisms.*** **FASEB J, 2000. 14(13): p. 2065-74.**

56. **Panther, E., et al.,** ***Adenosine affects expression of membrane molecules, cytokine and chemokine release, and the T-cell stimulatory capacity of human dendritic cells.*** **Blood, 2003. 101(10): p. 3985-90.**

57. **Han, K.L., et al.,** ***Adenosine A(2)A receptor agonist-mediated increase in donor-derived regulatory T cells suppresses development of graft-versus-host disease.*** **J Immunol, 2013. 190(1): p. 458-68.**

58. **Lee, D.J. and A.W. Taylor,** ***Both MC5r and A2Ar are required for protective regulatory immunity in the spleen of post-experimental autoimmune uveitis in mice.*** **J Immunol, 2013. 191(8): p. 4103-11.**

59. **Ohta, A. and M. Sitkovsky,** ***Extracellular adenosine-mediated modulation of regulatory T cells.*** **Front Immunol, 2014. 5: p. 304.**

60. **Iannone, R., et al.,** ***Adenosine limits the therapeutic effectiveness of anti-CTLA4 mAb in a mouse melanoma model.*** **Am J Cancer Res, 2014. 4(2): p. 172-81.**

61. **Waickman, A.T., et al.,** ***Enhancement of tumor immunotherapy by deletion of the A2A adenosine receptor.*** **Cancer Immunol Immunother, 2012. 61(6): p. 917-26.**

62. **Hein, T.W., L. Belardinelli, and L. Kuo,** ***Adenosine A(2A) receptors mediate coronary microvascular dilation to adenosine: role of nitric oxide and ATP-sensitive potassium channels.*** **J Pharmacol Exp Ther, 1999. 291(2): p. 655-64.**

63. **Desai, A., et al.,** ***Adenosine A2A receptor stimulation increases angiogenesis by down-regulating production of the antiangiogenic matrix protein thrombospondin 1.*** **Mol Pharmacol, 2005. 67(5): p. 1406-13.**

64. **de Lera Ruiz, M., Y.H. Lim, and J. Zheng,** ***Adenosine A2A receptor as a drug discovery target.*** **J Med Chem, 2014. 57(9): p. 3623-50.**

65. **Jarvis, M.F., et al.,** ***[3H]CGS 21680, a selective A2 adenosine receptor agonist directly labels A2 receptors in rat brain.*** **J Pharmacol Exp Ther, 1989. 251(3): p. 888-93.**

66. **Hutchison, A.J., et al.,** ***CGS 21680C, an A2 selective adenosine receptor agonist with preferential hypotensive activity.*** **J Pharmacol Exp Ther, 1989. 251(1): p. 47-55.**

67. **Palmer, T.M., et al.,** ***125I-4-(2-[7-amino-2-[2-furyl][1,2,4]triazolo[2,3-a][1,3,5] triazin-5-yl-amino]ethyl)phenol, a high affinity antagonist radioligand selective for the A2a adenosine receptor.*** **Mol Pharmacol, 1995. 48(6): p. 970-4.**

68. **Dall'Igna, O.P., et al.,** ***Neuroprotection by caffeine and adenosine A2A receptor blockade of beta-amyloid neurotoxicity.*** **Br J Pharmacol, 2003. 138(7): p. 1207-9.**

69. **Golembiowska, K. and A. Dziubina,** ***Striatal adenosine A(2A) receptor blockade increases extracellular dopamine release following l-DOPA administration in intact and dopamine-denervated rats.*** **Neuropharmacology, 2004. 47(3): p. 414-26.**

70. **Poucher, S.M., et al.,** ***The in vitro pharmacology of ZM 241385, a potent, non-xanthine A2a selective adenosine receptor antagonist.*** **Br J Pharmacol, 1995. 115(6): p. 1096-102.**

71. **Poucher, S.M., et al.,** ***Pharmacodynamics of ZM 241385, a potent A2a adenosine receptor antagonist, after enteric administration in rat, cat and dog.*** **J Pharm Pharmacol, 1996. 48(6): p. 601-6.**

72. **Keddie, J.R., et al.,** ***In vivo characterisation of ZM 241385, a selective adenosine A2A receptor antagonist.*** **Eur J Pharmacol, 1996. 301(1-3): p. 107-13.**

73. **Jaakola, V.P., et al.,** ***The 2.6 angstrom crystal structure of a human A2A adenosine receptor bound to an antagonist.*** **Science, 2008. 322(5905): p. 1211-7.**

74. **Lebon, G., et al.,** ***Agonist-bound adenosine A2A receptor structures reveal common features of GPCR activation.*** **Nature, 2011. 474(7352): p. 521-5.**

75. **Zhukov, A., et al.,** ***Biophysical mapping of the adenosine A2A receptor.*** **J Med Chem, 2011. 54(13): p. 4312-23.**

76. **Yasuda, M., et al.,** ***Pharmaceutical composition promoting defecation*****, 2006, Google Patents.**

77. **Czajkowsky, D.M., et al.,** ***Fc-fusion proteins: new developments and future perspectives.*** **EMBO Mol Med, 2012. 4(10): p. 1015-28.**

78. **Levin, D., et al.,** ***Fc fusion as a platform technology: potential for modulating immunogenicity.*** **Trends Biotechnol, 2015. 33(1): p. 27-34.**

79. **Matsumura, Y. and H. Maeda,** ***A new concept for macromolecular therapeutics in cancer chemotherapy: mechanism of tumoritropic accumulation of proteins and the antitumor agent smancs.*** **Cancer Res, 1986. 46(12 Pt 1): p. 6387-92.**

80. **Nimmerjahn, F. and J.V. Ravetch,** ***Fcgamma receptors as regulators of immune responses.*** **Nat Rev Immunol, 2008. 8(1): p. 34-47.**

81. **Buschor, P., et al.,** ***Improved FcgammaRIIb targeting functionally translates into enhanced inhibition of basophil activation.*** **Int Arch Allergy Immunol, 2014. 163(3): p. 206-14.**

82. **Saxon, A., C. Kepley, and K. Zhang,** ***"Accentuate the negative, eliminate the positive": engineering allergy therapeutics to block allergic reactivity through negative signaling.*** **J Allergy Clin Immunol, 2008. 121(2): p. 320-5.**

83. **Van Scott, M.R., et al.,** ***Systemic administration of an Fcgamma-Fc(epsilon)-fusion protein in house dust mite sensitive nonhuman primates.*** **Clin Immunol, 2008. 128(3): p. 340-8.**

84. **Ghosh, I., et al.,** ***Site-specific protein labeling by intein-mediated protein ligation.*** **Methods Mol Biol, 2011. 705: p. 87-107.**

85. **Zuger, S. and H. Iwai,** ***Intein-based biosynthetic incorporation of unlabeled protein tags into isotopically labeled proteins for NMR studies.*** **Nat Biotechnol, 2005. 23(6): p. 736-40.**

86. **Bolduc, D., et al.,** ***Phosphorylation-mediated PTEN conformational closure and deactivation revealed with protein semisynthesis.*** **Elife, 2013. 2: p. e00691.**

87. **Raghavan, R. and M.F. Minnick,** ***Group I introns and inteins: disparate origins but convergent parasitic strategies.*** **J Bacteriol, 2009. 191(20): p. 6193-202.**

88. **Chiang, M.J., et al.,** ***An Fc domain protein-small molecule conjugate as an enhanced immunomodulator.*** **J Am Chem Soc, 2014. 136(9): p. 3370-3.**

89. **Caulkett, P.W.R., et al.,** ***Adenine isosteres with bridgehead nitrogen. Part 1. Two independent syntheses of the [1,2,4]triazolo[1,5-a][1,3,5]triazine ring system leading to a range of substituents in the 2, 5 and 7 positions.*** **Journal of the Chemical Society, Perkin Transactions 1, 1995(7): p. 801-808.**

90. **Hutchison, A.J., et al.,** ***2-(Arylalkylamino)adenosin-5'-uronamides: a new class of highly selective adenosine A2 receptor ligands.*** **J Med Chem, 1990. 33(7): p. 1919-24.**

91. **Caulkett, P.W.R., et al.,** ***Azole Derivatives*****, 1991, Google Patents.**

92. **Synnestvedt, K., et al.,** ***Ecto-5'-nucleotidase (CD73) regulation by hypoxia-inducible factor-1 mediates permeability changes in intestinal epithelia.*** **J Clin Invest, 2002. 110(7): p. 993-1002.**

93. **Eltzschig, H.K., et al.,** ***Endogenous adenosine produced during hypoxia attenuates neutrophil accumulation: coordination by extracellular nucleotide metabolism.*** **Blood, 2004. 104(13): p. 3986-92.**

94. **Kobayashi, S., H. Zimmermann, and D.E. Millhorn,** ***Chronic hypoxia enhances adenosine release in rat PC12 cells by altering adenosine metabolism and membrane transport.*** **J Neurochem, 2000. 74(2): p. 621-32.**

95. **Morote-Garcia, J.C., et al.,** ***HIF-1-dependent repression of adenosine kinase attenuates hypoxia-induced vascular leak.*** **Blood, 2008. 111(12): p. 5571-80.**

96. **Ujhazy, P., et al.,** ***Ecto-5'-nucleotidase (CD73) in multidrug-resistant cell lines generated by doxorubicin.*** **Int J Cancer, 1994. 59(1): p. 83-93.**

97. **Sadej, R., J. Spychala, and A.C. Skladanowski,** ***Expression of ecto-5'-nucleotidase (eN, CD73) in cell lines from various stages of human melanoma.*** **Melanoma Res, 2006. 16(3): p. 213-22.**

98. **Zhi, X., et al.,** ***RNA interference of ecto-5'-nucleotidase (CD73) inhibits human breast cancer cell growth and invasion.*** **Clin Exp Metastasis, 2007. 24(6): p. 439-48.**

99. **Coustan-Smith, E., et al.,** ***New markers for minimal residual disease detection in acute lymphoblastic leukemia.*** **Blood, 2011. 117(23): p. 6267-76.**

100. **Hausler, S.F., et al.,** ***Ectonucleotidases CD39 and CD73 on OvCA cells are potent adenosine-generating enzymes responsible for adenosine receptor 2A-dependent suppression of T cell function and NK cell cytotoxicity.*** **Cancer Immunol Immunother, 2011. 60(10): p. 1405-18.**

101. **Serra, S., et al.,** ***CD73-generated extracellular adenosine in chronic lymphocytic leukemia creates local conditions counteracting drug-induced cell death.*** **Blood, 2011. 118(23): p. 6141-52.**

102. **Loi, S., et al.,** ***CD73 promotes anthracycline resistance and poor prognosis in triple negative breast cancer.*** **Proc Natl Acad Sci U S A, 2013. 110(27): p. 11091-6.**

103. **Quezada, C., et al.,** ***5'-ectonucleotidase mediates multiple-drug resistance in glioblastoma multiforme cells.*** **J Cell Physiol, 2013. 228(3): p. 602-8.**

104. **Yang, Q., J. Du, and L. Zu,** ***Overexpression of CD73 in prostate cancer is associated with lymph node metastasis.*** **Pathol Oncol Res, 2013. 19(4): p. 811-4.**

105. **Leclerc, B.G., et al.,** ***CD73 Expression Is an Independent Prognostic Factor in Prostate Cancer.*** **Clin Cancer Res, 2016. 22(1): p. 158-66.**

106. **Turcotte, M., et al.,** ***CD73 is associated with poor prognosis in high-grade serous ovarian cancer.*** **Cancer Res, 2015. 75(21): p. 4494-503.**

107. **Stagg, J., et al.,** ***Anti-CD73 antibody therapy inhibits breast tumor growth and metastasis.*** **Proc Natl Acad Sci U S A, 2010. 107(4): p. 1547-52.**

108. **Jin, D., et al.,** ***CD73 on tumor cells impairs antitumor T-cell responses: a novel mechanism of tumor-induced immune suppression.*** **Cancer Res, 2010. 70(6): p. 2245-55.**

109. **Terp, M.G., et al.,** ***Anti-human CD73 monoclonal antibody inhibits metastasis formation in human breast cancer by inducing clustering and internalization of CD73 expressed on the surface of cancer cells.*** **J Immunol, 2013. 191(8): p. 4165-73.**

110. **Ohta, A., et al.,** ***A2A adenosine receptor protects tumors from antitumor T cells.*** **Proc Natl Acad Sci U S A, 2006. 103(35): p. 13132-7.**

111. **Mittal, D., et al.,** ***Antimetastatic effects of blocking PD-1 and the adenosine A2A receptor.*** **Cancer Res, 2014. 74(14): p. 3652-8.**

112. **Cekic, C. and J. Linden,** ***Adenosine A2A receptors intrinsically regulate CD8+ T cells in the tumor microenvironment.*** **Cancer Res, 2014. 74(24): p. 7239-49.**

113. **Koszalka, P., et al.,** ***Specific Activation of A3, A2A and A1 Adenosine Receptors in CD73-Knockout Mice Affects B16F10 Melanoma Growth, Neovascularization, Angiogenesis and Macrophage Infiltration.*** **PLoS One, 2016. 11(3): p. e0151420.**

114. **Deslandes, A.,** ***Comparative clinical pharmacokinetics of antibody-drug conjugates in first-in-human Phase 1 studies.*** **MAbs, 2014. 6(4): p. 859-70.**

115. **Kitov, P.I. and D.R. Bundle,** ***On the nature of the multivalency effect: a thermodynamic model.*** **J Am Chem Soc, 2003. 125(52): p. 16271-84.**

116. **Martin, W.L. and P.J. Bjorkman,** ***Characterization of the 2:1 complex between the class I MHC-related Fc receptor and its Fc ligand in solution.*** **Biochemistry, 1999. 38(39): p. 12639-47.**

117. **Irani, V., et al.,** ***Molecular properties of human IgG subclasses and their implications for designing therapeutic monoclonal antibodies against infectious diseases.*** **Mol Immunol, 2015. 67(2 Pt A): p. 171-82.**

118. **Bruhns, P.,** ***Properties of mouse and human IgG receptors and their contribution to disease models.*** **Blood, 2012. 119(24): p. 5640-9.**

119. Justus, C.R., L. Dong, and L.V. Yang, *Acidic tumor microenvironment and pH-sensing G protein-coupled receptors.* Front Physiol, 2013. 4: p. 354.

Curriculum Vitae

The Johns Hopkins University School of Medicine

Po-Yuan Hsiao	September, 2016
Name	Date of this version

Educational History:

Ph.D. expected	2016	Pharmacology and Molecular Sciences Mentor: Philip A. Cole, MD PhD	Johns Hopkins School of Medicine
B.S.	2010	Cellular & Molecular Biology	University of Michigan, Ann Arbor

Other professional experience:

Graduate Research Assistant:

Present – 2011	Pharmacology and Molecular Sciences Mentor: Philip A. Cole, M.D. Ph.D.	Johns Hopkins School of Medicine

Consulting Associate Intern

2015-2015	Sage Growth Partners, LLC. Mentor: Chris DeMarco, Ph.D.

Research Rotations:

2011-2011 Lab of James T. Stivers, Ph.D., Johns Hopkins School of Medicine
2010-2011 Lab of Philip A. Cole, M.D. Ph.D., Johns Hopkins School of Medicine
2010-2010 Lab of Ronald L. Schnaar, Ph.D., Johns Hopkins School of Medicine

Research Intern

2010 – 2010	Biotin Nutritional & Biotechnical Product Co., Ltd.,

Research Assistant:

2009 – 2010	Michigan Nanotechnology Institute for Medicine and Biological Sciences (M-NIMBS) Lab of James R. Baker, Jr., M.D.

Research Assistant:

2008 – 2008	Faculty of Medical and Health Sciences, Lab of John D. Fraser, Ph.D.	University of Auckland

Awards and honors:

Phi Beta Kappa	2010	University of Michigan, Ann Arbor
Graduation *magna cum laude*	2010	University of Michigan, Ann Arbor
James B. Angell Scholar	2010	University of Michigan, Ann Arbor
University Honors	2010	University of Michigan, Ann Arbor

Posters:

Hsiao, P. Y., Chiang, M. J., Lo, Y. C., Kalin, J. H., Powell, J. D., Cole, P. A. (2014). A Small-Molecule Protein Conjugate for Cancer Immunotherapy, Sept. 2014, Baltimore, MD.

Hsiao, P. Y., Thomas, T. P., Zhang, Y., Desai, A., Zong, H., Leroueil, P. R., Majoros, I. J., Baker, J. R. Jr. (2009). Targeted Nanodendrimeric Anticancer Prodrug: Conjugation of Methotrexate, Folic acid, and Poly(amidoamine) Dendrimer – A novel rapid 'one pot' synthetic approach. October, 2009, Manhattan Beach, CA.

Publications

Hsiao, P. Y., Kalin, J. H., Sun, I. H., Amin, M. N., Lo, Y. C., Chiang, M. J., Giddens, J., Wang, L. X., Powell, J. D., Cole, P. A. (2016). An Fc-Small Molecule Conjugate for Targeted Inhibition of the Adenosine 2A Receptor. *Chembiochem*. [Epub 2016 Jul 19].

Chiang, M. J., Holbert, M. A., Kalin, J. H., Ahn, Y. H., Giddens, J., Amin, M. N., Taylor, M. S., Collins, S. L., Chan-Li, Y., Waickman, A., **Hsiao, P. Y.,** Bolduc, D., Leahy, D. J., Horton, M. R., Wang, L. X., Powell, J. D., & Cole, P. A. (2014). An Fc domain protein-small molecule conjugate as an enhanced immunomodulator. *Journal of the American Chemical Society, 9*, 3370–3373.

Prusevich, P., Kalin, J. H., Ming, S. A., Basso, M., Givens, J., Li, X., Hu, J., Taylor, M. S., Cieniewicz, A. M., **Hsiao, P. Y.,** Huang, R., Roberson, H., Adejola, N., Avery, L. B., Casero, R. A., Taverna, S. D., Qian, J., Tackett, A. J., Ratan, R. R., McDonald, O. G., Feinberg, A. P., & Cole, P. A. (2014). A selective phenelzine analogue inhibitor of histone demethylase LSD1. *ACS chemical biology, 6*, 1284–1293.

Taylor, M. S., Ruch, T. R., **Hsiao, P. Y.,** Hwang, Y., Zhang, P., Dai, L., Huang, C. R., Berndsen, C. E., Kim, M. S., Pandey, A., Wolberger, C., Marmorstein, R., Machamer, C., Boeke, J. D., & Cole, P. A. (2013). Architectural organization of the metabolic regulatory enzyme ghrelin O-acyltransferase. *The Journal of biological chemistry, 45*, 32211–32228.

Taylor, M. S., Hwang, Y., **Hsiao, P. Y.,** Boeke, J. D., & Cole, P. A. (2012). Ghrelin O-acyltransferase assays and inhibition. *Methods in enzymology*, 205–228.